

https://dspace.org/

Synthesis and characterization of hybrid silica and carbon on silica nanocomposites

Dube, Sibongile Mary-Anne

2010-03-24T11:40:18Z
http://hdl.handle.net/10539/7799

Downloaded from a DSpace repository. https://dspace.org/

SYNTHESIS AND CHARACTERIZATION OF HYBRID SILICA AND CARBON ON SILICA NANOCOMPOSITES

SIBONGILE MARY-ANNE DUBE

SYNTHESIS AND CHARACTERIZATION OF HYBRID SILICA AND CARBON ON SILICA NANOCOMPOSITES

SIBONGILE MARY-ANNE DUBE

A dissertation submitted to the Faculty of Science, University of Witwatersrand, Johannesburg, in fulfilment of the requirements for the degree of Master of Science.

Johannesburg, 2009

DECLARATION

I declare that this dissertation is my own, unaided work. It is being submitted for the Degree of Master of Science in the University of the Witwatersrand, Johannesburg. It has not been submitted before for any degree or examination in any other University.

_____

Sibongile Dube

_____ day of _____ 2009

ABSTRACT

As-synthesized and surfactant extracted periodic mesoporous organosilica (PMO) materials were synthesized by the sol-gel method under acidic and basic conditions. Five different silica sources were used: tetraethylorthosilicate (TEOS), 1,2-bis(trimethoxysilyl)ethane (BTME), 1,4-bis(triethoxysilyl)benzene (BTEB), 4,4-bis(triethoxysilyl)-1,1-biphenyl (BTEBP) and bis[3-trimethoxysilyl)propyl]-amine (BTMSPA). Two structure directing agents were used, triblock copolymer (Pluronic P123) and cetyltrimethylammonium bromide (CTAB). As-synthesized PMO materials were used as templates for the synthesis of silica on carbon nanocomposites with various nanostructures (nanotubes, bamboo nanotubes, spheres and beads).

FTIR spectroscopy and thermogravimetric analysis confirmed the formation of organosilica materials and show that the surfactants Pluronic P123 and CTAB were removed by solvent extraction. The use of the surfactant Pluronic P123 produced periodic mesoporous organosilica materials which had surface areas which followed a systematic trend. It was seen that the size of the organic group had an effect on the surface area obtained on the periodic mesoporous organosilica materials produced. From the results of the surface areas of solvent extracted samples, it was observed that the smaller the chain length of the organosilica precursor, the higher the surface area obtained. It can therefore be concluded that small organic groups (ethane) are more favorable for synthesizing PMOs with high surface areas followed by rigid organic groups (benzene and biphenyl) and lastly flexible organic groups (bis(propyl)amine). The surface areas are obtained for SE-TS-P123, SE-BMS-P123, SE-PS-P123, SE-BS-P123 and SE-BPS-P123 are 839.4, 802.3 and 344.3 m^2/g, 527.1 and 386.2 m^2/g.

The use of the surfactant CTAB yielded periodic mesoporous organosilica materials which followed a systematic trend, with the exception of SE-BS-CTAB. In the surfactant extracted samples the BET surface areas decrease as the chain length of the organic groups is increased. SE-TS-CTAB, SE-BMS-CTAB and SE-PS-CTAB have surface areas of 947.4, 901.1 and 331.6

m^2/g respectively. TEOS has no organic groups, BTME has two CH_2 chains and bis(propyl)amine has six CH_2 chains attached to a NH_2 group making it very flexible hence yielding the lower BET surface area. It is evident from BET that the materials are porous but the structural periodicity must have been confirmed by low angle XRD. Low angle XRD was not done for all the surfactant extracted periodic mesoporous organosilica samples formed due to inadequate resources.

PMOs synthesized using Pluronic P123 as the structure directing agent have lower surface areas than those obtained using CTAB. However SE-BS-CTAB had a higher surface area than SE-BMS-CTAB. This was higher than what was anticipated. It shows that 1,4-Bis(triethoxysilyl) benzene forms PMOs with better structural properties when CTAB as the structure directing agent is used. It can therefore be concluded that CTAB is a better structure directing agent for synthesizing PMOs with better structural properties than CTAB.

The carbonization of as-synthesized and surfactant extracted mesoporous materials in quartz tubes under an inert atmosphere resulted in a diverse range of carbon on silica nanostructures. AS-T-CS 1000 ^oC/5 h produced carbon on silica bamboo nanotubes with varying shapes and some amorphous material. The sample is thermally stable up to 581 ^oC in an air atmosphere. The presence of silica in the material was confirmed by TGA. AS-P-CS 1000 ^oC/5 h produced carbon on silica nanotubes with very thick internal diameters of between 160 – 170 nm, carbon spheres with average diameters of 400 nm and amorphous carbon. The sample is thermally stable up to 416 ^oC in an air atmosphere. EDX confirmed the presence of silica, carbon and oxygen in the various nanostructures obtained for this sample. AS-B-CS 1000 ^oC/5 h produced carbon on silica nanotubes with varying small internal diameters and amorphous carbon material. The sample was the most thermally stable of the three materials up to 650 ^oC in an air atmosphere. Raman spectroscopy revealed that all samples had a low degree of graphitization and are therefore amorphous. The I_D/I_G ratios of AS-T-CS 1000 ^oC/5 h, AS-B-CS 1000 ^oC/5 h and AS-P-CS 1000 ^oC/5 h samples are 0.81, 1.87 and 0.96. The disorder of the samples does not follow any systematic trend.

AS-BS-P123 samples heated at different carbonization temperatures produced different carbon on silica nanostructures which included spheres and nanotubes. Amorphous material (approximately 60%) was also produced. The presence of silicon and carbon in the carbon on silica nanocomposites produced was further confirmed by the use of scanning X-ray photoelectron spectroscopy (SXPS) (AS-B-CS 1000 ^{o}C/5 h sample). Raman spectral data showed that as the carbonization temperature is increased, the degree of disorder of the materials also increased. The temperature at which major loss changes occurred due to the oxidation of carbon increased as the carbonization temperature increased up to 1000°C. Low surface areas and pore volumes were obtained for all mesoporous phenyl-bridged organosilica/surfactant mesophases heated at different temperatures. This may be due to the high carbonization efficiency at temperatures from 700 ^{o}C to 1100 ^{o}C that there is rapid formation of carbon deposits which blocks some of the mesopores. Also at these high pyrolysis temperatures, the carbonization may be so fast that the surfactant molecules are directly converted to carbon which blocks the pores rather than being burnt off.

Longer pyrolysis times yield various shaped carbon on silica nanocomposites (nanotubes, spheres, beads and amorphous material) and shorter pyrolysis times yield only amorphous material and beads. AS-P-CS 1000 ^{o}C/5 h produced carbon on silica nanocomposites of nanotubes, spheres, beads and amorphous material. Both AS-P-CS 1000 ^{o}C/1 h and AS-P-CS 1000 ^{o}C/0.5 h carbon on silica nanocomposites produced amorphous material and beads. Most carbon on silica beads of AS-P-CS 1000 ^{o}C/1 h and AS-P-CS 1000 ^{o}C/0.5 h have sizes which range from 1.8 – 2.4 and 1.2 – 2.0 µm, respectively. Shorter pyrolysis times of 0.5 h produced carbon on silica beads with smaller diameters which ranged from 1.2 – 2.0 µm and pyrolysis times of 1 h produced carbon on silica beads with larger diameters of 1.8 – 2.4 µm. The Raman data showed that as the carbonization time is increased, the degree of disorder in the carbon on silica nanocomposites also increases. The thermal stability of the carbon on silica nanocomposite samples decreased as the carbonization time was increased.

This dissertation is dedicated to my parents,

Doreen and Russell Dube for their love, care and support throughout my studies.

ACKNOWLEDGEMENTS

I would like to express my sincere gratitude to the following people and institutions for their various roles in making this project a success:

- My supervisor, Professor N. J. Coville for his invaluable support, guidance and helpful suggestions and criticisms during this project.
- My Co-Supervisor, Dr A. M. Tshavhungwe for making a positive contribution through knowledge sharing and sacrificing his time to help.
- My husband, Bothwell Manikai for encouragement and support throughout my studies.
- Professor M. Witcomb and all members of the Electron Microscope Unit at the University of the Witwatersrand for assistance with electron microscopy work.
- Mr R. Erasmus for assistance with Raman spectroscopy analysis.
- Mr W. Jordaan of the CSIR Pretoria for XPS analysis.
- The glassblower, Mr S. Gannon for assistance with sealing and opening the quartz tubes used for this work.
- My family members for their patience in seeing me through this work.
- All members of the CAT-OM-MAT group of the school of chemistry at the University of the Witwatersrand for providing a conducive working environment.
- The DST/NRF Centre of Excellence in Strong Materials and the University of the Witwatersrand for financial support.
- Above all to God the almighty for providing strength and protection.

Poster presentations arising from this work

- In vacuo thermal transformations of nanoporous organosilica materials to silica/carbon nanocomposites. Workshop on "Structure and Properties of Nanomaterials", University of Zululand, Richards Bay, (29 July – 1 August 2007).
- Carbon on silica nanocomposites with variable morphologies synthesized by a simple carbonization process. 3rd NanoAfrica Conference, CSIR Convention Centre, Pretoria, (1-4 February 2009).

Table of Contents

Topic	Page
Title….....	i
Declaration	ii
Abstract…….....	iii
Dedication….....	vi
Acknowledgements….....	vii
Poster presentations….....	viii
Table of Contents…….....	ix
List of Figures.....	xv
List of Tables.....	xxii
List of Schemes.....	xxiv
Abbreviations and Symbols	xxv
Notations used to identify samples….....	xxviii
Chapter 1 Introduction.....	**1**
1.0 Background to the study.....	1
1.1 Objectives of the study.....	3
1.2.1 Dissertation outline.....	4
1.3 Sol-gel processing.....	5

1.3.1 History of sol-gel processing..... 5

1.3.2 The chemistry of sol-gel processing..... 6

1.3.3 Formation of mesoporous materials by the surfactant-templated sol-gel method..... 14

1.3.4 Advantages and disadvantages of sol-gel processing..... 17

1.3.4.1 Advantages..... 17

1.3.4.2 Disadvantages..... 19

1.4 Organic-Inorganic hybrid materials..... 19

1.5 Periodic mesoporous organosilica materials (PMOs..... 20

1.6 Nanotubes and related nanostructures..... 22

1.7 Carbon on silica nanocomposites..... 23

1.8 References..... 24

Chapter 2 Literature Review..... 29

2.1 Periodic mesoporous organosilica materials: A review..... 29

2.1.1 Synthesis of PMOs using structure directing agents with ionic surfactants..... 31

2.1.1.1 Aliphatic PMOs..... 31

2.1.1.2 Aromatic PMOs..... 33

2.1.1.3 Periodic mesoporous aminosilicas (PMAs)..... 35

2.1.2 Synthesis of PMOs through structure direction by non-ionic

surfactants..... 36

2.2 Background notes on the characterization of PMOs using nitrogen sorption studies..... 42

2.3 Mesoporous carbon materials: A review..... 47

2.4 Carbon/silica nanocomposites: A review..... 50

2.5 References..... 52

Chapter 3 Experimental..... 61

3.1 Brief Introduction 61

3.2 Reagents and Chemicals 62

3.3 Synthesis of periodic mesoporous organosilica materials 66

3.3.1 Mesoporous materials from structure directing agent Pluronic P123.....

3.3.1.1 Synthesis method 66

3.3.1.2 Surfactant extraction 67

3.3.2 Mesoporous materials from structure directing agent CTAB..... 68

3.3.2.1 Synthesis method 68

3.3.2.2 Surfactant extraction 68

3.3.3 Synthesis of carbon on silica nanocomposites..... 69

3.4 Characterization 70

3.4.1 Measurements 70

3.4.1.1 Thermogravimetric analysis (TGA)..... 70

3.4.1.2 Transmission electron microscopy (TEM)..... 70

3.4.1.3 High resolution transmission electron microscopy equipped with EDX (High resolution TEM)..... 70

3.4.1.4 Fourier transform infrared spectroscopy (FTIR)..... 71

3.4.1.5 Nitrogen adsorption/desorption analysis..... 71

3.4.1.6 Raman spectroscopy..... 71

3.4.1.7 Scanning electron microscopy (SEM)..... 72

3.4.1.8 Scanning X-ray photoelectron spectroscopy..... 72

3.5 References..... 72

Chapter 4 Results and Discussion..... 73

4.0 Brief Introduction – Overview of chapter……... 73

4.1 Synthesis of periodic mesoporous organosilica materials..... 74

4.1.1 As-synthesised and surfactant extracted periodic mesoporous organosilica materials synthesised using Pluronic P123 as a structure directing agent..... 74

4.1.1.1 Fourier transform infrared (FTIR) spectroscopy..... 75

4.1.1.2 Thermogravimetric analysis..... 78

4.1.1.3 Nitrogen sorption studies..... 84

4.1.2 As-synthesised and surfactant extracted periodic mesoporous organosilica materials synthesised using CTAB as a structure directing

agent..... 93

4.1.2.1 Fourier transform infrared (FTIR) spectroscopy..... 93

4.1.2.2 Thermogravimetric analysis..... 96

4.1.2.3 Nitrogen sorption studies..... 100

4.1.2.4 Summary of results..... 107

4.2 Synthesis of carbon on silica nanocomposite materials..... 109

4.2.1 Investigation of the effect of carbonization of different organic-inorganic hybrid materials at a constant temperature..... 109

4.2.1.1 Transmission electron microscopy..... 109

4.2.1.2 High magnification transmission electron microscopy..... 112

4.2.1.3 Raman spectroscopy..... 113

4.2.1.4 Thermogravimetric analysis..... 116

4.2.1.5 Summary of results..... 117

4.2.2 Effect of carbonization temperature on properties of AS-B-CS y ^{o}C/5 h (where y = 700, 800, 900, 1000 or 1100 ^{o}C) composites..... 118

4.2.2.1 Transmission electron microscopy..... 118

4.2.2.2 Raman spectroscopy..... 121

4.2.2.3 Thermogravimetric analysis..... 123

4.2.2.4 Nitrogen sorption studies..... 125

4.2.2.5 Scanning x-ray photoelectron spectroscopy..... 128

4.2.2.6 Summary of results..... 128

4.2.3 The effect of variation of carbonization time on the morphology of Carbon on silica nanocomposites formed from AS-PS-P123 organosilica materials..... 129

4.2.3.1 Transmission electron microscopy..... 129

4.2.3.2 Thermogravimetric analysis..... 134

4.2.3.3 Raman spectroscopy..... 135

4.2.3.4 Summary of results..... 137

4.3 References..... 138

Chapter 5 Conclusion 140

LIST OF FIGURES

Figure 1.1	The sol-gel process and the various products formed.....	13
Figure 1.2	Supramolecular structures for surfactants.....	15
Figure 1.3	Schematic phase diagram for CTAB in water.....	16
Figure 1.4	Reaction condition variables used to control the synthesis of PMOs.....	22
Figure 2.1	IUPAC classification of gas adsorption isotherms…….	43
Figure 2.2	IUPAC classification of adsorption-desorption hysteresis loops……..	45
Figure 3.1	Schematic showing the formation of as-synthesized and extracted periodic mesoporous organo-bridged silica, carbon/silica composites and mesoporous carbons.....	62
Figure 3.2	Pictures showing samples in quartz tubes, white sample before and black sample after the carbonization process…….	61
Figure 4.1	FTIR spectra of a) AS-TS-P123 and SE-TS-P123 and b) AS-BMS-P123 and SE-BMS-P123 mesoporous silica materials (*) modes assigned to Si – C stretching vibrations, (#) modes assigned to C – H stretching and deformation vibrations of Pluronic P123 and (^) modes assigned to C – H deformation vibrations of the ethane framework organic groups…….....	76
Figure 4.2	FTIR spectra of a) AS-BS-P123 and SE-BS-P123 and b) AS-BPS-P123 and SE-BPS-P123 mesoporous silica materials. (*)	

modes assigned to Si – C stretching vibrations, (#) modes assigned to C – H stretching and deformation vibrations of Pluronic P123, ($) modes assigned to C – C stretching vibrations of the aromatic ring and (+) modes assigned to C – H absorption bands of the aromatic ring……..... 77

Figure 4.3 FTIR spectra of a) AS-PS-P123 and SE-PS-P123 mesoporous silica materials. (*) modes assigned to Si – C stretching vibrations, (#) modes assigned to C – H stretching and deformation vibrations of Pluronic P123 and (//) modes assigned to N – H vibrations of the framework organic groups……. 78

Figure 4.4 TGA curves of a) AS-TS-P123 and SE-TS-P123, b) AS-BMS -P123 and SE-BMS-P123, c) AS-BS-P123 and SE-BS-P123, d) AS-BPS-P123 and SE-BPS-P123 and e) AS-PS-P123 mesoporous silica materials…… 80

Figure 4.5 Nitrogen adsorption isotherms and the corresponding BJH pore size distribution curves derived from adsorption and desorption isotherms of a) AS-TS-P123 and b) SE-TS-P123 organosilica materials…….…… 88

Figure 4.6 Nitrogen adsorption isotherms and the corresponding BJH pore size distribution curves derived from adsorption and desorption isotherms of a) AS-BMS-P123 and b) SE-BMS-P123 organosilica

materials……. 89

Figure 4.7 Nitrogen adsorption isotherms and the corresponding BJH pore size distribution curves derived from adsorption and desorption isotherms of a) AS-BS-P123 and b) SE-BS-P123 organosilica materials…… 90

Figure 4.8 Nitrogen adsorption isotherms and the corresponding BJH pore size distribution curves derived from adsorption and desorption isotherms of a) AS-BPS-P123 and b) SE-BPS-P123 organosilica materials…….. 91

Figure 4.9 Nitrogen adsorption isotherms and the corresponding BJH pore size distribution curves derived from adsorption and desorption isotherms of a) AS-PS-P123 and b) SE-PS-P123 organosilica materials…….. 92

Figure 4.10 FTIR spectra of a) AS-TS-CTAB and SE-TS-CTAB and b) AS-BMS-CTAB and SE-BMS-CTAB mesoporous silica (*) modes assigned to Si – C stretching vibrations, (#) modes assigned to C – H stretching and deformation vibrations of CTAB and (^) modes assigned to C – H deformations vibrations of the framework organic group…… 94

Figure 4.11 FTIR spectra of a) AS-BS-CTAB and SE-BS-CTAB and b) AS-PS-CTAB and SE-PS-CTAB mesoporous silica

(*) modes assigned to Si – C stretching vibrations, (#) modes assigned to C – H strectching and deformation vibrations of CTAB, ($) modes assigned to C – C strectching vibrations of the aromatic ring, (+) modes assigned to C – H strectching vibrations of the aromatic ring and (//) modes assigned to N – H bend vibrations……. 95

Figure 4.12 TGA curves of a) AS-TS-CTAB and SE-TS-CTAB, b) AS-BMS-CTAB and SE-BMS-CTAB, c) AS-BS-CTAB and SE-BS-CTAB and d) AS-PS-CTAB and SE-PS-CTAB mesoporous silica materials……..... 97

Figure 4.13 Nitrogen adsorption isotherms and the corresponding BJH pore size distribution curves derived from adsorption and desorption isotherms of a) AS-TS-CTAB and b) SE-TS-CTAB organosilica materials…….. 103

Figure 4.14 Nitrogen adsorption isotherms and the corresponding BJH pore size distribution curves derived from adsorption and desorption isotherms of a) AS-BMS-CTAB and b) SE-BMS-CTAB organosilica materials……. 104

Figure 4.15 Nitrogen adsorption isotherms and the corresponding BJH pore size distribution curves derived from adsorption and desorption isotherms of a) AS-BS-CTAB and b) SE-BS-CTAB organosilica

materials……. 105

Figure 4.16 Nitrogen adsorption isotherms and the corresponding BJH pore size distribution curves derived from adsorption and desorption isotherms of a) AS-PS-CTAB and b) SE-PS-CTAB organosilica materials…… 106

Figure 4.17 Graph showing the correlation between BET surface areas and Chain length of the organosilanes……. 108

Figure 4.18 Transmission electron microscopy images of AS-T-CS 1000 ^{o}C/5 h samples……..... 110

Figure 4.19 Transmission electron microscopy images of AS-B-CS 1000 ^{o}C/5 h samples…… 111

Figure 4.20 Transmission electron microscopy images of AS-P-CS 1000 ^{o}C/5 h samples……... 112

Figure 4.21 High magnification TEM images and corresponding EDX spectra of AS-P-CS 1000 ^{o}C/5 h carbon on silica nanocomposite sample….. 113

Figure 4.22 Raman spectra of a) AS-T-CS 1000 ^{o}C/5 h, b) AS-B-CS 1000 ^{o}C/5 h and c) AS-P-CS 1000 ^{o}C/5 h samples…… 115

Figure 4.23 TGA curves of a) AS-T-CS 1000 ^{o}C/5 h, b) AS-P-CS 1000 ^{o}C/5 h and c) AS-B-CS 1000 ^{o}C/5 h samples…….. 117

Figure 4.24 TEM images of a) AS-B-CS 700 ^{o}C/5 h, b) AS-B-CS 800 ^{o}C/5 h, c) AS-B-CS 900 ^{o}C/5 h, d) AS-B-CS 1000 ^{o}C/5 h and

e) AS-B-CS 1100 ^{o}C/5 h carbon on silica nanocomposite samples….. 120

Figure 4.25 Raman spectra of a) AS-B-CS 700 ^{o}C/5 h, b) AS-B-CS 800 ^{o}C/5 h, c) AS-B-CS 900 ^{o}C/5 h, d) AS-B-CS 1000 ^{o}C/5 h and e) AS-B-CS 1100 ^{o}C/5 h carbon on silica nanocomposite samples….. 123

Figure 4.26 TGA curves of a) AS-B-CS 700 ^{o}C/5 h, b) AS-B-CS 800 ^{o}C/5 h, c) AS-B-CS 900 ^{o}C/5 h, d) AS-B-CS 1000 ^{o}C/5 h and e) AS-B-CS 1100 ^{o}C/5 h carbon on silica nanocomposite samples….. 124

Figure 4.27 Derivative TGA curves of a) AS-B-CS 700 ^{o}C/5 h, b) AS-B-CS 800 ^{o}C, c) AS-B-CS 900 ^{o}C/5 h and AS-B-CS 1100 ^{o}C/5 h carbon on silica nanocomposite samples…… 125

Figure 4.28 TEM images of AS-P-CS 1000 ^{o}C/0.5 h and the corresponding diameter distribution graph of carbon on silica beads……. 130

Figure 4.29 TEM images of AS-P-CS 1000 ^{o}C/1 h and the corresponding diameter distribution graph of carbon on silica beads……. 132

Figure 4.30 TEM images of AS-P-CS 1000 ^{o}C/5 h samples……..... 133

Figure 4.31 TGA curves of a) AS-P-CS 1000 ^{o}C/5 h, b) AS-P-CS 1000 ^{o}C/1 h and c) AS-P-CS 1000 ^{o}C/0.5 h carbon on silica nanocomposite samples…… 134

Figure 4.32 Raman spectra of a) AS-P-CS 1000 ^{o}C/5 h, b) AS-P-CS 1000 ^{o}C/1 h and c) AS-P-CS 1000 ^{o}C/0.5 h carbon on silica nanocomposite samples…… 136

LIST OF TABLES

Table 1.1	Elements used to date in sol-gel processing.....	6
Table 2.1	Overview of mesoporous silica and PMO synthesis in the presence of ionic and non- ionic surfactants as structure directing agents…….	39
Table 3.1	Structure directing agents and organosilica precursors.....	64
Table 3.2	Tabular details of synthesis parameters.....	67
Table 4.1	TGA results of as-synthesized and solvent extracted PMOs prepared with Pluronic P123……..	81
Table 4.2	Structural properties of as-synthesized and surfactant extracted periodic mesoporous organosilicas synthesized using Pluronic P123 as structure directing agent……..	86
Table 4.3	TGA results of as-synthesized and solvent extracted PMOs prepared with CTAB as SDA.....	98
Table 4.4	Structural properties of as-synthesized and surfactant extracted PMOs synthesized using CTAB as a structure directing agent……	101
Table 4.5	D- and G- band positions and I_D/I_G ratios of carbon on silica nanocomposites produced by carbonization of different organic-inorganic hybrid materials at constant temperature and time…	114
Table 4.6	Morphologies of carbon on silica nanocomposite materials produced after carbonization of as-synthesized benzene-bridged silica samples	

at different temperatures……. 119

Table 4.7 D- and G- band positions and I_D/I_G ratios of AS-BS-P123 samples heated at different temperatures……. 122

Table 4.8 Textural properties of carbon on silica nanocomposites produced using as-synthesized benzene-bridged organosilica materials heated at different carbonization temperatures……. 127

Table 4.9 D- and G- band positions and I_D/I_G ratios of silica on carbon nanocomposites produced by the carbonization of AS-PS-P123 samples at different times……. 135

Table 4.10 Summary of TEM results obtained of AS-P-CS 1000 oC/x h (where x = 0.5, 1 and 5 hrs) of carbon on silica nanocomposite samples……. 138

LIST OF SCHEMES

Scheme 1.1	Schematic representation of hydrolysis of tetraalkylorthosilicate.....	8
Scheme 1.2	Hydrolysis mechanisms of tetraalkylorthosilicate……...	9
Scheme 1.3	Condensation mechanisms of tetraalkylorthosilicate……..	11

ABBREVIATIONS AND SYMBOLS

Abbreviation/Symbol	Meaning
2D/3D hex	2 Dimensional/3 Dimensional hexagonal
%	Percentage
Å	Angstrom
BET	Brunauer, Emmet and Teller
BJH	Barrett-Joyner-Halenda
B50-6600	Triblock copolymer $EO_{39}BO_{47}EO_{39}$
Brij 30	Polyoxyethylene-(4)-lauryl ether
	$C_{12}H_{25}EO4OH$
Brij 56	Polyoxyethylene-(10)-hexadecyl ether
	$C_{16}H_{33}EO10OH$
Brij 76	Polyoxyethylene-(10)-octadecyl ether
	$C_{18}H_{37}EO10OH$
BTEB	1,4-bis(triethoxysilyl)benzene
BTEBP	4,4-bis(triethoxysilyl)biphenyl
BTEE	1,2-bis(triethoxysilyl)ethene
BTET	2,5-bis(triethoxysilyl)thiophene
BTME	1,2-bis(trimethoxysilyl)ethane
BTMSPA	Bis[(3-trimethoxysilyl)propyl]-amine

CPB/CPC	Cetylpyridinium bromide/chloride
CTAB/CTAC	Cetyltrimethylammonium bromide/chloride
CVD	Chemical vapour deposition
d	XRD lattice spacing
EDX	Energy dispersive x-ray
EtOH	ethanol
FTIR	Fourier transform infrared
HCl	Hydrochloric acid
HF	Hydrofluoric acid
HRTEM	High resolution transmission electron microscopy
IUPAC	International Union of Pure and Applied Chemistry
LC	Liquid-crystalline
LGE 53	triblock copolymer poly(ethylene oxide)-poly(DL-lactic-acid-co-glycolic acid)-poly(ethylene oxide) $EO_{16}(L_{28}G_3)$ EO_{16}
MCM	Mobil Catalytic Material
MSU	Michigan State University
NaCl	Sodium chloride
NH_4OH	Aqueous ammonia solution
nm	Nanometre
OTAB/OTAC	Octadecyltrimethylammonium bromide/chloride

Pluronic F127	Triblock copolymer $EO_{106}PO_{70}EO_{106}$
Pluronic P123	Triblock copolymer $EO_{20}PO_{70}EO_{20}$
PMA	Periodic mesoporous aminosilica
PMO	Periodic mesoporous organosilica
SBA	Santa Barbara
S_{BET}	Specific surface area
SDA	Structure directing agent
SEM	Scanning electron microscopy
Si MASNMR	Silicon Magic Angle Spinning Nuclear Magnetic Resonance
SiO_2	Silica
SXPS	Scanning X-ray photoelectron spectroscopy
TEM	Transmission electron microscopy
TEOS	Tetra ethyl orthosilicate
TGA	Thermogravimetric analysis
TLCT	True liquid-crystal templating
XRD	X-ray diffraction

(Please note EO=ethylene oxide, PO=propylene oxide and BO=butylene oxide)

Notations used to identify samples

Notation	Meaning
	AS= As-synthesized, SE = Solvent extracted, TS, BMS, BS, BPS and PS = TEOS silica, BTME silica, Benzene silica, Biphenyl silica and Propylamine silica respectively (silica sources).
AS-TS-P123	As-synthesized TEOS silica prepared from Pluronic P123
SE-TS-P123	Solvent extracted TEOS silica prepared from Pluronic P123
AS-BMS-P123	As-synthesized BTME silica prepared from Pluronic P123
SE-BMS-P123	Solvent extracted BTME silica prepared from Pluronic P123
AS-BS-P123	As-synthesized Benzene silica prepared from Pluronic P123
SE-BS-P123	Solvent extracted Benzene silica prepared from Pluronic P123
AS-BPS-P123	As-synthesized Biphenyl silica prepared from Pluronic P123
SE-BPS-P123	Solvent extracted Biphenyl silica prepared from Pluronic P123

AS-PS-P123	As-synthesized Propylamine silica prepared from Pluronic P123
SE-PS-P123	Solvent extracted Propylamine silica prepared from Pluronic P123
AS-TS-CTAB	As-synthesized TEOS silica prepared from CTAB
SE-TS-CTAB	Solvent extracted TEOS silica prepared from CTAB
AS-BMS-CTAB	As-synthesized BTME silica prepared from CTAB
SE-BMS-CTAB	Solvent extracted BTME silica prepared from CTAB
AS-BS-CTAB	As-synthesized Benzene silica prepared from CTAB
SE-BS-CTAB	Solvent extracted Benzene silica prepared from CTAB
AS-BPS-CTAB	As-synthesized Biphenyl silica prepared from CTAB
SE-BPS-CTAB	Solvent extracted Biphenyl silica prepared from CTAB
AS-PS-CTAB	As-synthesized Propylamine silica prepared from CTAB
SE-PS-CTAB	Solvent extracted Propylamine silica prepared from CTAB CS = carbon silica, T, B and P = TEOS, Benzene and Propylamine respectively.
AS-T-CS 1000 ^{o}C/5 h	As-synthesized TEOS carbon silica composite heated at 1000 ^{o}C for 5 hours
AS-B-CS 1000 ^{o}C/5 h	As-synthesized Benzene carbon silica composite heated to 1000 ^{o}C for 5 hours

AS-P-CS 1000 ^{o}C/5 h	As-synthesized Propylamine carbon silica composite
	Composite heated to 1000 ^{o}C for 5 hours
AS-B-CS x ^{o}C/5 h	x = 700, 800, 900, 1000 or 1100 ^{o}C (carbonization
	temperature)
AS-P-CS 1000 ^{o}C/y h	y = 0.5, 1 or 5 hours (pyrolysis time)

CHAPTER ONE

INTRODUCTION

1.0 Background to the study

In the past decade, a lot of work has been put into the synthesis of well defined porous materials , because of their potential applications in catalysis [1 - 3], separation science [4,5], and environmental remediation [6, 7]. The scope of porous materials was expanded in 1999 when several research groups reported on a new class of organic-inorganic hybrid composites, called periodic mesoporous organosilica materials (PMOs) [8 – 10]. Silica/carbon composites are an example of a hybrid material and are particularly versatile materials that find many possible uses for example in electrochemical devices [11], and solar absorbers [12]. Silica/carbon composites may be prepared via many methods including sol-gel techniques followed by carbonization [13], pyrolysis of suitable carbon precursors in a porous silica matrix [14] or carbonization of organosilica/surfactant mesophases [15].

Silica/surfactant and organosilica/surfactant phases synthesized by sol-gel condensation of silica precursors and bridged silsesquioxanes have been used as precursors for the fabrication of a wide range of nanostructured materials under a flow of an inert gas [15 – 18]. By heating mesostructured benzene-bridged PMO with crystal like pore walls for 4 hours at 900 ^{o}C in a stream of nitrogen, Pang *et al* obtained mesoporous carbon/silica nanocomposite materials with pore walls uniformly constructed from molecular carbon and silica units [15]. Pinnavaia *et al* reported the formation of carbon nanotubes by in situ carbonization of a micellar non-ionic surfactant (Pluronic P123) under a flow of nitrogen [16]. Urban *et al* synthesized multiwalled carbon nanotubes by graphitization of as-synthesized mesoporous silicas templated by cetyltrimethylammonium bromide [17]. Mokaya *et al* showed that periodic mesoporous

organosilica surfactant mesophases can be transformed into silica/carbon nanocomposites and mesostructured forms of pure silica, carbon and silicon carbide [18].

In this study, the sol-gel process was used for the synthesis of as-synthesized and surfactant extracted periodic mesoporous organosilica materials. Five different silica sources were used: tetraethyl orthosilicate (TEOS), 1,2-bis(trimethoxysilyl) ethane (BTME), 1,4-bis(triethoxysilyl)benzene (BTEB), 4,4-bis (triethoxysilyl)-1,1 biphenyl (BTEBP) and bis[(3-trimethoxysilyl)propyl]-amine (BTMSPA). Two structure directing agents were used, triblock copolymer (Pluronic P123) and cetyltrimethylammonium bromide (CTAB). The chain length of the organic moiety and the nature of the structure directing agents were varied in order to study their effect on the morphology, thermal stability and on the surface properties (namely surface area, pore volume, pore size and pore size distribution) of the materials synthesized. The resulting as-synthesized periodic mesoporous organosilica materials were used as templates for the synthesis of carbon on silica nanocomposites using a simple carbonization process

Carbon on silica nanocomposites were synthesized by directly carbonizing the organosilica/surfactant phases at different temperatures under an inert atmosphere produced by first sealing the mesoporous silica materials in quartz tubes under vacuum. The carbonization process was done in a muffle furnace. No carbon precursor was impregnated in the pore walls of the mesoporous silica materials before carbonization. The effect of carbonization time, carbonization temperature, and the nature of the silica/organosilica precursor on the morphology, graphitic/amorphous nature, thermal stability, and textural properties of carbon/silica composites was investigated. This resulted in carbon on silica nanocomposites being formed with various nanostructures (e.g. nanotubes, spheres, etc). To the best of our knowledge, this is the first report on the direct preparation of carbon on silica nanocomposite materials with various nanostructures being produced by this process.

1.1 Objectives of the study

The objectives of the study are as follows:

- To synthesize periodic mesoporous organosilica materials using the sol – gel method.
- To study the effects of the variation of templates and organosilica precursors on the structural properties (namely surface area, pore volume, pore size and pore size distribution), morphology and thermal stability of the resulting periodic mesoporous organosilica materials formed.
- To use the periodic mesoporous organosilica materials formed as templates for the synthesis of silica on carbon nanocomposites.
- To study the effect of carbonization on different hybrid organic-inorganic materials at a constant temperature.
- To investigate the effects of varying carbonization time and temperature on the morphology, thermal stability and quality of carbon on silica nanocomposites produced.
- To characterize all materials formed by a variety of techniques such as thermogravimetric analysis, transmission electron microscopy, high magnification transmission electron microscopy equipped with EDX, fourier transform infrared spectroscopy, nitrogen sorption, Raman spectroscopy, scanning electron microscopy (SEM), and scanning X-ray photoelectron spectroscopy (SXPS).

1.2 Dissertation outline

Chapter 1 This chapter provides a brief review of the sol-gel method, its history, its chemistry and advantages and disadvantages. The background to hybrid organic-inorganic silica materials, periodic mesoporous organosilica materials, carbon on silica nanocomposites and nanotubes and related nanostructures are also discussed. The dissertation outline is also summarized.

Chapter 2 provides a review of the literature related to the synthesis of periodic mesoporous organosilica materials, mesoporous carbon materials and carbon/silica nanocomposites.

Chapter 3 describes the general preparation methods and characterization techniques of periodic mesoporous organosilica materials and carbon on silica nanocomposite materials used in this study.

Chapter 4. In this chapter, the results and discussion relating to the synthesis of periodic mesoporous organosilica materials and carbon on silica nanocomposites are presented.

Chapter 5. In this chapter, conclusions are drawn based on the results obtained with respect to the initial objectives of the study.

1.3 Sol-gel processing

1.3.1 History of sol-gel processing

Sol-gel processing methods were first used historically for decorative and constructional materials. They have also long been used for the powderless processing of glasses and ceramics. The first metal alkoxide was prepared from silicon tetrachloride ($SiCl_4$) and ethanol by Ebelmen in 1845 [10]. He found out that $SiCl_4$ and ethanol gelled on exposure to the atmosphere with normal humidity. This metal alkoxide was called tetraethylorthosilicate (TEOS). The commercial production of sol-gel coatings onto flat glasses appeared in the early sixties. However the development of sol-gel science only really started twenty years ago with the "First International Workshop on glasses and ceramics from Sols" in 1981. Many new applications for sol-gel prepared materials were developed in the 20th century. Sol-gel processes are now widely used for the synthesis of multicomponent ceramics [11], nanophase materials [12] and more than 6000 papers have been published during the past 22 years on the subject [13]. One of the major advances of sol-gel processing that has been seen during the last few years is undoubtedly the synthesis of hybrid organic-inorganic materials. This field was initiated in the 1980s by the pioneering work of Schmidt and co-workers at the Fraunhoffer Institute [14]. Intermediate between glasses and polymers, these nanocomposites open up new possibilities in the field of materials science. They have led to the development of functional coatings, optical devices, chemical sensors and even bio-sensors. Today sol-gel methods are reaching their full potential, enabling the preparation of new generations of advanced materials not easily accessible by other methods, yet using mild, low energy conditions. Table 1.1 shows the elements that have been used to this date in sol-gel processing [15].

Table 1.1 Elements used to date in sol-gel processing.

Li	Y	Cr	B	N
Na	La	Fe	Al	P
K	Nd	Co	In	As
Cs	Th	Ni	C	Sb
Mg	U	Pd	**Si**	O
Ca	Ti	Au	Ge	S
Sr	Zr	Zn	Sn	F
Ba	Hf	Cd	Pb	

1.3.2 The chemistry of sol-gel processing

The silicon based sol-gel process was employed in this work, therefore the fundamental reaction principles will be discussed using this process as a model system. The term sol-gel synthesis is defined broadly to mean the preparation of ceramic materials by the preparation of a sol, gelation of the sol, and removal of the solvent [15].

A **colloid** is a suspension in which the dispersed phase is so small (~1 nm – 1 µm) that gravitational forces are negligible and interactions are dominated by short range forces, such as van der Waals attractions as well as surface charges. A **sol** is a colloidal suspension of solid

particles in a liquid. A **gel** is a substance that contains a continuous solid skeleton enclosing a continuous liquid phase, with both the solid and liquid phases having colloidal dimensions.

The sol-gel process starts from a homogeneous solution of the precursor (starting compound) in a solvent, and leads to the formation of soluble species: oligomers, polymers, cross-linked chains and colloids. They result from the chemical reaction occurring in solution before the sol-gel transition. Then, once the gel is formed (solid), syneresis and ageing become important steps, since chemical and physical transformations still occur and strongly influence the characteristics of the material. Finally, xerogels are obtained after elimination of the solvent and drying. The following paragraphs will give a brief description of the stages involved in sol-gel processing.

In sol-gel processing, the precursors for the preparation of a colloid consist of a metal or metalloid element surrounded by ligands. Metal alkoxides are members of the family of metalorganic compounds, which have an organic ligand attached to a metal or metalloid atom. The most common of these is silicon tetraethoxide ($Si(OC_2H_5)_4$). This is also called tetraethoxysilane, or tetraethylorthosilicate (TEOS).

Sol-gel processing involves a series of stages (Fig 1.1). These are hydrolysis and condensation chemistry, gelation, aging, and drying through which an alkoxysilane monomer is converted into a hyper-cross-linked siloxane network. Principally $R_{4-n}SiX_n$ compounds (n = 1 – 4, X = OR', R = alkyl group) are used as molecular precursors, in which the Si – X bond is liable to hydrolyse forming unstable silanols (Si-OH) that condense leading to Si – O – Si bonds.

Hydrolysis

The first step in sol-gel processing of silica (SiO_2) is hydrolysis of silicon alkoxide to form a hydroxylated product and a corresponding alcohol (Scheme 1.1).

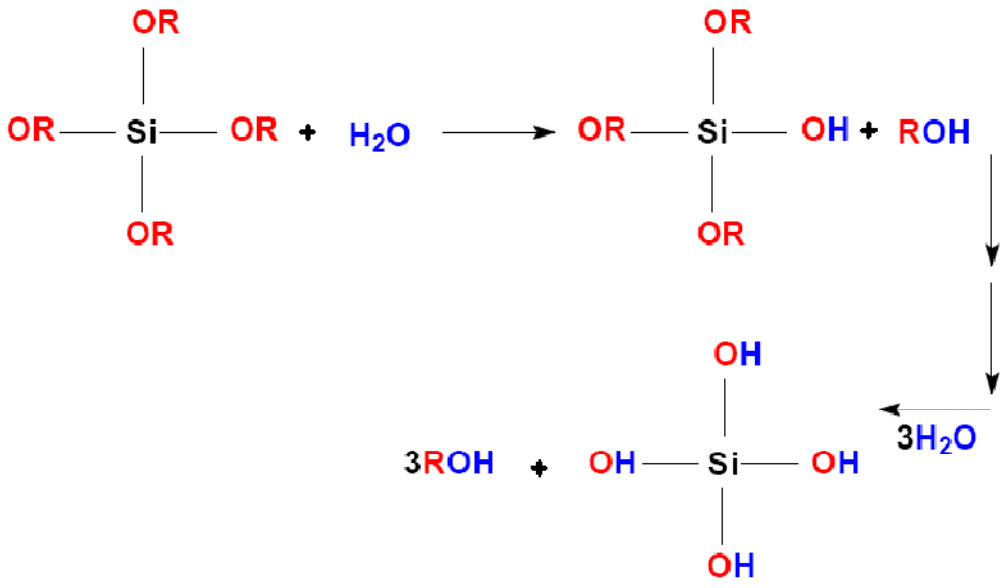

Scheme 1.1. Schematic representation of hydrolysis of tetraalkylorthosilicate (R = alkyl).

The process is catalysed by acids or bases resulting in different reaction mechanisms leading to the condensation reaction as shown in Scheme 1.2. The pH used therefore has an effect on the kinetics of the reaction which is usually expressed by the gel point of the sol-gel reaction.

Acid Catalysis

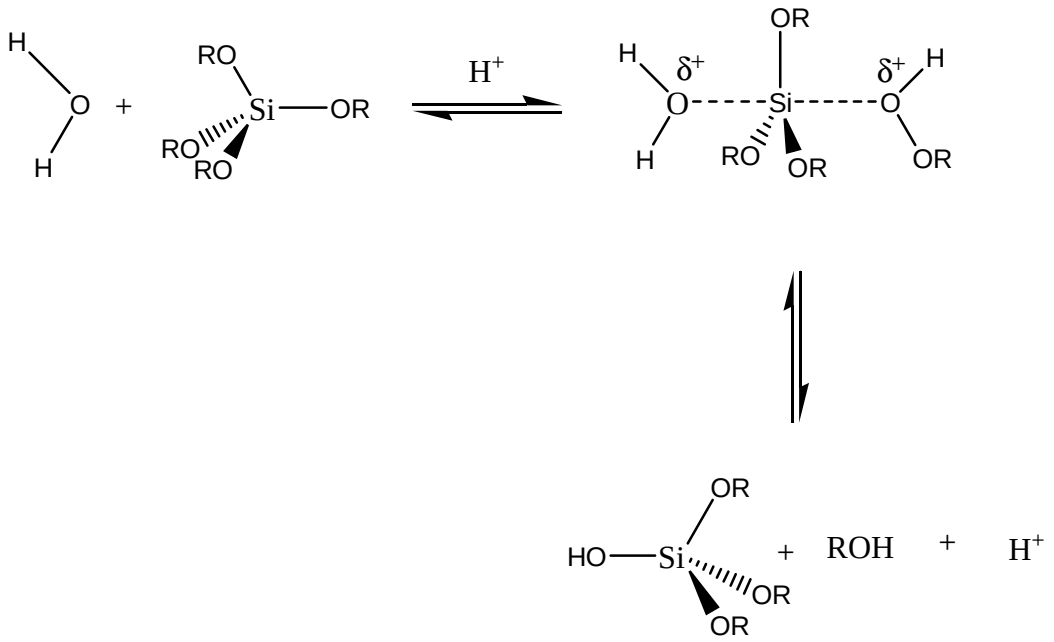

Base Catalysis

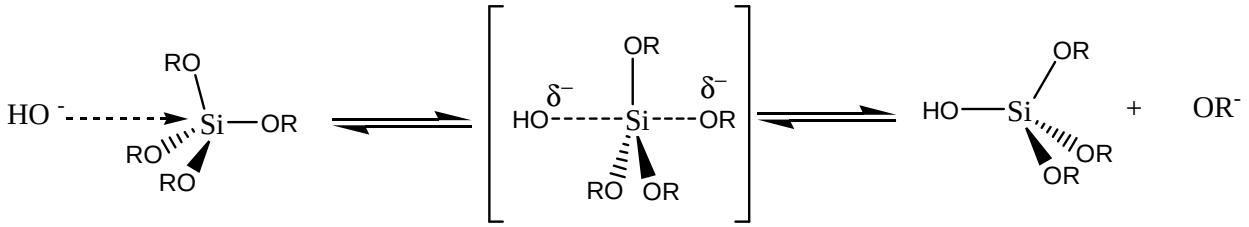

Scheme 1.2. Hydrolysis mechanisms of tetraalkylorthosilicate (R = alkyl).

The reaction is slowest at the isoelectronic point of silica (between 2.5 and 4.5 depending on different parameters) and the speed increases rapidly on changing the pH. Not only do the reaction conditions have a strong influence on the kinetics of the reaction but also on the

structure of the precursors. Generally, larger substituents decrease the reaction time due to steric hindrance. In addition, the substituents play a role in modifying the solubility of the precursor in the solvent. Water is required for the reaction and if organic substituents are quite large the precursor becomes immiscible in the solvent. By changing the solvent one has to take into account that it can interfere in the hydrolysis reaction. For example alcohols can undergo trans-esterification reactions leading to quite complicated equilibria in the mixture. Hence, for a well defined material the reaction conditions have to be fine-tuned.

The pH not only plays a major role in the mechanism but also affects the microstructure of the final material. Applying acid-catalysed reactions, an open network structure in the first steps of the reaction leads to condensation of small clusters. By contrast, the base-catalysed reaction leads to highly crosslinked sol particles in the first reaction steps. This can lead to variations in the homogeneity of the final materials. Commonly used catalysts are hydrochloric acid (HCl), sodium hydroxide (NaOH) or ammonium hydroxide (NH_4OH), but fluorides can be used as catalysts leading to fast reaction times.

Condensation

Condensation reactions can either be water condensation reactions



or alcohol condensation reactions:



The reverse reactions are hydrolysis and alcoholysis, respectively. As with initial hydrolysis, condensation reactions may be acid or base catalysed, and in either case the reaction proceeds via a rapid formation of a charged intermediate by reaction with a proton or hydroxide ion, followed by slow attack of a second neutral silicon species on this intermediate:

Acid catalysed

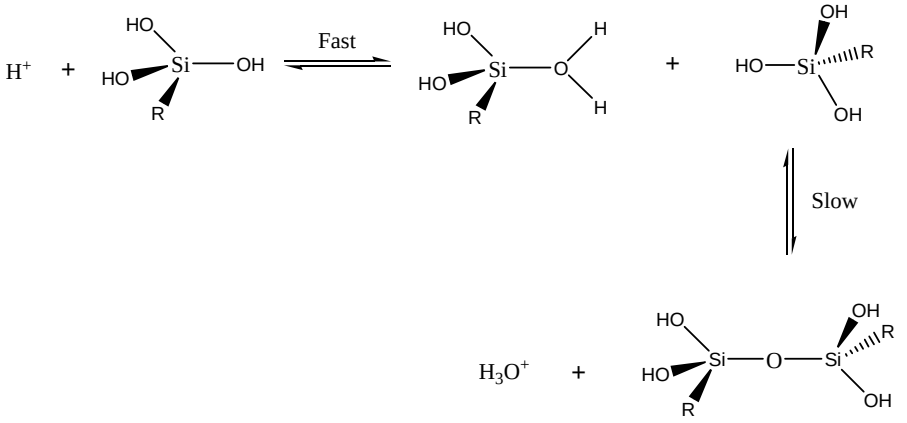

Base catalysed

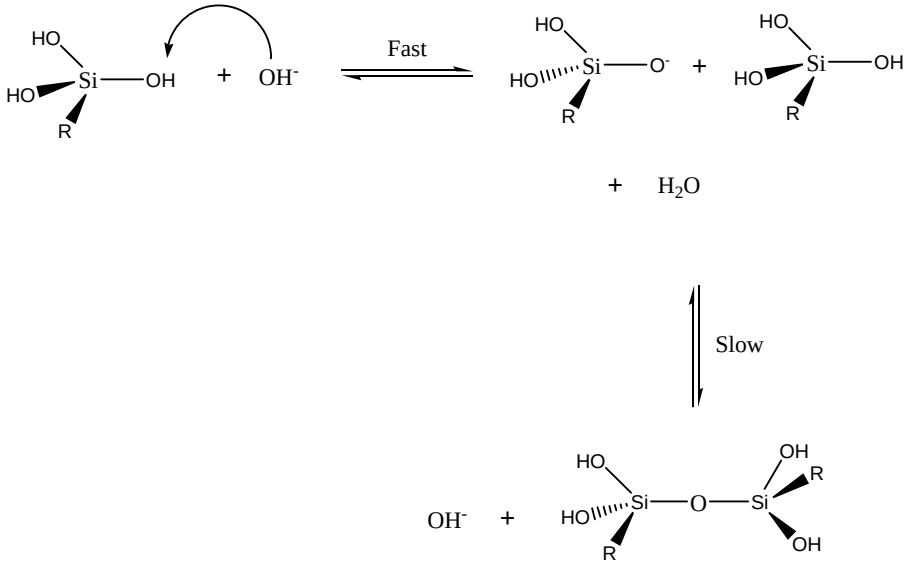

Scheme 1.3. Condensation mechanisms of tetraalkylorthosilicate (R = alkyl).

Gelation

During gelation, there is formation of a spanning cluster across the vessel, giving rise to a network which entraps the remaining solution. The gel has a high viscosity. Gelation does not affect the chemical composition of the mixture.

Ageing

During ageing, a series of processes including formation of further cross-links, associated shrinkage of the gel as covalent links replace nonbonded contacts, Ostwald ripening and structural evolution with changes in pore sizes and pore wall strengths occur.

Drying

After ageing of the gel, it is normally dried to remove the solvent thereby leaving a porous network. Depending on drying conditions, sol-gel derived products can be termed xerogels or aerogels. Drying by evaporation under normal conditions gives rise to capillary pressure that causes shrinkage of the gel network resulting in xerogels. Aerogels are gels that have been dried under supercritical conditions resulting in highly porous and extremely low density materials.

Densification

Further drying and heat treatment results in formation of dense ceramic or glass particles and thermal collapse of the open structure. A summary of the steps involved in the sol-gel process and the products formed is shown in Figure 1.1 [16].

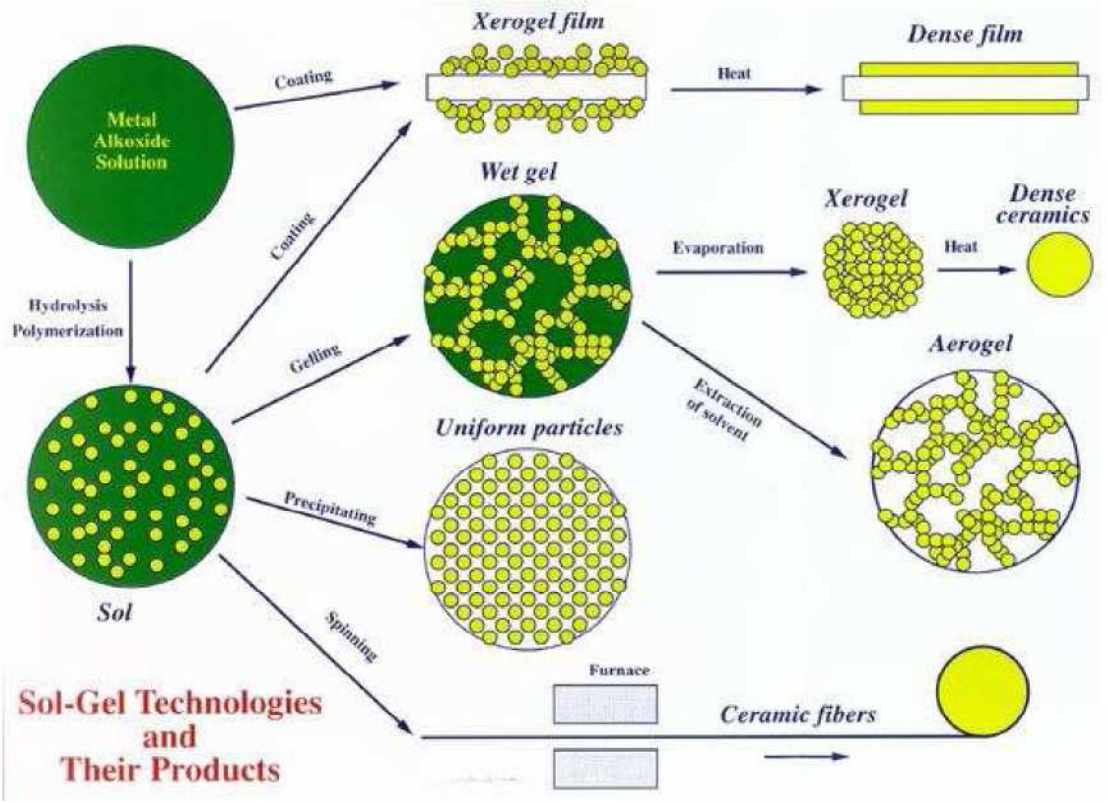

Figure 1.1 The sol-gel process and the various products formed.

The general properties of materials synthesized by the sol-gel method are high purity, better homogeneity, controlled porosity combined with the ability to form large surface area materials at low temperatures, possibility of preparing multi-component systems with broad ranges of compositions and good dispersion of minor components [17].

1.3.3 Formation of mesoporous materials by the surfactant-templated sol-gel method

For a standard synthesis of periodic mesoporous organosilica (PMO) materials, non-covalently bound templates are used, including molecules, supramolecular arrays, polymers [18 – 20] and colloids [21 – 23]. When dissolved in solution these species can template small inorganic precursors via electrostatic, van der Waals, and hydrogen bonding interactions to form nanostructured materials with tailorable pore shapes and sizes.

Surfactant templates consist of bi-functional molecules with a hydrophilic head group and a hydrophobic tail. As a result of their amphiphilic nature, surfactants can self assemble into supramolecular arrays. These molecules exist as monomers when the solution is dilute, but when their concentration exceeds a certain minimum (the so-called “critical micellar concentration”, cmc) the monomers organize spontaneously, forming aggregates of colloidal dimensions, the micelles.

The formation of micelles in aqueous media is generally seen as a compromise between the tendency for the hydrophobic groups to avoid the energetically unfavourable contacts with water and the desire for the polar parts to maintain contact with the aqueous environment. Depending on the size ratio between the hydrophobic chain and the head group of a surfactant different superstructures can be formed (Figure 1.2) [24].

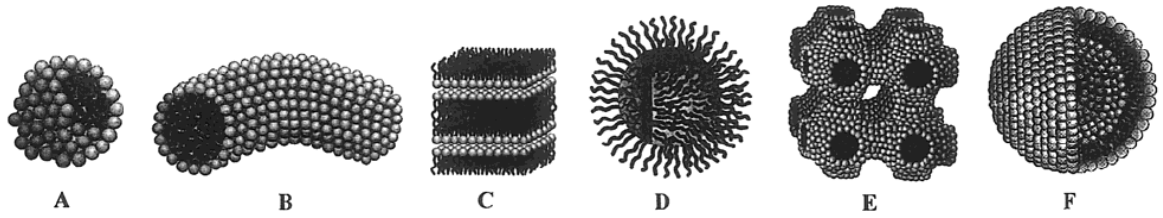

Figure 1.2 Supramolecular structures for surfactants. (A = sphere, B = cylinder, C = planar bilayer, D = reverse micelle, E = bicontinuous phase and F = liposomes).

Since these supramolecular structures are in thermodynamic equilibrium they are often called "phases" and a phase diagram can be constructed for each surfactant-solvent system. These phase diagrams allow prediction of the shape of the micelles that are dependent on the thermodynamic conditions, involved in the system under consideration. For example, cetyltrimethylammonium bromide (CTAB) in water will form spherical micelles above the critical micellar concentration in which the hydrophilic head group forms the outer surface and the hydrophobic tails point towards the centre (Figure 1.3) [25].

As the concentration of the surfactant increases, the spherical micelles can coalesce to form cylindrical micelles (cmc2). Further increase of the surfactant concentration leads to liquid-crystalline (LC) phases. The rod like micelles aggregate and form hexagonal close packed LC arrays. A further increase of the surfactant concentration can produce cubic bicontinuous LC phases and can even lead to LC lamellar phases. At very high concentrations, in some systems, inverse phases can exist, in which the water is inside the micelle, with the head group pointing inwards.

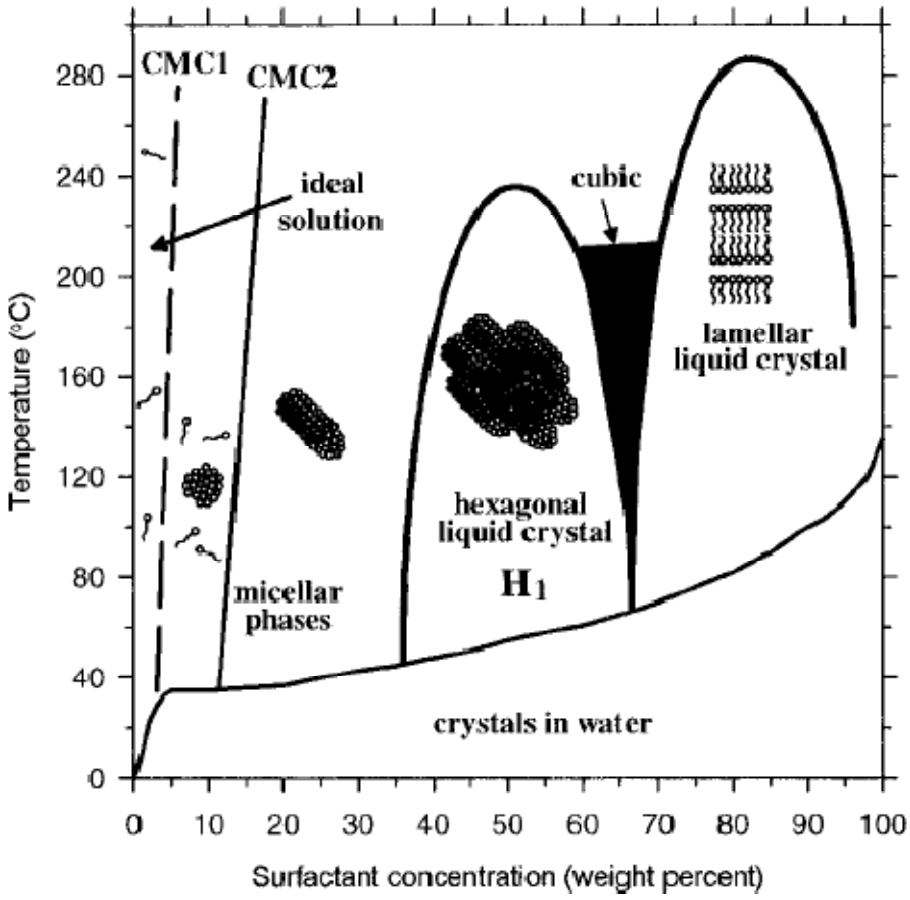

Figure 1.3. Schematic phase diagram for CTAB in water.

There are two different pathways for the preparation of mesoporous silica materials: the synthetic co-assembly mechanism introduced by Vartuli *et al* [26] and the nanocasting or true liquid crystal mechanism introduced by Attard and Goltner [27, 28]. While the co-assembly method works in a concentration range below the cmc of the surfactant and the assembly takes place due to the interaction of the surfactant with the precursor forming a molecule with a bigger head group, the true liquid crystal mechanism employs concentrations in which the surfactant forms LC phases. This process, which is also called nanocasting, therefore leads to a 1:1 replica of the surfactant phase in the final material as has been shown by X-ray diffraction [27 – 29]. Figure 1.2 shows supramolecular structures formed from using surfactants. An organic template

is dissolved in the precursor and an organic solvent, usually an alcohol. The concentrations are set in such a way that the template is one of its LC phases. The precursor assembles around the template due to van der Waals or Coulomb interactions. After condensation the template is removed to give the porous solid. The condensation is a two step reaction in which first the alkoxyl groups of the precursor are hydrolysed by the water in the reaction mixture and then the silanol group condenses with either an alkoxyl or a silanol group of another precursor (Schemes 1.1 - 1.3).

The hydrolysis and condensation reactions take place at different rates depending on the pH of the solution. At a pH between 2 and 5 the hydrolysis is faster leading to the formation of hydrolyzed monomeric units, which then slowly form small particles [30, 31]. At a pH higher than 5 the condensation is instead favoured, leading to the formation of larger condensed particles, which will slowly grow into a 3D network [31 – 33]. The nanocasting process is usually performed at a pH lower than 5 therefore leading to monolithic materials, whereas the co-assembly method is often used at a higher pH leading to powders. However, procedures have been developed for controlling the morphology of the materials in the form of films, fibres and spheres to name a few.

1.3.4 Advantages and disadvantages of sol-gel processing.

1.3.4.1 Advantages

a) The temperatures required for all reaction stages apart from densification are low and frequently close to room temperature. Thus thermal degradation of both the material and any entrapped species is minimised and high purity and stoichiometry can be achieved.

Also the low temperatures of sol-gel processes which are generally below the crystallization temperature for oxide materials allows for the production of unusual amorphous materials.

b) Precursors such as metal alkoxides and mixed alkyl/alkoxides are frequently volatile and easily purified to very high levels. This further contributes to high purity products.

c) Since organometallic precursors involving different metals are frequently miscible, homogeneous controlled doping is easy to achieve.

d) The chemical conditions are mild. Hydrolysis and condensation reactions are catalysed by acids and bases, but extreme pH conditions may easily be avoided, by rapid neutralisation or buffering of the synthesis mixture after hydrolysis.

e) Highly porous materials and nanocrystalline materials may be prepared by the sol-gel process.

f) By appropriate chemical modification of the precursors, control may be achieved over the rates of hydrolysis and condensation, and over colloid particle size and the pore size, porosity and pore wall chemistry of the material. Also by controlling the ageing and drying conditions, further pore size and mechanical strength control may be achieved.

g) By using organometallic precursors containing polymerisable organic ligands, materials may be produced which contain both inorganic and organic polymer networks.

h) Entrapped organic species may serve as templates for creation of pores with controlled size and shape. Subsequent removal of these species leaves “molecular footprints” with potential applications as catalytic sites.

1.3.4.2 Disadvantages

a) The precursors are often very expensive and sensitive to moisture, limiting large scale production plants to specialised applications such as optical coatings.
b) The process is also time-consuming, particularly where careful ageing and drying are required.
c) The problems of dimensional change on densification, and of shrinkage and stress cracking on drying, although not insurmountable, do require careful attention [34].

1.4 Organic-inorganic hybrid materials

Preparation of functionalised mesoporous silica with organic moieties has been a major topic of research because it offers further possibilities of tailoring the physical and chemical properties of the porous materials. One important way of modifying the physical and chemical properties of mesoporous silicates has been the incorporation of organic components, either on the silicate surface, as part of the silicate wall, or trapped within the channels [35, 36]. The organic functionalization of these solids permits the tuning of the surface properties (hydrophobicity, hyprophilicity and binding to guest molecules, alteration of surface reactivity, protection of the surface from attack) and modification of the bulk properties (e.g. mechanical or optical properties) of the material [37]. These materials are called hybrid mesoporous materials. Organic moieties containing hybrid mesoporous silica materials facilitate the chemistry in the channels and provides new opportunities for controlling the chemical, physical, mechanical and dielectric properties of the materials. Before calcination or solvent extraction, all silica based mesophases may be regarded as organic-inorganic composite materials.

Hybrid materials did not originate in a chemical laboratory but in nature. A hybrid material is a material that includes two moieties blended on the molecular scale. Commonly one of these compounds is inorganic and the other one organic in nature. Many natural materials consist of inorganic and organic building blocks distributed on the (macro) molecular or nanoscale level. In most cases the inorganic part provides mechanical strength and an overall structure to the natural objects while the organic part delivers bonding between the inorganic building blocks and/or the soft tissue. Typical examples of such materials are bone or nacre.

1.5 Periodic mesoporous organosilica materials (PMOs)

Periodic mesoporous organosilicas (PMOs) represent a new class of organic-inorganic hybrid materials suitable for a broad range of applications. PMOs emerged in 1999 [8 - 10] as a new family of inorganic-organic hybrid materials. In 1999, three different research groups were successful in applying the concept for the synthesis of ordered pure mesoporous silica phases through structure directing agents. The presence of uniform mesopores in the PMOs distinguishes them from the traditional inorganic-organic hybrid materials [47]. These materials are synthesized via hydrolysis and subsequent condensation reactions of bridged organosilsesquioxane precursors of the type $(OR`)_3Si\text{-}R\text{-}Si(OR`)_3$, with R` being hydrolysable methoxy or ethoxy groups and R being a non-hydrolysable organic bridge group in the presence of cationic, anionic and polymeric surfactants [48 – 50]. PMOs have several unique features built into their structure: high loading of organic content, insignificant pore blockage, chemically reactive sites, homogeneously distributed functional groups, and the physical and materials properties can be easily modified by tinkering with the composition of the bridge-bonded silsequioxane precursor. These PMOs exhibit a distinct advantage over other mesoporous silica materials because there exist a large number of organic functional groups homogeneously distributed throughout the pore wall of PMOs [51 – 53]. They therefore have better hydrothermal and mechanical stabilities [54], favourable surface, physical and chemical properties which are

promising for potential applications in catalysis, sensor, drug delivery, adsorption separation and nanocasting [55]. Research on organosilica materials is motivated by applications in materials science (reverse-phase chromatography columns, silicone oils, resins), and because the formation of nanoporous structures can enhance the material properties.

To date PMOs have been prepared using various bridged organic groups ranging from saturated groups like methane or ethane groups [8 – 10] to unsaturated or aromatic groups [56, 57] to very large organometallic complexes [58]. Most commonly cetyltrimethylammonium bromide/chloride (CTAB/CTAC), octadecyltrimethylammonium bromide/chloride (OTAB/OTAC) or cetylpyridinium bromide (CPB/CPC) are used as ionic structure-directing agents. These molecules undergo a self-assembly process under specific conditions (temperature, concentration, solvent etc) into a lyotropic liquid crystal phase in the presence of a silica precursor. The organosilica precursor molecules can be hydrolyzed and condensed to form an ordered organobridged composite material. After removal of the surfactant the hybrid material reveals accessible pores with uniform sizes (in the range of 2 – 5 nm) and shapes.

PMOs with larger pores (6 – 20 nm) can be obtained using non-ionic triblock copolymers such as Pluronic P123 ($EO_{20}PO_{70}EO_{20}$), Pluronic F127 ($EO_{106}PO_{70}EO_{106}$) or B50-6600 ($EO_{39}BO_{47}EO_{39}$) as structure directing agents (SDAs). These have been known for quite some time and have been used for the preparation of large pore silica mesophases such as SBA-15, SBA-16 or FDU-1. The degree of order of these materials structured by triblock copolymers could be improved by the addition of inorganic salts such as NaCl to the reaction mixture. The salts have a specific effect on the interaction between the positively charged head group of the surfactant and the inorganic species. In this way, Guo *et al* [59] were able to obtain a highly ordered large pore (6.4 nm), ethane bridged PMO with 2D hexagonal symmetry (*p6mm*).

A number of conditions can be varied: temperature, concentrations, alkoxyl leaving groups, templates, catalyst, ageing conditions, template removal method and solvent (Fig. 1.4) [60]. Control of pore size and shape, pore connectivity, surface functionality, hydrophobicity, particle morphology, channel orientation, framework composition, wall thickness, and crystallinity is possible by adjusting these variables.

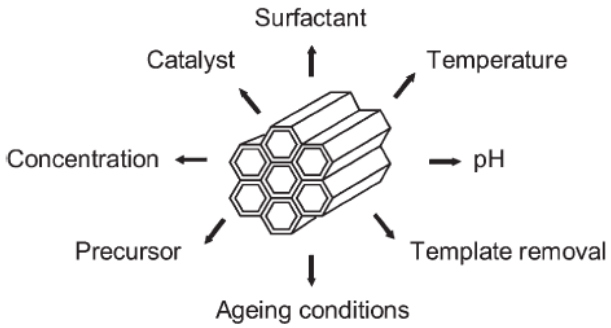

Figure 1.4. Reaction condition variables used to control the synthesis of PMOs.

1.6 Nanotubes and related nanostructures

Since their discovery in 1991 [61], carbon nanotubes and related nanostructures have attracted much attention because of their remarkable electrical, mechanical, and thermal properties. There are various types of shaped carbon nanostructures and these include spheres, balls, onions, beads, nanotubes and bamboo nanotubes. These various shaped nanostructures have been produced under a variety of reaction conditions. All of these shaped nanostructures are of interest in their own right but the high yield synthesis of “pure” materials is still to be achieved. The outcome of making mixtures is that subsequent purification processes are needed to remove impurities but these procedures can also modify or destroy the material of interest.

Shaped nanostructures can be made by a variety of procedures. Generally the most frequently applied techniques differ either in the carbon source or the method used to generate the high temperatures at which the carbon precursor is converted to the desired nanostructure and these include numerous variations of the arc discharge, the laser ablation and the chemical vapour deposition (CVD) processes. Another type of nanostructure synthesis method has been developed in recent years that does not use a gas flow system. Rather the reaction to make the shaped nanostructured materials takes place in a closed container (e.g. autoclave or sealed quartz tube), at elevated pressures. Typically, in this method mesoporous materials containing an external carbon source are used as starting materials to synthesize the shaped nanostructured materials.

1.7 Carbon on silica nanocomposites

Silica-based composites such as metal/silica, metal oxide/silica, and polymer/silica and silica/ carbon materials are attractive because of their optical, magnetic, thermal, mechanical, and electric properties. Silica/carbon nanocomposites may be synthesized by carbonization or pyrolysis of various carbon precursors [59 – 65]. In addition to their interesting properties, nanostructured silica/carbon composites are potentially useful as starting points for the simple and direct preparation of nanoporous silica and carbon materials. This is particularly attractive for mesoporous carbons given that the conventional hard templating process for their formation involves several steps [66].

Recently there have been efforts to prepare mesoporous carbon via more direct routes by carbonization of silica organic-inorganic hybrid composites [67] or organosilica/surfactant mesophases [64] followed by removal of silica. Mesoporous carbons have also been fabricated via direct carbonization of organic-organic nanocomposites comprising of a thermosetting

polymer and thermally decomposable surfactant [68]. The synthesis and application of mesostructured materials has attracted substantial interest because of their high surface areas and ordered large pores.

1.8 References

[1] J. P. G. Pater, P. A. Jacobs, J. A. Martens, *Journal of Catalysis*, **184**, 262 (1999).

[2] M. S. Morey, A. Davidson, G. D. Stucky, *Journal of Porous Materials*, **5**, 195 (1998).

[3] E. Armengol, A. Corma, H. Garcia, J. Primo, *Applied Catalysis A – General*, **126**, 391 (1995).

[4] S. V. Mattigod, X. D. Feng, G. E. Fryxell, J. Liu, M. L. Gong, *Seperation Science and Technology*, **34**, 2329 (1999).

[5] D. Y. Zhao, P. D. Yang, Q. S. Huo, B. F. Chmelka, G. D. Stucky, *Current Opinion in Solid State and Materials Science*, **3**, 111 (1998).

[6] L. Mercier, T. J. Pinnavaia, *Advanced Materials*, **9**, 500 (1997).

[7] J. Y. Ying, C. P. Mehnert, M. S. Wong, *Angewandte Chemie International Edition*, **38**, 56 (1999).

[8] B. J. Melde, B. T. Holland, C. F. Blandgord, A. Stein, *Chemistry of Materials*, **11**, 3302 (1999).

[9] S. Inangaki, S. Guan, Y. Fukushima, T. Ohsuna, O. Terasaki, *Journal of the American Chemical Society*, **121**, 867 (1999).

[10] T. Asefa, M. J. MacLachlan, N. Coombs, G. A. Ozin, *Nature*, **402**, 867 (1999).

[11] V. G. Gavalas, R. Andrews, D. Bhattacharyya, L.G. Bachas, *Nanotechnology Letters*, **1**, 719 (2001).

[12] Y. Mastai, S. Polarz, M. Antoniette, *Advanced Functional Materials*, 12, **197** (2002).

[13] J. Aguado-Serrano, M. J. Rojas-Cervantes, A. J. Lopez-Peinado, V. Gomez-Serrano, *Microporous and Mesoporous Materials*, **74**, 111 (2004).

[14] P. R. Giunta, L. J. Van de Burgt, A. E. Stiegman, *Chemistry of Materials*, **17**, 1234 (2005).

[15] J. Pang, V. T. John, D. A. Loy, Z. Zhang, Y. Lu, *Advanced Materials*, **17**, 704 (2005).

[16] T. J. Pinnavaia, S. Kim, D. Lee, J. Shah, *Chemical Communications*, 1436 (2003).

[17] M. Urban, D. Mehn, Z. Konya, I. Kiricsi, *Chemical Physics Letters*, **359**, 95 (2002).

[18] R. Mokaya, Z. Yang, Y. Xia, *Journal of Materials Chemistry*, **16**, 3417 (2006).

[19] J. J. Ebelmen, *Ann*, **57,** 331 (1846).

[20] M. Kakihama, *Journal of Sol-Gel Science Technology*, **6**, 7 (1996).

[21] S. Komarneni, *Journal of Sol-Gel Science Technology*, **6**, 127 (1996).

[22] J. D. Mackenzie, *Ceramic Transformations*, **55**, 25 (1995).

[23] H. Schmidt, *Materials Research Society Symposium Proceedings*, **32**, 327 (1984).

[24] C. J. Brinker, G.W. Scherer, *Sol-Gel Science: The Physics and Chemistry of Sol-Gel Processing*, Academic Press, California (1990).

[25] L. V. Interrante, M.J. Hampden – Smith, *Chemistry of Advanced Materials, An Overview*, Wiley-Vch (1998).

[26] S. J. Teichner, G. A. Nicolaon, M. A. Vicarini, G. E. E. Gardes, *Advances in Colloidal Sc*ience, **5**, 245, (1976).

[27] B. Smarsly, S. Polarz, M. Antoniette, *Journal of Physical Chemistry B*, **105**, 10473 (2001).

[28] A. Thomas, H. Schlaad, B. Smarsly, M. Antonietti, *Langmuir*, **19**, 4455 (2003).

[29] D. Zhao, J. Feng, Q. Huo, N. Melosh, G. H. Frederickson, B. F. Chmelka, G. D. Stucky, *Science*, **279**, 548 (1998).

[30] A. Stein, *Microporous and Mesoporous Materials*, **44**, 227 (2001).

[31] Y. Zhou, S. H. Yu, A. Thomas, B. H. Han, *Chemical Communications*, 262 (2003).

[32] S. M. Yang, N. Coombs, G. A. Ozin, *Advanced Materials*, **12**, 1940 (2000).

[33] G. D. J. Soler – illia, C. Sanchez, B. Lebeau, J. Patarin, *Chemical Reviews*, **102**, 4093 (2002).

[34] N. K. Raman, M. T. Anderson, C. J. Brinker, *Chemistry of Materials*, **8**, 1684 (1996).

[35] J. C. Vartuli, K. D. Schmitt, C. T. Kresge, W. J. Roth, M. E. Leonowicz, S. B. McCullen, S. D. Hellring, J. S. Beck, J. L. Schlenker, D. H. Olson, E. W. Sheppard, *Chemistry of Materials*, **6**, 2317 (1994).

[36] G. S. Attard, C. G. Goltner, J. M. Corker, S. Henke, R. H. Templer, *Angewandte Chemie International Edition*, **36**, 1315 (1997).

[37] G. S. Attard, J. C. Glyde, C. G. Goltner, *Nature*, **378**, 366 (1995).

[38] C. G. Goltner, S. Henke, M. C. Weissenberger, M. Antoniette, *Angewandte Chemie International Edition*, **37**, 613 (1998).

[39] N. Husing, U. Schubert, *Angewandte Chemie International Edition*, **37**, 23 (1998).

[40] D. W. Schaefer, *Science*, **243**, 1023 (1989).

[41] D. W. Schaefer, K. D. Keefer, *Physical Review Letters*, **53**, 1383 (1984).

[42] K. D. Keefer, D. W. Schaefer, *Physical Review Letters*, **56**, 2376 (1986).

[43] J. D. Wright, Nico. A. J. M. Sommerdijk, *Sol-Gel Materials: Chemistry and Applications*, Gordon and Breach Science Publishers, Amsterdam (2001).

[44] K. Moller, T. Bein, *Chemistry of Materials*, **10**, 2950 (1998).

[45] G. A. Ozin, E. Chomski, D. Khushalani, M. J. MacLachlan, *Current Opinions in Colloid and Interface Science*, **3**, 181 (1998).

[46] A. Stein, B. J. Melde, R. C. Schroden, *Advanced Materials*, **12**, 1403 (2000).

[47] D. A. Loy, K. J. Shea, *Chemical Reviews*, **95**, 1431 (1995).

[48] M. P. Kapoor, S. Inangaki, *Chemistry of Materials*, **14**, 3509 (2002).

[49] S. Hamoudi, Y. Yang, I. L. Moudrakovski, S. Lang, A. Sayari, *Journal of Physical Chemistry B*, **105**, 9118 (2001).

[50] S. Hamuudi, S. Kaliaguine, *Chemical Communications*, 2118 (2002).

[51] Y. Goto, S. Inangaki, *Chemical Communications*, 2410 (2002).

[52] C. Yoshina-Ishii, T. Asefa, N. Coombs, M.J. MacLachlan, G. A. Ozin, *Chemical Communications*, 2539 (1999).

[53] S. Inangaki, S. Guan, Y. Fukushima, T. Ohsuna, O. Terasaki, *Journal of the American Chemical Society*, **121**, 9611 (1999).

[54] X. Feng, G. E. Fryxell, L. Q. Wang, A. Y. Kim, J. Liu, K. M. Kemner, *Science*, **276** 923 (1997).

[55] M. H. Lim, C. F. Blanford, A. Stein, *Chemistry of Materials*, **10**, 467 (1998).

[56] M. H. Lim, C. F. Blanford, A. Stein, *Chemistry of Materials*, **11**, 3285 (1999).

[57] Y. Lu, H. Fan, N. Doke, D. Y. Loy, R. A. Assink, D.A. LaVan, C. J. Brinker, *Journal of the American Chemical Society*, **122**, 5258 (2000).

[58] J. F. Diaz, K .J. Balkus, *Journal of Molecular Catalysis B: Enzymes*, **2**, 115 (1996).

[59] W. Guo, J. Park, M. Oh, H. Jeong, W. Cho, I. Kim, C. Ha, *Chemistry of Materials*, **15**, 2296 (2003).

[60] W. J. Hunks, G. A. Ozin, *Journal of Materials Chemistry*, **15**, 3716 (2005).

[61] S. Iijima, *Nature*, **354**, 56 (1991).

[62] J. Aguado-Serrano, M. L. Rojas-Cervantes, A. J. Lopez-Peinado, V. Gomez-Serrano, *Microporous and Mesoporous Materials*, **74**, 111 (2004).

[63] P. R. Giunta, L. J. van de Burgt, A. E. Stiegman, *Chemistry of Materials*, **17**, 1234 (2005).

[64] J. Pang, V. T. John, D. A. Loy, Z. Yang, Y. Lu, *Advanced Materials*, **17**, 704 (2005).

[65] Z. Yang, Y. Xia, R. Mokaya, *Journal of Materials Chemistry*, **16**, 3417 (2006).

[66] S. Jun, S. H. Joo, R. Ryoo, M. Kruk, M. Jaroniec, Z. Liu, T. Ohsuna, O. Terasaki, *Journal of American Chemical Society*, **122**, 10712 (2000).

[67] B. H. Han, W. Zhou, A. Sayari, *Journal of the American Chemical Society*, **125**, 3444 (2003).

[68] S. Tanaka, N. Nishiyama, Y. Egashira, K. Ueyama, *Chemical Communications*, 2125 (2005).

CHAPTER TWO

LITERATURE REVIEW

2.1 Periodic mesoporous organosilica materials: A review

In the last decade, a lot of interest has been put into the synthesis of well defined porous materials, because of their potential applications in catalysis [1 - 3], separation science [4, 5], and environmental remediation [6, 7]. Porous materials can be classified by size, network forming material and degree of order. A material will be called microporous if the pores are smaller than 2 nm, macroporous if they are over 50 nm and mesoporous for all the sizes in between. In this work mesoporous material with a silica framework and periodic mesoporous organosilica materials will be considered in more detail. One of the methods to synthesize these materials is to use a surfactant-templated sol-gel system, which was reported for the first time by Kresge and co-workers in 1992 [8], who discovered surfactant-assembled silica mesostructures. Unfortunately pure silica materials are not that interesting chemically, and different synthetic methods have been examined to create materials with chemical functionality.

One way to create functionality is to anchor a functional group on the surface of the pores in a post synthesis procedure. After removal of the surfactant the silica surface usually contains hydroxyl groups, which can function as chemical tethering sites for a wide range of organic molecules with interesting functionality. The disadvantages of this approach are that the organic groups are dangling into the pore void and therefore block off space and sometimes even clog the entire pore. Also not every silanol is necessarily modified and this creates a non uniform distribution of grafted organics. Nevertheless, amine functions [9, 10], ephedrine [11, 12], and organometallic complexes [13] have been introduced into mesoporous silica materials by this method.

Another way to create functionality is to change the framework of the silicas by introducing organic groups in the precursor. This can be done by using molecules with the formula R-Si-$(OR)_3$ in the condensation process [14]. This has been successfully achieved for R = alkyl, aryl, thiol, amine side chains as well as metal complexes and chiral complexes [14 - 16]. However, only about 25% of a modified precursor can be used in this synthesis approach without causing collapse of the framework. Another potential disadvantage of this method is the uneven distribution of organic groups on the surface of a pore. These problems may be exacerbated by microphase separation, which leads to some parts of the material containing more of the functional group than the others [17].

As mentioned earlier in the previous chapter, in 1999 three different research groups independently introduced organically bridged precursors for the synthesis of mesoporous hybrid organic-inorganic silica compounds [18 - 20]. This method enabled materials to be made exclusively from organic modified precursors, leading to a uniform distribution of organic functionality in the solid. These materials have been labelled “periodic mesoporous organosilica” (PMO) materials. Some of the organic groups contained in PMOs are alkyl bridges (ethane and methane), double bonds (ethylene, phenylene, benzene and derivatives thereof), and heteroatoms functionalities (ferrocene, thiophene, 4-phenyl ether and 4-phenyl sulphide) and amines [18 - 23]. The incorporation of organic groups inside the channel walls of silica-based materials leads to the possibility to fine tune the chemical, physical and mechanical properties of the material through synthetic chemistry. Compared to the other methods described above, the “functional” groups do not take space in the pores and pure organic precursor molecules can be condensed without compromising the mechanical stability of the material or the short and long range order.

2.1.1 Synthesis of PMOs by using structure directing agents with ionic surfactants

2.1.1.1 Aliphatic PMOs

The most frequently used ionic structure directing agents are the bromide and chloride salts of long – chain alkyltrimethylammonium compounds and the corresponding salts of long – chain alkylpyridinium derivatives (hexadecyltrimethylammonium bromide/chloride (CTAB/CTAC), octadecyltrimethylammonium bromide/chloride (OTAB/OTAC), hexadecylpyridinium bromide/chloride (CPB/CPC). Under certain conditions (temperature, concentration, solvent, pH, etc) and in the presence of organosilica precursors, these surfactants self-assemble to form a lyotropic liquid crystalline phase. The hydrolysis and condensation reactions of the precursors in this phase produce the ordered periodic hybrid material, which after removal of the surfactant exhibits accessible pores of uniform size and shape.

Inagaki *et al* [19] were able to prepare a new organic-inorganic hybrid material by conversion of 1,2-bis(trimethylsilyl)ethane (BTME) under basic conditions in the presence of OTAC as structure-directing agent (SDA). The symmetry of the pore arrangement depended on the ratios of the components in the reaction mixture. Materials with a 2-dimensional hexagonal (2D hex) pore arrangement as well as those with 3D hexagonal (3D hex) periodicity were obtained. Nitrogen physisorption measurements revealed specific inner surface areas of 750 (2D hex) and 1170 m^2g^{-1} (3D hex). Silicon Magnetic Angle Spinning Nuclear Magnetic Resonance (Si MAS NMR) measurements showed that the Si-C bond was not cleaved during synthesis [24]. Both materials decomposed at temperatures above 400 ^oC. Nitrogen adsorption measurements showed a uniform pore size distribution with pore diameters of 3.1 and 2.7 nm for the 2D hex and 3D hex mesoporous materials respectively. Well defined external morphologies of the materials

were observed in the scanning electron microscopy (SEM) images. In the 2D hex sample, rodlike particles predominated and in the 3D hex sample spherical particles were observed.

Ozin and co-workers reported the synthesis of a PMO that contained an unsaturated organic spacer [18]. They used 1,2-bis(triethoxysilyl)ethene as a precursor, which was transformed under basic conditions in the presence of CTAB as a SDA to obtain an ethane-bridged PMO material with a 2D hexagonally ordered pore system (specific surface area S_{BET} = 640 m^2/g^{-1}, pore diameter = 3.9 nm). Bromination reactions were carried out to test the accessibility to the C = C bonds incorporated into the silica framework. Elemental analysis showed a degree of bromination of 10 % relative to the C = C bond content.

Around the same time, Stein and co-workers [20] published the synthesis of an ethene-bridged PMO material that was obtained under similar conditions and with the same precursor and surfactant. The material exhibited a very high surface area of approximately 1200 m^2g^{-1} but a comparably low-range order. Transmission electron microscopic (TEM) investigations suggested the presence of wormlike rather than strictly parallel 2D hexagonally arranged pores with diameters of 2.2 – 2.4 nm.

An ethane-bridged PMO material with cubic symmetry (*Pm3n*), the analogous mesoporous pure silica phase with identical symmetry to SBA-1, was synthesized for the first time by Guan *et al* [25] and Sayari *et al* [26]. They both used BTME as organosilica source in the presence of CTAC as SDA in basic media. The crystal like external morphology of the particle, determined by SEM was described as 18 faced, consisting of 6 squares and 12 hexagonals. In a further study, Sayari and co-workers [27] investigated the influence of the chain length of the surfactant on the synthesis of ethane-bridged PMOs whereby the length of the hydrocarbon chain varied between 10 and 18 carbon atoms. They also compared two different synthetic pathways: in one, the last

step comprised merely aging at room temperature, whereas the second included hydrothermal treatment at 95 ^{o}C in an autoclave. They found that the pore diameter increased with increasing length of the surfactant used. In contrast, the specific surface areas followed no clear trend. With, but one exception, the PMO materials were always obtained with a 2D hexagonal pore system. The exception was the sample that was synthesized with CTAC as SDA and treated hydrothermally. This sample exhibited a cubic structure.

2.1.1.2 Aromatic PMOs

Hydrocarbon chains of the organosilica precursors can be at most two carbon atoms long to produce periodic ordered mesoporous materials [28]. The organic group must not be too flexible if pure PMO materials and not disordered hybrid materials are desired. This requirement is fulfilled by (hetero) aromatic compounds. Thus, numerous attempts have been made to introduce aromatic bridges into PMOs.

The first synthesis of PMO materials with aromatic bridges was reported by Yoshina-Ishii *et al* [29] as early as 1999. They used 1,4-bis(triethoxysilyl)benzene (BTEB) and 2,5-bis(triethoxysilyl)thiophene (BTET) as precursors in the presence of CTAB as SDA. Interesting synthesis in the presence of ammonia led to cleavage of the Si - C bonds, thus almost all the organic bridges were cleaved in the reaction products obtained. By using mild acidic conditions, which were realized by the use of hexadecylpyridinium chloride as SDA, well ordered products (pore diameter = 2.0 nm) with a high degree of structural integrity of the organic bridges were formed. Even under these conditions Si - C bond cleavage could not be avoided entirely.

Temstin *et al* [30] prepared the aromatic precursors 1,4-bis(triethoxysilyl)-2-methylbenzene, 1,4-bis(triethoxysilyl)-2,5-dimethylbenzene and 1,4-bis(triethoxysilyl)-2,5-dimethoxybenzene by a Grignard reaction using the respective brominated compounds with chlorotriethoxysilane and were able to use these precursors to obtain PMO materials. They used CPC as SDA under acidic conditions, neutralized the reaction mixture, and then treated the reactants with ammonium fluoride, which acted as a catalyst. 2D hexagonal products were obtained with pore diameters of 2.3 nm and specific surface areas between 560 and 1100 m^2g^{-1}. Thermogravimetric analysis showed that the aryl bridges are cleaved from the silica framework at temperatures above 360 ^oC.

Several research groups have also produced PMO materials that have periodic, ordered mesopores and also show crystal-like organization of the organic bridges within the pore walls. The first report of PMOs with crystal-like pore walls was reported by Inagaki *et al* [31], who like Yoshina-Ishii *et al* [29], used BTEB as a precursor in the presence of OTAC as SDA under basic conditions. The powder X-ray diffraction (XRD) pattern of the benzene-bridged PMO showed reflections that were assigned to the highly ordered 2D hexagonal mesophase (p6mm). The four reflections (10, 20, 30, 40) in the wide - angle range ($2\theta > 10^o$) showed the existence of a periodicity of 0.76 nm. This crystal like organization of the organic bridges within the pore walls was confirmed by high resolution transmission electron microscopy (HRTEM) images, which showed numerous lattice fringes along the pore axis and also indicated a separation distance of 7.6 Å. The product (pore diameter = 3.8 nm, S_{BET} = 818 m^2g^{-1}) was thermally stable up to 500 ^oC. Bion *et al* [32] also synthesized 1,4-benzene-bridged PMO materials with crystal-like pore walls. The pore diameter could be varied between 2.3 and 2.9 nm by variation of the length of the hydrocarbon chain (C14 to C18) of the trimethylammonium halide surfactant used.

Another aromatic PMO system that shows both periodic ordered mesoporosity and a periodicity at a molecular level was prepared by Inagaki and co-workers [33], who used 4,4'-bis(triethoxysilyl)biphenyl (BTEBP) as the organosilica source in the presence of OTAC under

basic conditions. The material obtained (pore diameter = 3.5 nm, S_{BET} = 869 m^2g^{-1}), showed one reflection in the low-angle region of the powder XRD pattern and five additional reflections in the wide-angle region that can be attributed to a crystal – like arrangement of the biphenyl units within the pore walls. The periodicity of the organic bridges (1.16 nm) derived from the diffraction pattern was confirmed by a corresponding separation of the lattice fringes in the HRTEM images.

The effect of the precursor on the ordering of cetyltrimethylammonium bromide templated and acid catalysed benzene silica materials was demonstrated by Goletto et al [34]. A 2D hexagonal phase was formed from 1,3-bis(triethoxysilyl)benzene, whereas 1,4-bis(triethoxysilyl) benzene led to a cubic phase.

2.1.1.3 Periodic mesoporous aminosilicas (PMAs)

There have been a few attempts to introduce nitrogen-containing groups into PMOs. These include the synthesis of a pyridine-bridged PMO and the synthesis of ordered materials with a fraction of nitrogen containing bis-(trialkoxysilyl)organic groups supposedly incorporated in the silica framework [35]. In the latter cases, the bridging organic groups include flexible chain fragments that likely lead to mechanically unstable organosilicate frameworks. Moreover these bridging groups are probably too large to be intimately mixed with the silica frameworks.

Wahab *et al* [36] reported a further attempt to prepare bridged amine-functionalized ethane-silica materials by co-condensation of 1,2-bis(triethoxysilyl)ethane (BTEE) and bis[(3-trimethoxysilyl)propyl]-amine (BTMSPA) in the presence of CTAB. Unfortunately, they obtained poorly ordered materials with a content of BTMSPA in the reaction mixture of up to 18 mol %. A further increase in amine content worsened the mesostructure further. An interesting

transition of the mesostructure of this system with increasing BTMSPA content in the starting mixture was observed by Froba *et al* [37] in the co-condensation of BTME and BTMSPA in the presence of OTAC. When the ratio of BTME/BTMSPA was changed from 90: 10 to 55: 45, a change from a 2D hexagonal (*p6mm*) to a cubic mesophase took place. Higher BTMSPA concentrations in the reaction mixture led to collapse of the structure.

Asefa *et al* [38] prepared periodic mesoporous aminosilica materials that contained amine functional groups in the framework of the mesoporous network via thermal ammonolysis of PMOs under a flow of nitrogen gas. The quantity of amine groups introduced into the materials was found to depend strongly on the ammonolysis temperature. The largest loading of amine groups was obtained when a well ordered cubic methylene PMO material without prior vacuum drying was thermolyzed in ammonia.

2.1.2 Synthesis of PMOs through structure direction by non-ionic surfactants

After the initial reports on the synthesis of PMOs, considerable effort was made to enlarge the pore diameters of these materials with a view to potential applications in such areas as catalysis, sorption, and host guest chemistry. The pore diameters of the PMOs prepared by structure directing agents with alkyl ammonium surfactants (with chain lengths from C12 to C20) were restricted to the range between 2 and 5 nm. This limitation was finally surmounted by using different non-ionic triblock copolymers such as P123, F127 or B50 – 6600 as SDAs under acidic conditions. These triblock copolymers had been used previously in the synthesis of large-pore mesoporous pure silica phases such as SBA-15, SBA-16 and FDU-1. The synthesis proposed to take place by the $S^{+}X^{-}I^{+}$ pathway when non-ionic surfactants in acidic media are used.

The first synthesis of large pore PMOs by structuring with triblock copolymers was reported by Muth *et al* [39] in 2001. BTME was used as an organosilica precursor in the presence of P123 as supramolecular template under acidic conditions to synthesize the corresponding ethane-bridged silica, which exhibited a 2D hexagonal pore structure analogous to SBA-15 (pore diameter = 6.5 nm, S_{BET} = 913 m^2g^{-1}). Burleigh et al [40] used BTME and P123, and the reaction mixtures were treated with various amounts of swelling agent 1,3,5-trimethylbenzene (TMB). The pore diameters increased from 6 to 20 nm with increasing concentrations of TMB, while the pore structure changed from wormlike motifs to a hexagonal arrangement of spherical pores.

The degree of order in these materials structured by triblock copolymers could be improved by the addition of inorganic salts such as NaCl to the reaction mixture. The salts have a specific effect on the interaction between the positively charged head group of the surfactant and the inorganic species. Guo *et al* [41] were able to obtain a highly ordered large pore (pore diameter = 6.4 nm), ethane-bridged PMO with 2D hexagonal symmetry (*p6mm*). More recently Guo et al [42] have reported that the addition of a large amount of K_2SO_4 to a synthesis mixture containing BTME and pluronic F127 ($EO_{106}PO_{70}EO_{106}$) under acidic conditions affords a high quality cubic (*Im3m*) ethane-silica mesophase with large cavities, 9.8 nm in diameter.

Bao *et al* [43 - 45] investigated the influence of the ratio of an organosilica precursor and P123 in the reaction mixture in the synthesis of ethane-bridged PMOs, as well as the effect of acid concentration on the degree of structural order and the external morphology of the products. By optimization of the synthetic conditions, they were able to obtain highly ordered materials without needing to add inorganic salts. In contrast to the corresponding pure silica phases, the pore properties and the external morphologies of the ethane-bridged PMOs were considerably dependent on the acid concentration in the polymer solution.

Zhu *et al* [46] reported the synthesis of a large pore ethane-bridged silica phase by the true liquid-crystal templating approach (TLCT). As SDA they used a lyotropic liquid-crystalline phase formed from the binary P123/water mixture to which the precursor was added. Using this approach they obtained well organized monolith 2D hexagonal PMO materials (pore diameter = 7.7 nm, S_{BET} = 957 m^2g^{-1}).

Most of the large-pore PMOs that have been reported are ethane-bridged materials, which may be due to the commercial availability of the respective precursors BTME and BTEE. Unfortunately the ethane bridge offers few possibilities for further chemical modification. Only a few syntheses of large pore PMO materials have been reported so far.

The first benzene-bridged PMO with large pores was synthesized by Goto and Inagaki [47]. They obtained a well-ordered material with 2D hexagonal symmetry (pore diameter = 7.4 nm, S_{BET} = 1029 m^2g^{-1}). However, unlike the corresponding benzene – bridged silicas synthesized under basic conditions in the presence of alkylammonium surfactants, this material showed no reflections in the wide – angle region of the powder XRD pattern, and thus exhibited no crystal-like pore walls. Thermogravimetric analysis showed that the material was stable up to 550 ^oC and thus exceeded the thermal stability of the benzene-bridged silicas prepared with the help of alkylammonium surfactants by 50 ^oC.

An overview of PMO materials that have been synthesized in the presence of ionic and non-ionic surfactants as structure directing agents is given in Table 2.1. The data includes information on the precursors, surfactants and pH used in the preparation of PMO materials and the types of mesophases formed. The data in the table only tabulates studies involving precursors used in this work.

Table 2.1 Overview of mesoporous silica and PMO synthesis in the presence of ionic and non-ionic surfactants as structure directing agents.

Precursor	Surfactant	pH	Mesophase	Reference
Tetraethylorthosilicate	CTAB	basic	2D hex (MCM-41)	[58, 59]
	CTAB	basic	3D cubic (MCM-48)	[58, 59]
	Pluronic F127	acidic	cubic case structure (SBA-16)	[60]
	Brij 56	acidic	cubic (SBA-11)	[60]
	Brij 76	acidic	3D hex (SBA-12)	[60]
	P123	acidic	2D hex (SBA-15)	[60]
1,2-Bis(trimethoxysilyl)ethane	CPB	acidic	wormlike	[48]
	CTAB	acidic – basic	2D hex / wormlike	[20]
	P123	acidic	2D hex / wormlike	[38 – 45]
	F127	acidic	cubic	[41, 49]

Precursor	Surfactant	pH	Mesophase	Reference
	LGE53	acidic	2D hex	[50]
1,2-Bis(trimethoxysilyl)ethane	B50-6600	acidic	FDU – 1 like	[51]
	Brij 76	acidic	2D hex	[26, 52 – 54]
		Neutral $NiCl_2$ / NH_4F	2D hex	[55]
	Brij 56	acidic	2D hex	[52, 56]
	Brij 30 / OTAC	basic	2D hex	[57]
1, 4-Bis (triethoxysilyl)benzene	CPC	acid	2D hex	[18]
	OTAC	basic	2D hex cryst	[31]

Precursor	Surfactant	pH	Mesophase	Reference
	C_{14} – C_{18} TAB / / TAC	basic	2D hex cryst	[32]
	P123	acidic	2D hex	[46]
	Brij 76	acidic	2D hex	[53]
	Brij 56	acidic	2D hex	[58]
4, 4’-bis(triethoxysilyl)-1, 1’-biphenyl	OTAC	basic	2D hex crystal	[33]
Co – condensation of bis[(3-trimethoxysilyl)propyl]-amine and 1,2-bis(triethoxysilyl)ethane	CTAB	basic	Hexagonal	[35]

2.1.3 Background notes on characterization of PMOs using nitrogen sorption studies

According to the IUPAC classification, porous solids can be classified into three domains, depending on their pore size. These are called microporous – (< 2 nm), mesoporous – (2 – 50 nm), and macroporous (> 50 nm) materials [62, 63]. This classification can be done by using nitrogen sorption studies. Adsorption of nitrogen (or argon) on PMO materials is the standard analytical method to measure the surface area, the total pore volume and the pore size distribution [61]. The simplest model for a porous material is that of non-intersecting cylindrical tubes. There are two possible modes of filling/ emptying of these pores with a liquid like adsorbate. The first model is "adsorptive filling". A multilayered film of the liquid is formed on the wall of the capillary and with increasing thickness of this layer it gradually fills. In the "bulk filling" model, a thin monolayer is formed, but then additional adsorbate fills the capillary completely at one point. The addition of more liquid causes the meniscus to gradually move, filling the pore.

IUPAC classification of isotherms

Gas adsorption isotherms generally fall into six categories (Figure 2.1) [62, 63]. Type I isotherms are an indication for microporous materials as well as strong adsorbent-adsorbate interactions. However Type I isotherms can also be found in mesoporous materials with cylindrical pores, which have a pore size close to the microporous range.

Type II isotherms are found in many macroporous solids, which show a gradual increase in the amount of adsorbate with relative pressure due to multilayer formation following the "adsorptive filling" model. A material showing a Type II isotherm exhibits a pronounced monolayer formation, whereas in the case of a Type III isotherm no monolayer formation is observed. This

lack of monolayer formation results from strong lateral interactions between the adsorbed molecules compared to weak adsorbent surface – adsorbate interactions [64].

Type IV and Type V isotherms are found in mesoporous materials. At low pressures the materials show isotherms similar to macroporous materials, but at higher pressures the amount adsorbed rises steeply due to capillary condensation in the pores ("bulk filling" model). The difference between Type IV and Type V isotherms is the same as between Type II and Type III isotherms. The capillary condensation and evaporation are usually taking place at different pressures giving rise to the formation of a hysteresis loop. If capillary condensation – evaporation in the mesopores is reversible, then an isotherm of Type IV occurs. This is often the case for materials with a pore diameter close to the micropore range.

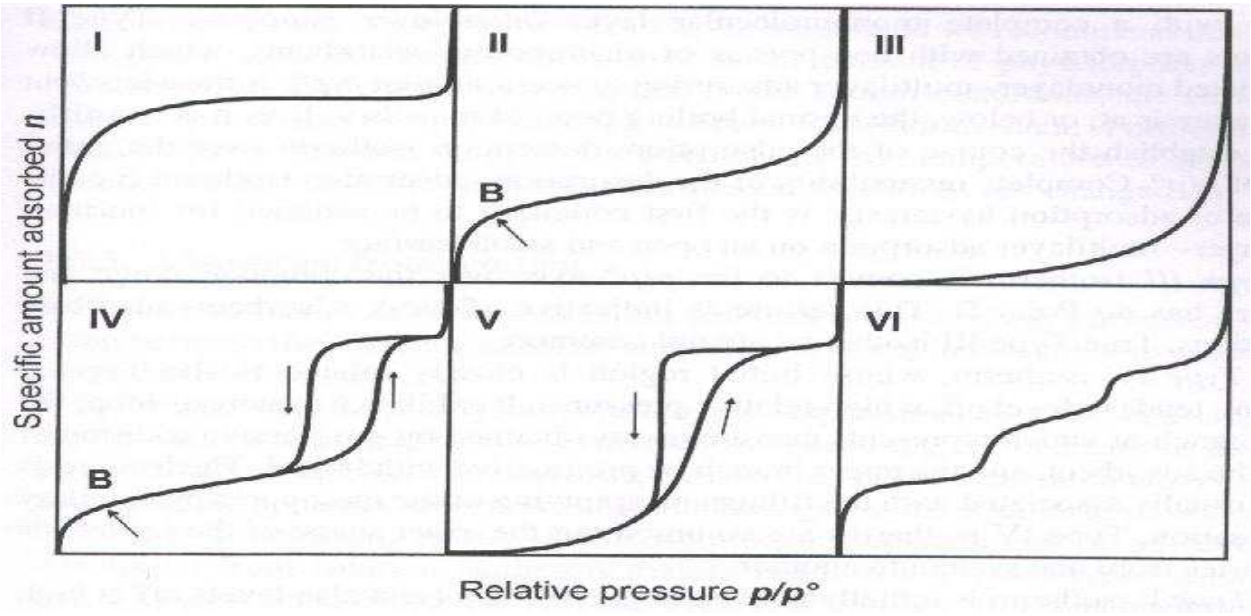

Figure 2.1 IUPAC classification of gas adsorption isotherms

Adsorption hysteresis

The origin of the hysteresis loop in mesoporous materials is usually attributed to thermodynamic and/or network effects [62, 65 - 68]. The hysteresis loops can be classified into four types (Figure 2.2) [63] depending on their shape, which is related to the form of pores in the material. Type H1 loops are found for cylindrical pores with a high degree of uniformity, [64, 69] whereas type H2 shapes can come from ink – bottle shaped ones [67]. Slit-like pores show a type H3 hysteresis loop and a type H4 loop is observed for mesopores, which are embedded in a matrix of smaller pores [70, 71]. Some porous materials also show a low pressure, nonclosing hysteresis loop, which arises when the adsorbent is swollen or deformed by the adsorbate or when reversible or irreversible chemisorptions takes place in the material.

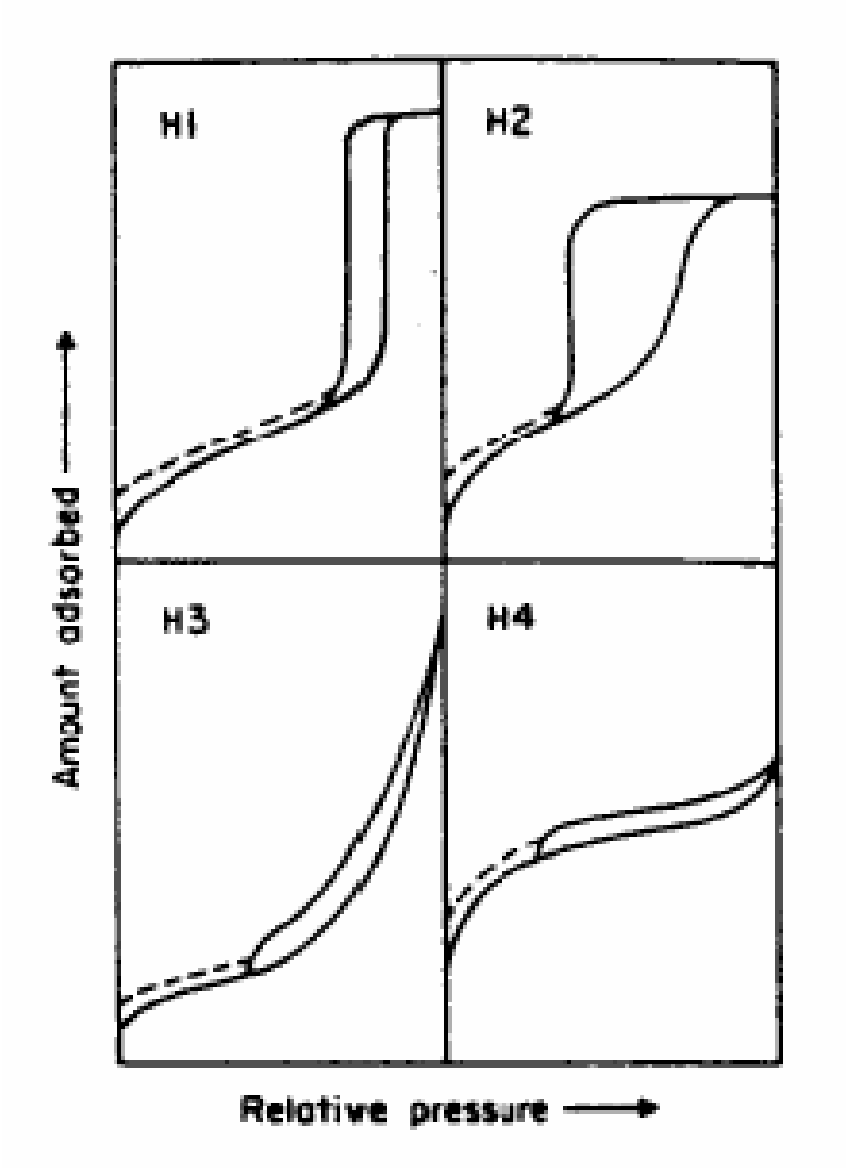

Figure 2.2 IUPAC classification of adsorption-desorption hysteresis loops

The specific surface area, pore volume and pore size distribution can be calculated by the Brunauer, Emmet, and Teller (BET) method [62, 63, 65, 72]. The BET method is based on the monolayer capacity, which is found by fitting the gas adsorption data to the BET equation. The BET equation reduces to a Langmuir equation in the area of low relative pressures of 0.05 – 0.35. The specific surface area, a_s(BET), is obtained from the equation

$$A_s\ (BET) = n^a_m x L x a_m$$

where L is Avogadro`s number, n^a_m is the monolayer capacity (defined as the amount of the adsorbate required to form a complete monolayer on the surface of unit mass of the adsorbate), a_m is the molecular cross-sectional area (i.e. the average area occupied by the adsorbate molecule). For nitrogen, $a_m\ (N_2) = 0.162\ nm^2$ at 77K.

Pore size. The traditional method for analyzing pore size distributions (PSDs) in the mesopore range is the Barrett-Joyner-Halenda (BJH) method [73] which is based on the Kelvin equation [15] and, thus has a thermodynamic origin. In the BJH method, the derived mesopore size distribution is usually expressed in the graphical form $\Delta Vp\ /\ \Delta rp$ versus *rp* (or d_p) (where *Vp* is the mesopore volume and *rp* is the pore radius for cylindrical pores, and d_p is the width for parallel sided slits). The mesopore pore volume is assumed to be completely filled at high relative pressure. The derived pore size distribution is dependent on whether the adsorption or desorption branch of the hysteresis loop is used for computation.

The total pore volume of a material is calculated from the amount adsorbed at a relative pressure close to the saturation vapor pressure. This is done by converting the amount adsorbed into the corresponding volume of liquid adsorbate at the analysis temperature. In the case of nitrogen at liquid nitrogen temperature, this conversion value is 0.0015468 [74]. It is assumed that the density of the condensed adsorbate is the same as the one of the bulk liquid.

2.3 Mesoporous carbon materials: A review

Mesoporous carbon materials are an active area of research because of their many applications in the field of science and technology which include adsorbents for bulky pollutants, catalysis and energy storage [75 - 77]. These mesoporous carbon materials have a large surface area, large pore volume and narrow pore size distribution. The general synthesis procedure for ordered mesoporous carbons using mesoporous silica templates is outlined as:

(a) preparation of the mesoporous silica as the hard template,
(b) introduction of the carbon source into the channels of mesoporous silica through impregnation or chemical vapour deposition (CVD),
(c) carbonization of the hybrid sample to gain a carbon / silica nanocomposite, and
(d) removal of the silica template [78].

Various forms of mesoporous silicas and aluminosilicas, including MCM-48, SBA-15, HMS, MSU-H, SBA-12, SBA-16, and mesocellular silica foams, have been used as sacrificial templates for the preparation of mesoporous carbons [79 – 83]. Two techniques, i.e. liquid phase impregnation [79, 83] and chemical vapour deposition (CVD) [84] have been well established for the infiltration of carbon precursors, and many carbon precursors such as sucrose, glucose, xylose, furfuryl alcohol, mesophase pitch, acenaphthene and benzene have been demonstrated to be suitable for preparing mesoporous carbon materials [85]. For liquid impregnation, catalysts such as sulphuric acid, aluminium, etc were required to ensure the polymerization and carbonization of carbon precursors.

The pore channel system of mesoporous carbons is usually inversely replicated from the inorganic templates, and in general the carbons retain the particle morphology of the template [79 – 83, 86, 87]. Therefore to prepare mesoporous carbon materials with particular porosity

and/or morphology, it is necessary to control the textural properties and particle morphology of the inorganic templates [86, 87].

Ryoo *et al* [79, 80] reported the first synthesis of a new type of mesoscopically ordered carbon molecular sieve CMK-1 and CMK-3 (cubic and hexagonal respectively) by carbonizing sucrose inside the pores of the cubic MCM-48 and hexagonal SBA-15 mesostructured silica materials. CMK-1 had two pore size distributions one centred in the nanoporous region with pores ranging from 0.5 to 0.8 nm and one centred in the mesoporous region with pores near 3.0 nm. Yu and co-workers [88] synthesized mesoporous carbon using as synthesized MCM-48 silica/surfactant composite as a template. This mesoporous carbon, however, was not synthesized only by converting the organic template directly into the carbonaceous material. Rather an additional carbon precursor, poly(divinylbenzene) was synthesized inside the empty space of the silica/surfactant composite prior to the carbonization process.

Sayari and co-workers [89] reported the direct preparation of wormhole like large sized microporous carbon through the carbonization of a silica/cyclodextrin – template nanocomposite. The carbon material produced was a disordered wormhole – like microporous material. The synthesis of mesoporous carbon by a one step vapour deposition polymerization process using colloidal silica particles as templates and polyacrylonitrile as a carbon precursor was reported by Jang and co-workers [90]. Kruk *et al* [91] studied MCM-48 silica as a template for mesoporous carbons by synthesizing a variety of MCM-48 samples and impregnating them with sucrose in the presence of sulphuric acid. In order to provide a comparison, they also impregnated MCM-41 with sucrose and MCM-48 with polyfurfuryl alcohol. For the impregnation of polyfurfuryl alcohol to take place it was necessary to convert the pure silica MCM-48 sample into an aluminosilicate via a post synthetic aluminosilicate method [92]. They found that the templating of MCM-41 and MCM-48 showed that after the removal of silica template, CMK-1 retained long

range order mesoporosity. Upon removal of the MCM-41 template, the resulting carbon lost all long range order and become completely nanoporous.

Saadallah *et al* [93] synthesized new ordered carbon materials using pitch and mesoporous silica materials as the carbon precursor and templates respectively. The new ordered carbon materials were prepared by first impregnating MCM-48 and SBA-15 with pitch then carbonizing them. This was followed by removal of the silica by acid treatment. They found out that by using pitch as a carbon precursor, a graphitizable carbon material with ordered porosity could be obtained. The carbon materials obtained were found to be thermally stable up to 1402 ^{o}C, the material was thermally stable and porosity was preserved. The liquid impregnation of the pitch showed several advantages compared to that of sucrose. In particular, a lower unit cell contraction during the carbonization step was noted.

Katok *et al* [94] studied the pyrolytic decomposition of acetylene over the surfaces of nickel, cobalt and iron containing mesoporous MCM-41 silicas. They developed two efficient methods of synthesizing carbon nanostructures. The two methods were a) chemisorption of acetylacetonates onto MCM-41 silica at 150 ^{o}C, followed by reduction of the supported metal acetylacetonates with hydrogen at 450 ^{o}C and subsequent treatment with acetylene at 450 ^{o}C, and b) direct treatment of the supported metal acetylacetonates with acetylene at 700 ^{o}C. Both routes, depending on metal conditions, led to carbon deposition either in the form of nanotubes (diameter, 14 – 84 nm) or carbon fibres (diameter, 86 – 111 nm). Longer pyrolysis times using acetylene, increased the yield of amorphous carbon particles. It was observed that in the absence of a catalyst on the mesoporous silica matrices, only low yields (up to 2 %) of carbon nanotubes were obtained.

Li *et al* [95] prepared ordered mesoporous carbons with high surface areas using SBA-15 as a template at different carbonization temperatures. Ferric acetylacetonate was first dissolved in ethanol and mixed with the SBA-15 powder and dried. The dried powders of SBA-15 were then carbonized at different temperatures under a stream of a 1:1 mixture of argon and hydrogen gas. The silica/carbon nanocomposite obtained was washed with 20 % HF solution. The carbon materials they obtained replicated the structures of SBA-15 template and the growth was limited within the pores. The structure and the degree of crystallinity of the ordered mesoporous carbons (OMCs) depended strongly on the growth temperature. As the temperature increased from 650 to 850 ^{o}C, the pore volume, surface area and average pore size of OMCs were enhanced from 0.87 to 1.54 cm^3g^{-1}, 826 to 1236 m^2g^{-1} and 4.2 to 4.9 nm respectively. Extensive work has been done on the synthesis of mesoporous carbon materials from mesoporous silica templates mostly by the route proposed by Kim *et al*. [78].

2.4 Carbon/silica nanocomposites: A review

Mesoporous silica is the most commonly used starting material or hard template for the nanocasting of mesoporous carbon and other non-siliceous mesoporous materials. Nanoporous silicas may also be used to fabricate silica based composite materials such as metal/silica or metal alkoxide/silica, polymer/silica and carbon/silica [96]. Silica/carbon composites are particularly versatile materials that find many possible uses for example electrochemical devices [97], and as solar absorbers [98]. Silica/carbon composites may be prepared via a lot of methods including sol-gel techniques followed by carbonization [99], pyrolysis of suitable carbon precursors in a porous silica matrix [100] or carbonization of organosilica/surfactant mesophases [101].

A further possibility for the transformation of PMOs into other mesoporous materials has been described by Pang *et al* [101]. By heating mesostructured benzene-bridged PMO with crystal like pore walls for 4 hours at 900 ^{o}C in a stream of nitrogen, they obtained mesoporous carbon/silica nanocomposite materials with pore walls uniformly constructed from molecular carbon and silica units. During the carbonization process, the surfactant contained within the mesostructured starting material was decomposed. The benzene units in the pore walls were transformed into carbon. Thermogravimetric analysis showed that the carbon in the composite originated almost exclusively from the aromatic units of the PMO and not from the surfactant. The order of the mesostructure in the end product was essentially retained after the carbonization, but crystal-like regions were only partially present in the pore walls. The mesostructure following thermal treatment was contracted, as was evidenced by both a reduction in the XRD d spacing value (from 4.8 to 4.0 nm) and in the pore size (from 2.5 to 2.0 nm). Polarz and his co-workers [98] reported the synthesis of porous silica-carbon hybrid materials from the direct carbonization of silica/cyclodextrin nanocomposite and showed their application as selective solar absorber materials.

Yang *et al* [102] reported on the direct preparation of mesoporous silica/carbon composites, mesoporous silica and nanostructured carbon and silica carbide materials from mesoporous ethyl-bridged organosilica/surfactant mesophases. Well ordered mesoporous silica/carbon composites with surface area of 820 m^2g^{-1} and pore volume of 0.4 cm^3g^{-1} were obtained via pyrolysis of organosilica mesophases under argon flow at between 800 – 950 ^{o}C. The mesoporous silica/carbon composites, mesoporous silica and mesoporous carbon materials retained the particle morphology of the organosilica mesophases.

Pinnavaia *et al* reported the formation of carbon nanotubes by in-situ carbonization of a micellar non-ionic surfactant (Pluronic P123) under a flow of nitrogen [103]. Urban *et al* synthesized multiwalled carbon nanotubes by graphitization of as-synthesized mesoporous silicas templated

by cetyltrimethylammonium bromide [104]. They employed a non-catalytic, templating process wherein the surfactant of a micelle-templated silica was transformed directly into carbon nanotubes on the walls of the silica template.

From the review on carbon/silica nanocomposites, it can be seen that some work has been done on mesoporous carbon/silica composites. However most authors used either liquid phase impregnation or the CVD technique for the infiltration of carbon precursors. Their inert atmosphere was created by the use of inert gases and where some used sealed quartz tubes, they would have first impregnated a carbon source into the template. In this study carbon/silica nanocomposites were prepared by directly carbonizing the organosilica/surfactant phases in an evacuated closed system created by sealing the materials in quartz tubes under vacuum. No carbon precursor was impregnated in the pore walls of the nanoporous materials before carbonization. To the best of our knowledge, this will be the first report on the direct preparation of silica on carbon nanocomposite materials with various nanostructures (spheres, beads, bamboo-shaped multiwalled nanotubes and multiwalled nanotubes) from mesoporous silica and PMOs under vacuum.

2.5 References

[1] J. P. G. Pater, P. A. Jacobs, J. A. Martens, *Journal of Catalysis*, **184**, 262 (1999).

[2] M. S. Morey, A. Davidson, G. D. Stucky, *Journal of Porous Materials*, **5**, 195 (1998).

[3] E. Armengol, A. Corma, H. Garcia, J. Primo, *Applied Catalysis A – General*, **126**, 391 (1995).

[4] S. V. Mattigod, X. D. Feng, G. E. Fryxell, J. Liu, M. L. Gong, *Seperation Science and Technology*, **34**, 2329 (1999).

[5] D. Y. Zhao, P. D. Yang, Q. S. Huo, B. F. Chmelka, G. D. Stucky, *Current Opinion in Solid State and Materials Science*, **3**, 111 (1998).

[6] L. Mercier, T. J. Pinnavaia, *Advanced Materials*, **9**, 500 (1997).

[7] J. Y. Ying, C. P. Mehnert, M. S. Wong, *Angewandte Chemie International Edition*, **38**, 56 (1999).

[8] J. S. Beck, J. C. Vartuli, W. J. Roth, M. E. Leonowicz, C. T. Kresge, K. D. Schmitt, C. T. W. Chu, D. H. Olson, E. W. Sheppard, S. B. McCullen, J. B. Higgins, J. L. Schlenker, *Journal of the American Chemical Society*, **114**, 10834 (1992).

[9] J. H. Clark, J. C. Ross, D. J. Macquarrie, S. J. Barlow, T. W. Bastock, *Chemical Communications*, 1203 (1997).

[10] M. A. Marshall, H. A. Mottola, *Analytical Chemistry*, **55**, 2089 (1983).

[11] D. Brunel, N. Bellocq, P. Sutra, A. Cauvel, M. Lasperas, P. Moreau, F. Di Renzo, A. Galarneau, F. Fajula, *Coordinattion Chemistry Reviews*, **180**, 1085 (1998).

[12] M. Lasperas, N. Bellocq, D. Brunel, P. Moreau, *Tetrahedron – Asymmetry*, **9**, 3053 (1998).

[13] T. Maschmeyer, F. Rey, G. Sankar, J. M. Thomas, *Nature*, **378**, 159 (1995).

[14] K. Moller, T. Bein, *Chemistry of Materials*, **10**, 2950 (1998).

[15] G. A. Ozin, E. Chomski, D. Khushalani, M. J. MacLachlan, *Current Opinion in Colloid and Interface Science*, **3**, 181 (1998).

[16] S. L. Burkett, S. D. Sims, S. Mann, *Chemical Communications*, 1367 (1996).

[17] M. C. Burleigh, M. A. Markowitz, M. S. Spector, B. P. Gaber, *Journal of Physical Chemistry B*, **105**, 9935 (2001).

[18] T. Asefa, M. J. MacLachlan, N. Coombs, G. A. Ozin, *Nature*, **402**, 867 (1999).

[19] S. Inagaki, S. Guan, Y. Fukushima, T. Ohsuna, O. Terasaki, *Journal of the American Chemical Society*, **121**, 9611 (1999).

[20] B. J. Melde, B. T. Holland, C. F. Blandford, A. Stein, *Chemistry of Materials*, **11**, 3302 (1999).

[21] W. J. Hunks, G. A. Ozin, *Chemistry of Materials*, **16,** 5465 (2004).

[22] G. Temtsin, T. Asefa, S. Bittner, G. A. Ozin, *Journal of Materials Chemistry*, **11**, 3202 (2001).

[23] M. Kuroki, T. Asefa, W. Whitnal, M. Kruk, C. Yoshina – Ishii, M. Jaroniec, G. A. Ozin, *Journal of the American Chemical Society*, **124**, 13886 (2002).

[24] C. Tourne-Peteilh, D. Brunel, S. Begu, B. Chiche, F. Fajula, D. A. Lernera, J. M. Devoisselle, *New Journal of Chemistry*, **27**, 1417 (2003).

[25] S. Guan, S. Inagaki, T. Ohsuna, O. Terasaki, *Journal of the American Chemical Society*, **122**, 5660 (2000).

[26] A. Sayari, S. Hamoudi, Y. Yang, I. L. Moudrakovski, J. R. Ripmeester, *Chemistry of Materials*, **12**, 3857 (2000).

[27] S. Hamoudi, Y. Yang, I. L. Moudrakovski, S. Lang, A. Sayari, *Journal of Physical Chemistry B*, **105**, 9118 (2001).

[28] F. Hoffmann, M. Cornelius, J. Morell, M. Froba, *Angewandte Chemie International Edition*, **45**, 3216 (2006).

[29] C. Yoshina-Ishii, T. Asefa, N. Coombs, M. J. MacLachlan, G. A. Ozin, *Chemical Communications*, 2539 (1999).

[30] G. Temstin, T. Asefa, S. Bittner, G. A. Ozin, *Journal of Materials Chemistry*, **11**, 3202 (2001).

[31] S. Inagaki, S. Guan, T. Ohsuna, O. Terasaki, *Nature*, **416**, 304 (2002).

[32] N. Bion, P. Ferreria, A. Valente, I. S. Goncalves, J. Rocha, *Journal of Materials Chemistry*, **13**, 1910 (2003).

[33] M. P. Kapoor, Q. Yang, S. Inagaki, *Journal of the American Chemical Society*, **124**, 15176 (2002).

[34] V. Goletto, A. Bled, G. Trimmel, M. Man, W. C. Michel, H. Woo, D. Durand, F. Babonneau, *Materials Research Society Symposium Proceedings*, **726** (Organic/Inorganic Hybrid Materials), 123 (2002).

[35] M. Alvaro, B. Ferrer, V. Fornes, H. Garcia, *Chemical Communications*, 2546 (2001).

[36] M. A. Wahab, I. Kim, C. S. Ha, *Journal of Solid State Chemistry*, **177**, 3439 (2004).

[37] F. Hoffman, M. Cornelius, J. Morell, M. Froba, *Journal of Nanoscience and Nanotechnology*, **6,** 265 (2006).

[38] T. Asefa, M. Kruk, N. Coombs, H. Grondey, M. J. MacLachlan, M. Jaroniec, G. A. Ozin, *Journal of the American Chemical Society*, **125**, 11662 (2003).

[39] O. Muth, C. Schellbach, M. Froba, *Chemical Communications*, 2032 (2001).

[40] M. C. Burleigh, M. A. Markowitz, E. M. Wong, J. S. Lin, B. P. Gaber, *Chemistry of Materials*, **13**, 4411 (2001).

[41] W. Guo, J. Y. Park, M. O. Oh, H. W. Jeong, W. J. Cho, I. Kim, C. S. Ha, *Chemistry of Materials*, **15**, 2295 (2003).

[42] W. Guo, I. Kim, C. S. Ha, *Chemical Communications*, 2692 (2003).

[43] X. Y. Bao, X. S. Zhao, X. Li, P. A. Chia, J. Li, *Journal of Physical Chemistry B*, **108**, 4684 (2004).

[44] X. Bao, X. S. Zhao, X. Li, J. Li, *Applied Surface Science*, **237**, 380 (2004).

[45] X. Y. Bao, X. S. Zhao, S. Z. Qiao, S. K. Bhatia, *Journal of Physical Chemistry B*, **108**, 16441 (2004).

[46] H. Zhu, D. J. Jones, J. Zajac, J. Roziere, R. Dutartre, *Chemical Communications*, 2568 (2001).

[47] Y. Goto, S. Inagaki, *Chemical Communications*, 2410 (2002).

[48] T. Ren, X. Zhang, J. Suo, *Microporous and Mesoporous Materials*, **54**, 139 (2002).

[49] L. Zhao, G. Zhu, D. Zhang, Y. Di, Y. Chen, O. Terasaki, S. Qiu, *Journal of Physical Chemistry B*, **109**, 765 (2005).

[50] E. B. Cho, K. Char, *Chemistry of Materials*, **16**, 270 (2004).

[51] J. R. Matos, M. Kruk, L. P. Mercuri, M. Jaroniec, T. Asefa, N. Coombs, G. A. Ozin, T. Kamiyama, O. Terasaki, *Chemistry of Materials*, **14**, 1903 (2002).

[52] M. C. Burleigh, M. A. Markowitz, B. P. Gaber, *Journal of Physical Chemistry B*, **106**, 9712 (2002).

[53] M. C. Burleigh, S. Jayasundera, C. W. Thomas, M. S. Spector, M. A. Markowitz, B. P. Gaber, *Colloid and Polymer Science*, **282**, 728 (2002).

[54] M. C. Burleigh, M. A. Markowitz, M. S. Spector, C. W. Thomas, B. P. Gaber, *Journal of Physical Chemistry B*, **107**, 12628 (2003).

[55] L. Zhang, Q. Yang, W. H. Zhang, Y. Li, J. Yang, D. Jiang, G. Zhu, C. Li, *Journal of Materials Chemistry*, **15**, 2562 (2005).

[56] S. Hamoudi, S. Kaliaguine, *Chemical Communications*, 2118 (2002).

[57] M. P. Kapoor, S. Inagaki, *Chemistry of Materials*, **14**, 3509 (2002).

[58] C. T. Kresge, M. E. Leonowicz, W. J. Roth, J. C. Vartuli, J. S. Beck, *Nature*, **359**, 710 (1992).

[59] J. S. Beck, C. T. Chu, I. D. Johnson, C. T. Kresge, M. E. Leonowicz, W. J. Roth, J. C. Vartuli, *US Patent 5, 108, 725 to Mobil Coorporation* (1992).

[60] D. Zhao, Q. Huo, J. Feng, B. F. Chmelka, G. D. Stucky, *Journal of the American Chemical Society*, **120**, 6024 (1998).

[61] M. Kruk, M. Jaroniec, *Chemistry of Materials*, **13,** 3169 (2001).

[62] F. Rouquerol, J. Rouquerol, K. Sing, *Adsorption by Powders and Porous Solids. Principles, Methodology and Applications.* Academic Press, London, 1999.

[63] K. S. W. Sing, D. H. Everett, R. A. W. Haul, L. Moscou, R. A. Pierotti, J. Rouquerol, T. Siemieniewska, *Pure and Applied Chemistry*, **57**, 603 (1985).

[64] M. Kruk, M. Jaroniec, A. Sayari, *Langmuir*, **13**, 6267 (1997).

[65] S. J. Gregg, K.S.W. Sing, *Adsorption, Surface Area and Porosity*. 2nd Edition,(1982).

[66] P. C. Ball, R. Evans, *Langmuir*, **5**, 714 (1989).

[67] H. L. Liu, L. Zhang, N. A. Seaton, *Journal of Colloid and Interface Science*, **156**, 285 (1993).

[68] P.I. Ravikovitch, S. C. Odomhnaill, A. V. Neimark, F. Schuth, K.K. Unger, *Langmuir*, **11**, 4765 (1995).

[69] Q. S. Huo, D. I. Margolese, G. D. Stucky, *Chemistry of Materials*, **8**, 1147 (1996).

[70] H. P. Lin, S. T. Wong, C. Y. Mou, C. Y. Tang, *Journal of Physical Chemistry B*, **104**, 8967 (2000).

[71] P. J. Kooyman, M. J. Verhoef, E. Prouzet, *Studies in Surface Science and Catalysis*, **129**, 535 (2000).

[72] J. Rouquerol, D. Avnir, C. W. Fairbridge, D.H. Everett, J. H. Haynes, N. Pernicone, J. D. F. Ramsay, K. S. W. Sing, K. K. Unger, *Pure and Applied Chemistry*, **66**, 1739 (1994).

[73] E. P. Barrett, L.G. Joyner, P. P. Halenda, *Journal of the American Chemical Society*, **73**, 373 (1951).

[74] M. Kruk, M. Jaroniec, *Chemistry of Materials*, **12**, 222 (2000).

[75] H. Marsh, E. A. Heintz, F. Rodriguez-Reinoso, *Introduction to Carbon Technology*, Universidad de Alicante, Secretariado de Publications , Alicante (1997).

[76] K. Kinoshita, *Carbons: Electrochemical and Physicochemical Properties*, Wiley, New York (1988).

[77] T. Kyotani, *Carbon*, **38**, 269 (2000).

[78] J. Kim, J. Lee, T. Hyeon, *Carbon*, **42**, 2711 (2004).

[79] R. Ryoo, S. H. Joo, S. Jun, *Journal of Physical Chemistry B*, **103**, 7743 (1999).

[80] S. Jun, S. H. Joo, R. Ryoo, M. Kruk, M. Jaroniec, Z. Liu, T. Ohsuna, O. Terasaki, *Journal of the American Chemical Society*, **122**, 10712 (2000).

[81] J. Lee, S. Yoon, T. Hyeon, S. M. Oh, K. B. Kim, *Chemical Communications*, 2177 (1999).

[82] M. Kruk, B. Dufuor, E. B. Celer, T. Kowalewski, M. Jaroniec, K. Matyjaszewski, *Journal of Physical Chemistry B*, **109**, 9216 (2005).

[83] S. S. Kim, T. J. Pinnavaia, *Chemical Communications*, 2418 (2001).

[84] W. Zhang, C. Liang, H. Sun, Z. Shen, Y. Guan, P. Ying, C. Li, *Advanced Materials*, **14**, 1776 (2002).

[85] A. Lu, F. Schuth, *Advanced Materials*, **18**, 1793 (2006).

[86] C. Yu, J. Fan, B. Tian, D. Zhao, G. D. Stucky, *Advanced Materials*, **14**, 1742 (2002).

[87] Y. Xia, R. Mokaya, *Advanced Materials*, **16**, 886 (2004).

[88] S. B. Yoon, J. Y. Kim, J. S. Yu, *Chemical Communications*, 1536 (2002).

[89] B. H. Han, W. Zhou, A. Sayari, *Journal of the American Chemical Society*, **125**, 3444 (2003).

[90] J. Jang, B. Lim, M. Choi, *Chemical Communications*, 4214 (2005).

[91] M. Kruk, M. Jaroniec, R. Ryoo, S. H. Joo, *Journal of Physical Chemistry B*, **104**, 7960 (2000).

[92] S. Jun, R. Ryoo, *Journal of Catalysis*, **195**, 237 (2000).

[93] C. Vix-Guterl, S. Saadallah, L. Vidal, M. Reda, J. Parmentier, J. Patarin, *Journal of Materials Chemistry*, **13**, 2535 (2003).

[94] K. V. Katok, V. A. Tertykh, S. Ya Brichka, G. P. Prikhod'ko, *Journal of Therm*al *Analysis and Calorimetry*, **86**, 109 (2006).

[95] Z. Li, J. Zhang, Y. Li, Y. Guan, Z. Feng, C. Li, *Journal of Materials Chemistry*, **16**, 1350 (2006).

[96] J. Lee, S. Han, T. Hyeon, *Journal of Materials Chemistry*, **14**, 478 (2004).

[97] V. G. Gavalas, R. Andrews, D. Bhattacharyya, L.G. Bachas, *Nanotechnology Letters*, **1**, 719 (2001).

[98] Y. Mastai, S. Polarz, M. Antoniette, *Advanced Functional Materials*, 12, **197** (2002).

[99] J. Aguado-Serrano, M. J. Rojas-Cervantes, A. J. Lopez-Peinado, V. Gomez-Serrano, *Microporous and Mesoporous Materials*, **74**, 111 (2004).

[100] P. R. Giunta, L. J. Van de Burgt, A. E. Stiegman, *Chemistry of Materials*, **17**, 1234 (2005).

[101] J. Pang, V. T. John, D. A. Loy, Z. Zhang, Y. Lu, *Advanced Materials*, **17**, 704 (2005).

[102] Z. Yang, Y. Xia, R. Mokaya, *Journal of Materials Chemistry*, **16**, 3417 (2006).

[103] T. J. Pinnavaia, S. Kim, D. Lee, J. Shah, *Chemical Communications*, 1436 (2003).

[104] M. Urban, D. Mehn, Z. Konya, I. Kiricsi, *Chemical Physics Letters*, **359**, 95 (2002).

CHAPTER THREE

EXPERIMENTAL

3.1 Brief introduction

This chapter covers the synthesis of periodic mesoporous organosilica materials and carbon on silica nanocomposite materials. The characterization techniques will also be described.

The PMOs were synthesized via hydrolysis and subsequent condensation reactions of bridged organosilsesquioxane precursors in the presence of supramolecular aggregates of long chain surfactants as illustrated in Fig. 3.1. An ionic structure directing agent cetyltrimethylammonium bromide (CTAB) and a non ionic triblock copolymer P123 structure directing agent were used. Figure 3.1 also shows formation of mesoporous carbon-silica composites and mesoporous carbon composites from as-synthesized and extracted periodic mesoporous organobridged silica.

Carbon on silica nanocomposites in this work are obtained from PMO mesophases via pyrolysis under an inert atmosphere at 800 – 1000 ^{o}C. These were synthesized through a simple direct synthetic method of as synthesized silica/surfactant nanocomposites.

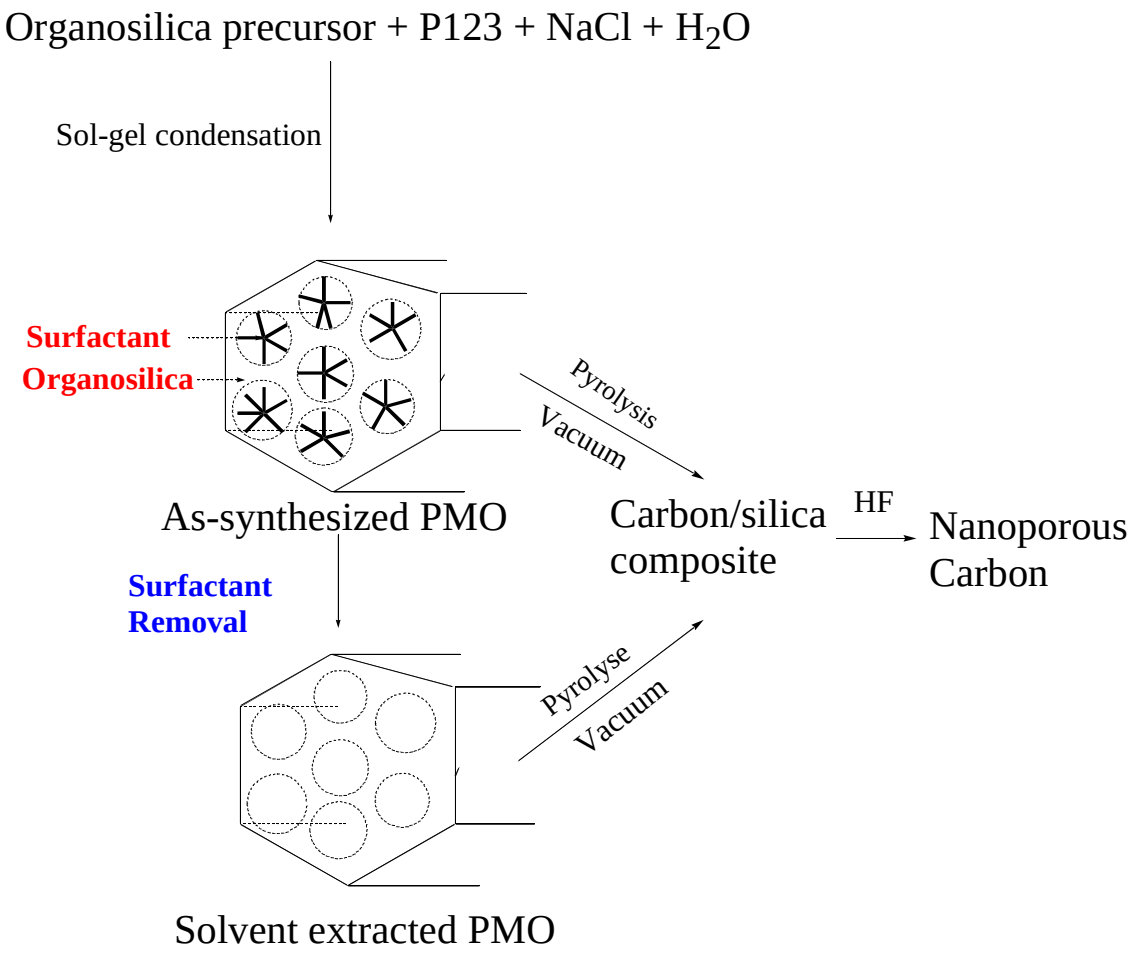

Figure 3.1 Schematic showing the formation of as-synthesized and extracted periodic mesoporous organo-bridged silica, carbon/silica composites and mesoporous carbons.

3.2 Reagents and chemicals

The organically bridged silica sources and structure directing agents (Table 3.1) were all purchased from Sigma Aldrich. The deionised water and ethanol (C_2H_5OH, 99.5 %, Merck) were used as co-solvents. Fuming hydrochloric acid (HCl, 32%, Promark Chemicals) was used as a

catalyst and for removal of surfactant. Aqueous ammonia (NH_4OH, 33 %, Riedel-de-Haen) was used as a catalyst. Sodium chloride (NaCl, Associated Chemical Enterprises) was used as an additive under low acid concentrations. Hydrofluoric acid (HF, 40 %) and nitric acid (HNO_3, 55 %) were purchased from Merck Chemicals. All chemicals were used as received without further purification

Table 3.1 Structure directing agents and organosilica precursors

Name	Structure
Organically bridged silica sources	
Tetra ethyl orthosilicate (TEOS)	$Si(OC_2H_5)_4$ 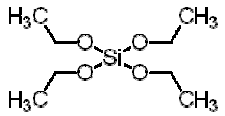
1,2 – Bis(trimethoxysilyl) ethane (BTME)	$[-CH_2Si(OCH_3)_3]_2$ 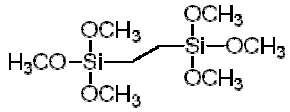
1, 4 – Bis (triethoxysilyl) benzene (BTEB)	$C_6H_4(Si(OC_2H_5)_3)_2$ 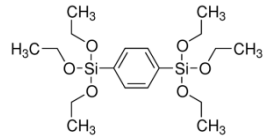

Name	Structure
4, 4 – Bis (triethoxysilyl) – 1, 1 biphenyl (BTEBP)	$[-C_6H_4Si(OC_2H_5)_3]_2$ 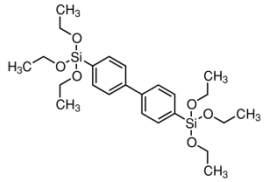
Bis [3 – trimethoxysilyl) propyl] – amine (BTMSPA)	$[(CH_3O)_3Si(CH_2)_3]_2NH_2$ 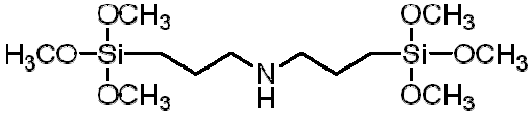
Structure directing agents	
Triblock Copolymer (Pluronic P123)	$EO_{20}PO_{70}EO_{20}$ $HO(CH_2CH_2O)_{20}(CH_2(CH_3)CH_2O)_{70}$ $(CH_2CH_2O)_{20}H)$
Cetyltrimethylammonium bromide (CTAB)	$CH_3(CH_2)_{15}N(Br)(CH_3)_3$ 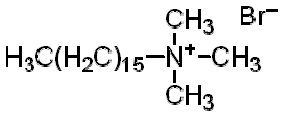

3.3 Synthesis of periodic mesoporous organosilica materials

3.3.1 Mesoporous materials from structure directing agent Pluronic P123

The synthesis of periodic mesoporous organosilica materials using Pluronic P123 as the structure directing agent was performed according to the procedure reported by Guo and coworkers [1] with a few modifications.

3.3.1.1 Synthesis method

Pluronic P123 (1.2 g) and NaCl (3.5 g) were dissolved in deionised water (10 g) and 2.0 M HCl (52 ml) solution with stirring at 40 ^{o}C. To this homogeneous solution was added the organosilica precursor and then the mixture was stirred for 24 hours at the same temperature. The resulting mixture was transferred into a round bottomed flask and refluxed by soxhlet at 80 ^{o}C for an additional 24 hours with stirring. The final reactant molar composition of organosilica precursor: P123: HCl: NaCl: H_2O used was 0.5: 0.017: 5.07: 5.07: 178. The solid products were collected by filtration, washed thoroughly with water, and air dried at room temperature. This material is referred to as the as-synthesized material. The as-synthesized materials are designated as AS-TS-P123, AS-BMS-P123, AS-BS-P123, AS-BPS-P123 and AS-PS-P123. See appendix for notations used to identify samples. See Table 3.2 for amounts of organosilica precursor used for synthesis of the as-synthesized and surfactant extracted periodic mesoporous organosilica materials.

3.3.1.2 Surfactant extraction

The surfactant was removed by stirring 1.0 g of as-synthesized sample in 150 ml of ethanol in 3.8 g of 36 % HCl solution at 50 ^{o}C for 6 hours. The resulting solid was recovered by filtration, washed with ethanol, and dried in air. This extraction procedure was repeated to remove the surfactant completely. This material is referred to as the surfactant extracted material. The surfactant extracted materials are designated as SE-TS-P123, SE-BMS-P123, SE-BS-P123, SE-BPS-P123 and SE-PS-P123. See appendix for notations used to identify samples.

Table 3.2 Tabular details of synthesis particulars

Sample	Amount of organosilica precursor Used (ml)	Type of organosilica precursor used
AS-TS-P123	2.64	TEOS
SE-TS-P123	2.64	TEOS
AS-BME-P123	2.98	BTME
SE-BME-P123	2.98	BTME
AS-BS-P123	4.69	BTEB
SE-BS-P123	4.69	BTEB
AS-BPS-P123	5.41	BTEBP
SE-BPS-P123	5.41	BTEB
AS-PS-P123	3.89	BTMSPA
SE-PS-P123	3.89	BTMSPA

3.3.2 Mesoporous materials from structure directing agent CTAB

The synthesis of periodic mesoporous organosilica materials using CTAB as the structure directing agent was performed according to the procedure reported by Kumar and coworkers [2] with a few modifications.

3.3.2.1 Synthesis method

CTAB (2.4 g) was dissolved in 50 g of deionized water. To this was added, 50 ml of technical grade ethanol and 12 ml of aqueous ammonia. The solution was stirred for 10 minutes after which an appropriate amount of organosilica precursor was added. The molar composition of the gel was 1 M organosilica precursor: 12.5 M NH_4OH: 54 M EtOH: 0.4 M CTAB: 174 M H_2O. The solution was then stirred for 2 hours at room temperature. The resulting mixture was then transferred into a round bottomed flask and refluxed in a soxhlet at 80 ^oC for an additional 24 hours with stirring. The resulting solid was recovered by filtration, washed with deionized water and air dried in air at room temperature. The as-synthesized materials are designated as AS-TS-CTAB, AS-BMS-CTAB, AS-BS-CTAB and AS-PS-CTAB. See appendix for notations used to identify samples.

3.3.2.2 Surfactant extraction

The surfactant was removed by stirring 1.0 g of as-synthesized sample in 150 ml of ethanol in 3.8 g of 36 % HCl solution at 50 ^oC for 6 hours. The resulting solid was recovered by filtration, washed with ethanol, and dried in air. This extraction procedure was repeated to remove the surfactant completely. This material is referred to as the surfactant extracted material. The

surfactant extracted materials are designated as SE-TS-CTAB, SE-BMS-CTAB, SE-BS-CTAB and SE-PS-CTAB. See appendix for notations used to identify samples.

3.3.3 Synthesis of silica on carbon nanocomposites

Carbonization experiments were performed by heating samples which had been sealed under vacuum in quartz tubes. An appropriate amount of sample (as-synthesized/surfactant extracted) was weighed into a quartz tube. The quartz tube was sealed under vacuum. The tube was heated in an oven from 25 ^{o}C to the required temperatures (700, 800, 900, 1000 or 1100 ^{o}C) at a heating rate of 10 ^{o}C/minute, dwell time of x (5 hours, 1 hour or 30 minutes). The temperature was then lowered to 30 ^{o}C at a heating rate of 10 ^{o}C/minute. Samples were heated in a muffle furnace. Figure 3.2 below shows a picture of the samples in quartz tubes before and after the carbonization process.



Figure 3.2: Pictures showing samples in quartz tubes, white sample before and black sample after the carbonization process.

3.4 Characterization

Characterization of samples was performed using different techniques which included thermogravimetric analysis (TGA), transmission electron microscopy (TEM), High magnification transmission electron microscopy (HMTEM) equipped with EDX, Fourier transform infrared spectroscopy (FTIR), nitrogen sorption, Raman spectroscopy, scanning electron microscopy (SEM), and scanning X-ray photoelectron spectroscopy (SXPS).

3.4.1 Measurements

3.4.1.1 Thermogravimetric analysis (TGA) – Thermal analysis was performed using a Thermogravimetric analyzer (Perkin Elmer Pyris 1 TGA) instrument. The heating rate was 10 ^{o}C/min in both nitrogen and air atmosphere and materials were heated from 30 – 1000 ^{o}C. Thermogravimetric analysis was used to probe the thermal stability as well as the hydrophobicity and hydrophilic character of the hybrid materials.

3.4.1.2 Transmission electron microscopy (TEM) - A JOEL 2010 electron microscope operated at an acceleration voltage of 80 kV for data collection. The TEM technique was used to elucidate the morphology of the carbon-silica nanocomposite materials. To prepare samples for TEM analysis, a small amount of the material was first suspended in absolute alcohol by sonication in an ultrasonication water bath for 10 minutes. A drop of this suspension was then placed onto a carbon – coated 200 mesh copper grid, followed by drying at room temperature.

3.4.1.3 High magnification Transmission Electron Microscopy (High magnification TEM) equipped with EDX – a Philips CM200 electron microscope was used to record EDX spectra

and to take images. This technique was used to determine the elemental composition of carbon-silica nanocomposites. To prepare samples for TEM analysis, a small amount of the material was first suspended in absolute alcohol by sonication in an ultrasonication water bath for 10 minutes. A drop of this suspension was then placed onto a carbon – coated 200 mesh copper grid, followed by drying at room temperature.

3.4.1.4 Fourier transform infrared (FTIR) spectroscopy - FTIR measurements were performed on a Bruker Vector FTIR spectrometer in the range 4000 – 400 cm^{-1}. The FTIR spectra were recorded at room temperature using KBr pellets, 32 scans were signal averaged. FTIR was used to confirm the removal of surfactants and the formation of organosilica materials.

3.4.1.5 Nitrogen adsorption/desorption analysis – A Micrometrics Tristar Surface Area and Pore Analyzer was used to measure N_2 adsorption/desorption isotherms according to the Brunauer, Emmett and Teller (BET) method at -196 ^oC. The samples were degassed using a Micrometrics Flow Prep 060 Sample Degas System at 120 ^oC for 12 hours prior to nitrogen adsorption. The BET surface areas were calculated based on the adsorption data in the relative pressure range of 0.001 – 0.20. Pore size distributions were determined based on the Barrett-Joyner-Halender (BJH) adsorption curve. The pore volumes were estimated at a relative pressure of 0.94, assuming full surface saturation of nitrogen. This technique was used to determine the BET surface area, pore volume, pore size distributions and nitrogen adsorption - desorption isotherms.

3.4.1.6 Raman spectroscopy – Measurements were made using the micro - Raman attachment of a Jobin - Yvon T64000 Raman spectrometer, configured in single spectrograph mode. A grating with 600 grooves / mm was used to disperse the spectrum onto a charge couple device (CCD) detector. The laser spot size on the sample was approximately 1.5 microns in diameter, and the excitation wavelength was 514.5 nm from a green line of an argon ion laser.

3.4.1.7 Scanning electron microscopy (SEM) – Scanning electron microscopy images were recorded on a JSM 840 Scanning electron microscope with an acceleration voltage of 15 kV. This technique was used to observe the external morphologies of the as synthesized and surfactant extracted materials. Samples were prepared by depositing solids onto carbon coated copper grids and sputtering with gold and palladium.

3.4.1.8 Scanning X-ray photoelectron spectroscopy – Elemental composition was determined using Scanning X-ray photoelectron spectroscopy (SXPS). The binding energy was recorded on a Physical electronics quantum 2000 instrument using AlKα X-rays at a power of 20 W. The beam diameter was 100 µm.

3.5 References

[1] W. Guo, J. Park, M. Oh, H. Jeong, W. Cho, I. Kim, C. Ha, *Chemistry of Materials*, **15**, 2296 (2003).

[2] D. Kumar, K. Schumacher, C. du Fresne von Hohenesche, M. Grun, K.K. Unger, *Colloids and Surfaces A: Physicochemical and Engineering Aspects*, **187 – 188**, 110 (2001).

CHAPTER FOUR

RESULTS AND DISCUSSION

4.0 Brief introduction – Overview of chapter

The sol-gel process was used for the synthesis of as-synthesized and surfactant extracted periodic mesoporous organosilica materials. Five different silica sources were used: tetraethyl orthosilicate (TEOS), 1,2-bis(trimethoxysilyl) ethane (BTME), 1,4-bis(triethoxysilyl)benzene (BTEB), 4,4-bis (triethoxysilyl)-1,1 biphenyl (BTEBP) and bis[(3-trimethoxysilyl)propyl]-amine (BTMSPA). Two structure directing agents were used, triblock copolymer (Pluronic P123) and cetyltrimethylammonium bromide (CTAB) (Section 3.0). The chain length of the organic moiety and the nature of the structure directing agents were varied in order to study their effect on the morphology, thermal stability and on the surface properties (namely surface area, pore volume, pore size and pore size distribution) of the materials synthesized. The resulting as-synthesized periodic mesoporous organosilica materials were used as templates for the synthesis of carbon on silica nanocomposites using a simple carbonization process. These samples were characterized by FTIR, TGA, nitrogen physisorption studies and SEM (Section 3.4.2).

Carbon on silica nanocomposites were synthesized by directly carbonizing the organosilica/surfactant phases at different temperatures under an inert atmosphere produced by first sealing the mesoporous silica materials in quartz tubes under vacuum (Section 3.3.3). The carbonization process was done in a muffle furnace. No carbon precursor was impregnated in the pore walls of the mesoporous silica materials before carbonization. This resulted in carbon on silica nanocomposites with various nanostructures (e.g. nanotubes, spheres, etc). To the best of our knowledge, this will be the first report on the direct preparation of carbon on silica nanocomposite materials with various nanostructures being produced by this process. Mokaya *et al* [1] did similar work to this study but there are differences. They obtained their silica/carbon composites by pyrolysis of ethyl-bridged organosilica/surfactant mesophases under an argon

flow. Their silica source was BTME and their SDA was CTAB whereas in this study BTEB, TEOS and BTMSPA were used as silica sources and P123 as the SDA. The following investigations were conducted in this section:

- The effect of carbonization of different hybrid organic-inorganic materials at a constant temperature.
- The effect of variation of carbonization temperature of AS-BS-P123 organosilica materials.
- The effect of variation of carbonization time on the morphology of the resulting carbon on silica nanocomposites produced from AS-PS-P123 organosilica materials.

These samples were characterized by TEM, High magnification TEM, SXPS, TGA, Raman spectroscopy and nitrogen physisorption studies (Section 3.4.2). The results will be reported in the order in which the various studies were done.

4.1 Synthesis of periodic mesoporous organosilica materials

4.1.1 As-synthesized and surfactant extracted periodic mesoporous organosilica materials synthesized using Pluronic P123 as a structure directing agent.

The methodology for the synthesis of the as-synthesized and surfactant extracted periodic mesoporous organosilica materials made using Pluronic P123 as a structure directing agent can be found in section 3.3.1.1 and 3.3.1.2. For sample notations refer to the table of contents.

4.1.1.1 Fourier transform infrared (FTIR) spectroscopy

FTIR spectroscopy was used to detect the presence of organic groups in the as - synthesized and solvent extracted samples (Figures 4.1 - 4.3). The as-synthesized and surfactant extracted samples clearly show absorption bands assigned to Si – C stretching vibrations (*) at 695 and 770 cm^{-1}. Absorption bands which could be attributed to the triblock copolymer (#) at 1347, 1381, 1465, 2904 and 2980 cm^{-1} can only be seen in the spectra of all the as-synthesized samples indicating that the surfactant is almost completely removed by solvent extraction. The small absorption bands at 2903 cm^{-1} of the triblock copolymer Pluronic P123 (#) in the surfactant extracted samples shows that the surfactant is not completely removed. The AS-BMS-P123 and SE-BMS-P123 organosilica samples all show absorption bands at 1272 and 1412 cm^{-1} which are characteristic of C – H deformations vibrations (^). The AS-BS-P123, SE-BS-P123, AS-BPS-P123 and SE-BPS-P123 organosilica samples all show medium absorption bands for C – C stretching vibrations ($) at 1447 and 1598 cm^{-1} and weak absorption bands due to C – H absorption bands (+) at 720 and 812 cm^{-1}. There is an additional weak band at 3025 cm^{-1} indicating also a C – H stretch vibration (+) that indicates the presence of aromatic rings in the sample. The AS-PS-P123 and SE-PS-P123 samples show absorption bands at 3375 and 1645 cm^{-1} due to N – H vibrations (//).

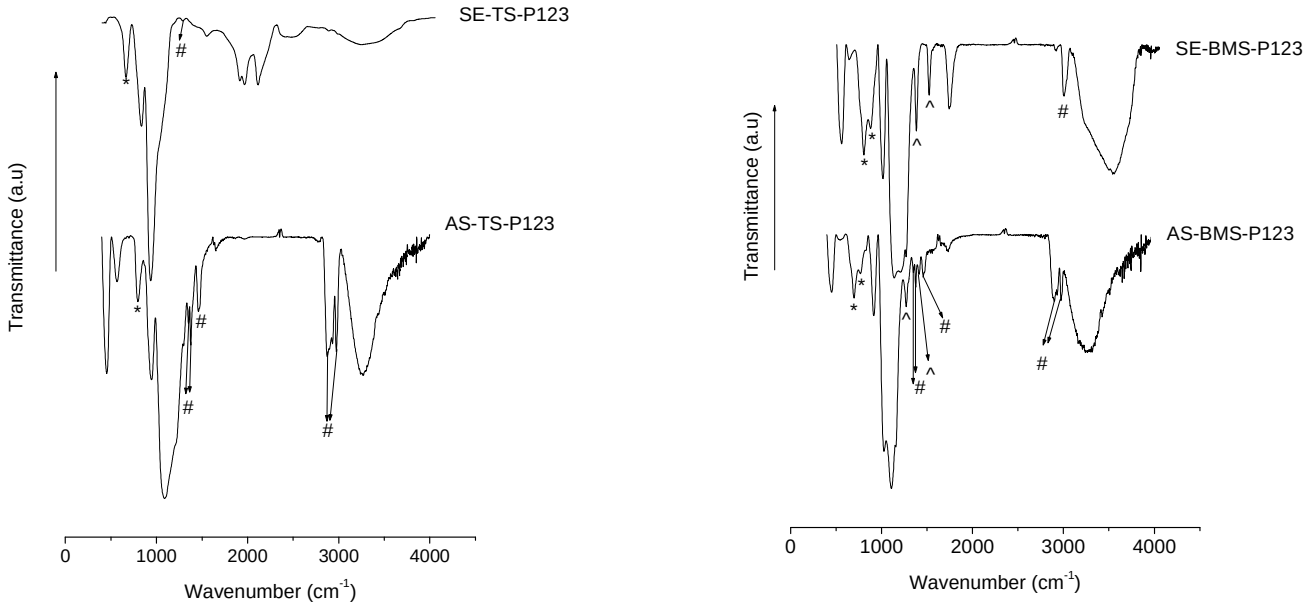

Figure 4.1 FTIR spectra of a) AS-TS-P123 and SE-TS-P123, b) AS-BMS-P123 and SE-BMS-P123 mesoporous silica materials. (*) modes assigned to Si – C stretching vibrations, (#) modes assigned to C – H stretching and deformation vibrations of Pluronic P123 and (^) modes assigned to C – H deformation vibrations of the ethane framework organic groups.

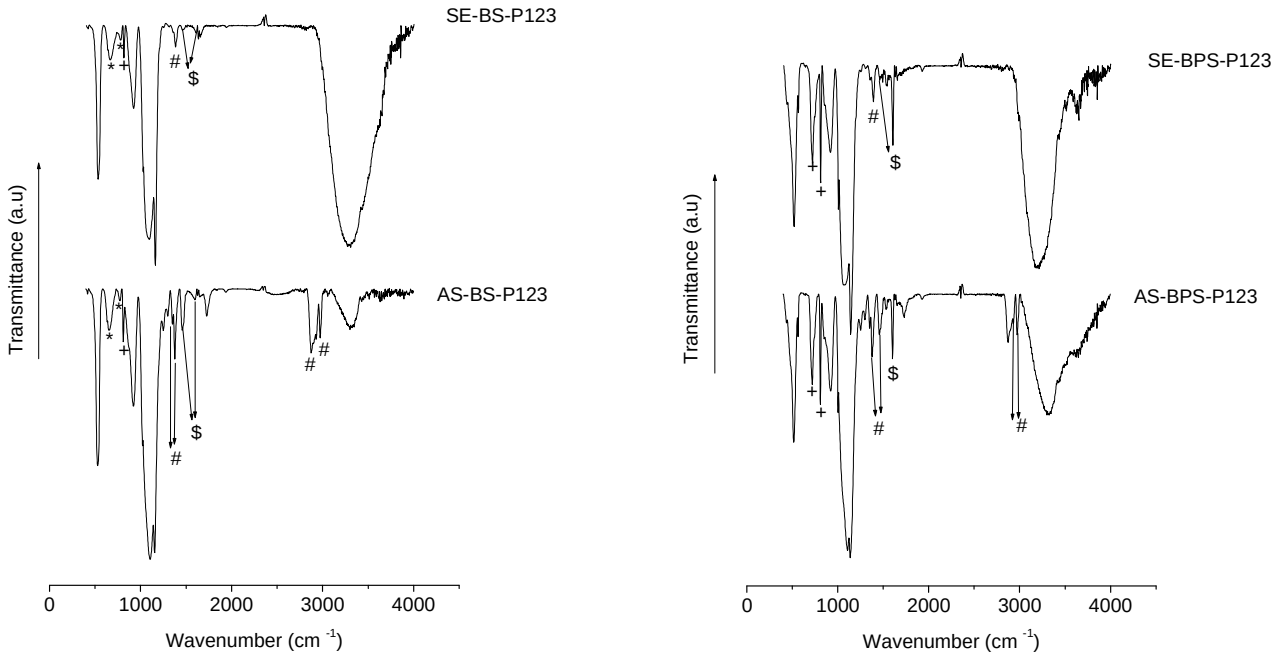

Figure 4.2 FTIR spectra of a) AS-BS-P123 and SE-BS-P123, b) AS-BPS-P123 and SE-BPS-P123 mesoporous silica materials. . (*) modes assigned to Si – C stretching vibrations, (#) modes assigned to C – H stretching and deformation vibrations of Pluronic P123, ($) modes assigned to C – C stretching vibrations of the aromatic ring and (+) modes assigned to C – H absorption bands of the aromatic ring.

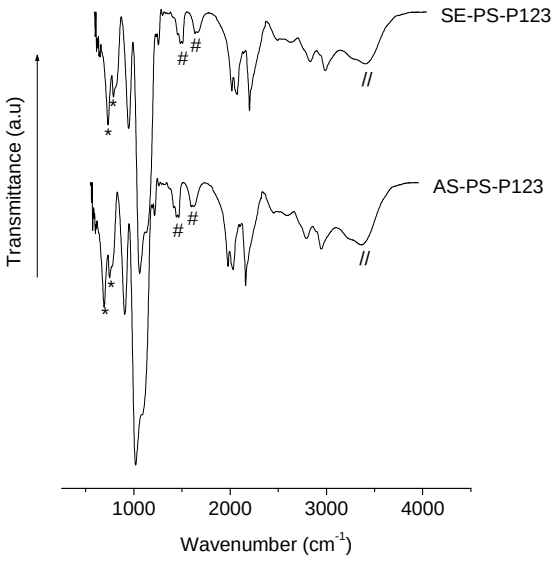

Figure 4.3 FTIR spectra of AS-PS-P123 and SE-PS-P123 mesoporous silica materials. (*) modes assigned to Si – C stretching vibrations, (#) modes assigned to C – H stretching and deformation vibrations of Pluronic P123 and (//) modes assigned to N – H vibrations of the framework organic groups.

4.1.1.2 Thermogravimetric analysis

Samples were analyzed before and after solvent extraction using thermogravimetric analysis (TGA). Analysis was conducted from room temperature to 1000 ^{o}C at a heating rate of 10 ^{o}C/min under a nitrogen atmosphere. The TGA curves of as-synthesized and solvent extracted organosilica materials are shown in Figure 4.4. Explanation of the weight losses shown in the TGA curves is given in Table 4.1. Thermogravimetric analysis was also used to further confirm the removal of P123 upon solvent extraction in the surfactant extracted samples.

AS-TS-P123 shows a sharp significant weight loss of approximately 57 % in the temperature range 203-514 ^{o}C due to surfactant decomposition. SE-TS-P123 shows a small weight loss in the temperature range of 25-100 ^{o}C of 12 % due to physisorbed water and ethanol molecules. There is a small weight loss in the temperature range 100-400 ^{o}C due to surfactant decomposition of approximately 5 %. This shows that the surfactant was nearly completely removed.

The thermogravimetric curve for SE-PS-P123 sample was also obtained. It is similar to that of AS-PS-P123 sample. However evidence that the surfactant had been removed partially in this sample is shown by its FTIR spectrum (Figure 4.3). The increase in BET surface area of SE-PS-P123 sample also shows that some of the surfactant which was blocking the pores was removed. The profiles indicate that the samples are thermally stable.

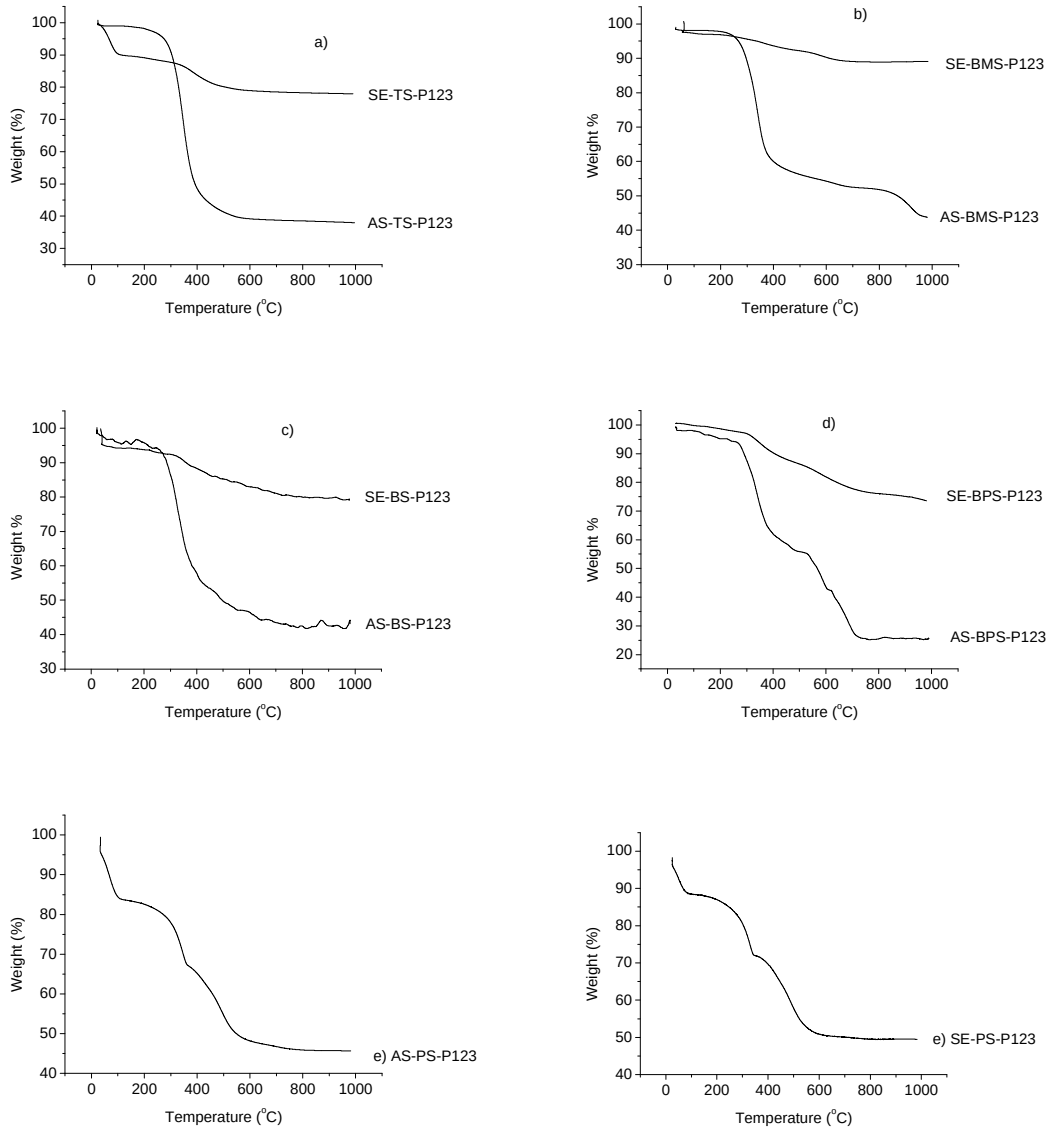

Figure 4.4 TGA curves of a) AS-TS-P123 and SE-TS-P123, b) AS-BMS-P123 and SE-BMS-P123, c) AS-BS-P123 and SE-BS-P123, d) AS-BPS-P123 and SE-BPS-P123 and e) AS-PS-P123 mesoporous silica materials.

Table 4.1 TGA results of as-synthesized and solvent extracted PMOs prepared with Pluronic P123.

Sample	Temperature range (^{o}C)	% Mass loss	Source of mass loss
AS-TS-P123	203 – 514	57	Surfactant decomposition
SE-TS-P123	25 – 100	12	Physisorbed water and ethanol molecules
	100 – 400	5	Surfactant decomposition
AS-BMS-P123	238 – 438	41	Surfactant decomposition
	821 – 1000	7	Matrix decomposition and water from condensation of internal hydroxyls
SE-BMS-P123	228 – 1000	10	Decomposition of surfactant, matrix and water from condensation of internal hydroxyls
AS-BS-P123	20 – 119	3	Desorption of water and ethanol molecules
	255 – 545	47	Surfactant decomposition

Sample	Temperature range (^{o}C)	% Mass loss	Source of mass loss
	545 – 1000	4	Decomposition of matrix and water from condensation of internal hydroxyls
SE-BS-P123	317 – 590	13	Residual surfactant and benzene framework decomposition
AS-BPS-P123	38 – 120	1	Physisorbed water and ethanol molecules
	266 – 401	38	Surfactant decomposition
	527 – 1000	29	Decomposition of organic groups in the fragment of the material
SE-BPS-P123	267 – 1000	13	Decomposition of residual surfactant, breaking of the aromatic groups and water from condensation of internal hydroxyls.
AS-PS-P123	37 – 104	11	Desorption of water and ethanol molecules
	104 – 358	16	Surfactant decomposition

Sample	Temperature range (^{o}C)	% Mass loss	Source of mass loss
	358 – 560	18	Loss of organic groups of bis(propyl)amine in framework
	560 – 1000	4	Loss of water from condensation of internal hydroxyls and matrix decomposition

4.1.1.3 Nitrogen sorption studies

The structural properties of the as-synthesized and surfactant extracted mesoporous organosilicas are listed in Table 4.2. Generally all as-synthesized samples have low surface areas. The reason for the low surface areas is due to the organic groups filling the pores and reducing the area available for nitrogen sorption. This therefore indicates that the as-synthesized composites are not porous powders prior to ethanol extraction. In the surfactant extracted mesoporous organosilicas, the surface areas decrease as the organic group chain length increases. It can be seen that the size of the organic group has an effect on the surface area of the periodic mesoporous organosilica materials formed. The surface areas of solvent extracted samples increase in the order:

SE-TS-P123> SE-BMS-P123 > SE-BS-P123 > SE-BPS-P123 > SE-PS-P123.

From the results of the surface areas of solvent extracted samples, it can be seen that the smaller the chain length of the organosilica precursor, the higher the surface area obtained. It can therefore be concluded that small organic groups (ethane) are more favorable for the synthesis of PMOs with high surface areas followed by rigid organic groups (benzene and biphenyl) and lastly flexible organic groups (bis(propyl)amine). The surface areas obtained for SE-TS-P123, SE-BMS-P123 and SE-PS-P123 are 839.4, 802.3 and 344.3 m^2/g respectively. The surface areas obtained for SE-BS-P123 and SE-BPS-P123 are 527.1 and 386.2 m^2/g respectively.

The pore volumes do not correlate with the increase in size of the organosilica precursor/organotrialkoxysilanes. SE-TS-P123 and SE-BMS-P123 periodic mesoporous organosilica materials have pore diameters which are narrow 3.3 and 3.1 nm. The pore size diameters do not follow any systematic trend as well. The calculated pore diameters for the as-synthesized and surfactant samples of TEOS, BTME, benzene, biphenyl and bis(propyl)amine all

are within the range of mesopores. All samples can be termed mesoporous materials because their pore sizes lie between within 2 and 50 nm.

Table 4.2 Structural properties of as-synthesized and surfactant extracted periodic mesoporous organosilicas synthesized using Pluronic P123 as structure directing agent.

Sample Name	BET Surface Area (m^2/g)	Total Pore Volume (cm^3/g)	Average Pore Diameter (nm)	BJH Adsorption Pore Diameter (nm)	BJH Desorption Pore Diameter (nm)
AS-TS-P123	34.0	0.1	10.9	8.3	4.5
SE-TS-P123	839.4	0.7	3.3	4.5	3.9
AS-BMS-P123	19.7	0.1	11.8	10.6	9.7
SE-BMS-P123	802.3	0.6	3.1	5.2	4.7
AS-BS-P123	57.0	0.3	19.3	17.2	13.7
SE-BS-P123	527.1	0.8	6.2	9.0	7.4
AS-BPS-P123	56.6	0.2	17.1	15.1	13.7
SE-BPS-P123	386.2	0.7	7.7	8.3	8.0
AS-PS-P123	1.2	0.0	20.7	44.0	44.4
SE-PS-P123	344.3	0.7	8.3	7.8	7.3

Nitrogen adsorption-desorption isotherms and the corresponding BJH pore size distributions derived from the isotherms for periodic mesoporous organosilica materials using different organosilica sources and P123 as the structure directing agent are shown in Figures 4.5 – 4.9. The structural properties (BET surface area, pore volume and average pore size diameter) of these materials are listed in Table 4.2. All surfactant extracted samples exhibit Type IV isotherms according to the IUPAC classification, which is typical of mesoporous materials [2]. The type H3 hysteresis loops obtained for all solvent extracted PMOs synthesized using P123 do not exhibit any limiting adsorption at high pressures. Type H3 hysteresis loops are observed with aggregates of plate-like particles giving rise to slit-shaped pores. The AS-TS-P123 sample exhibits a Type IV isotherm, with a H4 hysteresis loop which is attributed to adsorption-desorption in narrow slit – shaped pores. The AS-BMS-P123 sample exhibits Type II reversible isotherms that describe the gas adsorption with a non porous or macroporous solid in which multilayer adsorption involve a strong interaction between adsorbate molecules. All the other as-synthesized materials exhibit Type III isotherms, which originates from both non porous and macroporous solids. These isotherms are characteristic of weak adsorbate-adsorbent interactions. Type H3 hysteresis loops are observed from AS-BMS-P123 to AS-PS-P123 materials.

The pore size distribution derived from the adsorption isotherms of AS-TS-P123, SE-TS-P123, AS-BMS-P123 and AS-PS-P123 materials show one narrow pore size with maxima at 5.7, 1.4, 6.2 and 1.6 nm respectively. AS-TS-P123 and AS-BMS-P123 contain mesopores while SE-TEOS and AS-PS-P123 contains micropores. The pore size distribution of SE-BMS-P123 shows two maxima of 1.1 and 7.7 nm, which indicates a bimodial pore size distribution. The pore size distribution curves for SE-BS-P123, SE-BPS-P123 and SE-PS-P123 organosilica materials contain both mesopores and macropores. The pore size distribution curves for SE-BS-P123, SE-BPS-P123 and SE-PS-P123 mesoporous materials (Figures 4.7b), 4.8b) and 4.9b) respectively) show many maxima for the pore diameters and these do not correlate with those in Table 4.2. This could be due to interparticle absorption in the agglomerates.

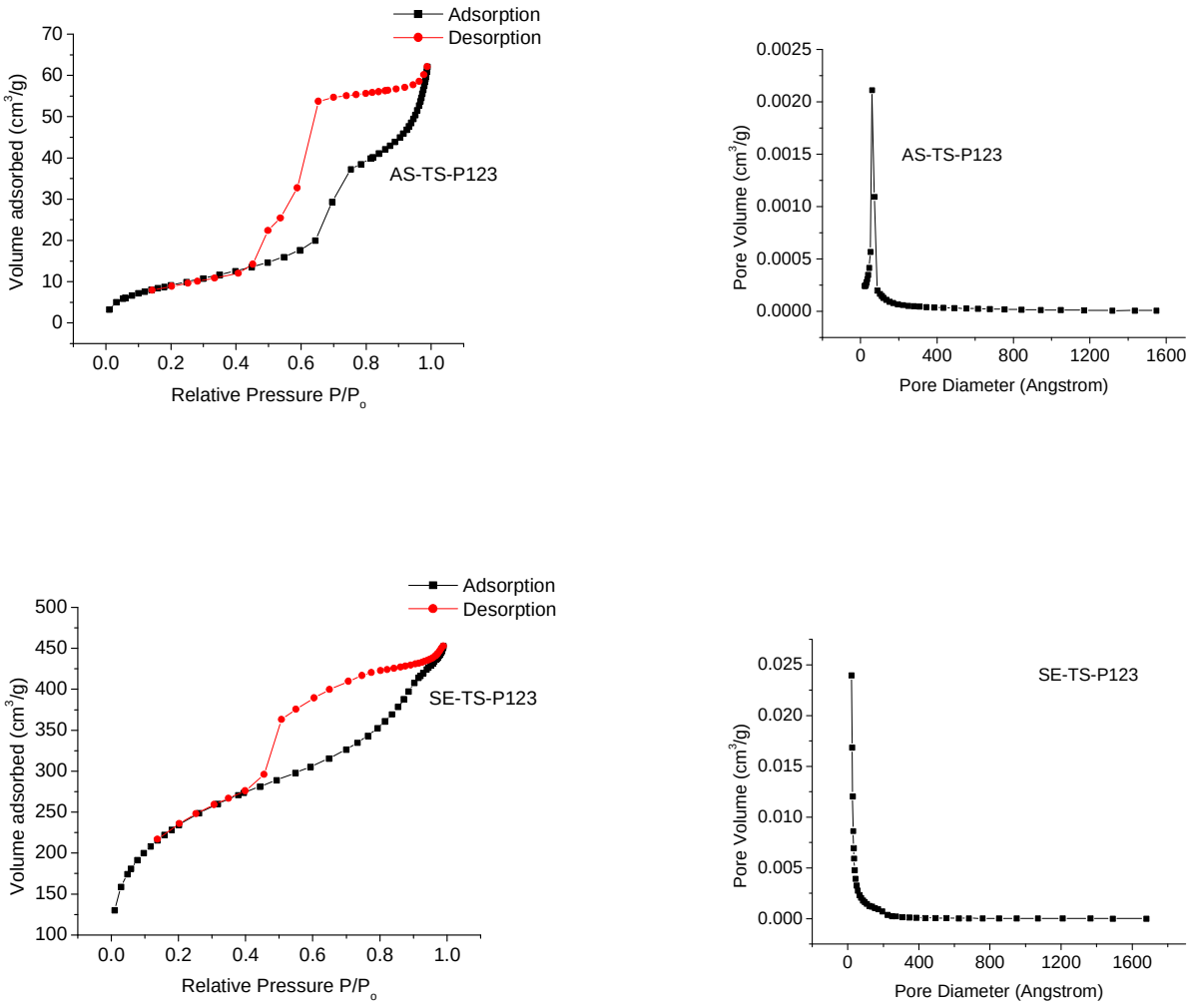

Figure 4.5 Nitrogen adsorption isotherms and the corresponding BJH pore size distribution curves derived from adsorption and desorption isotherms for a) AS-TS-P123 and b) SE-TS-P123 organosilica materials.

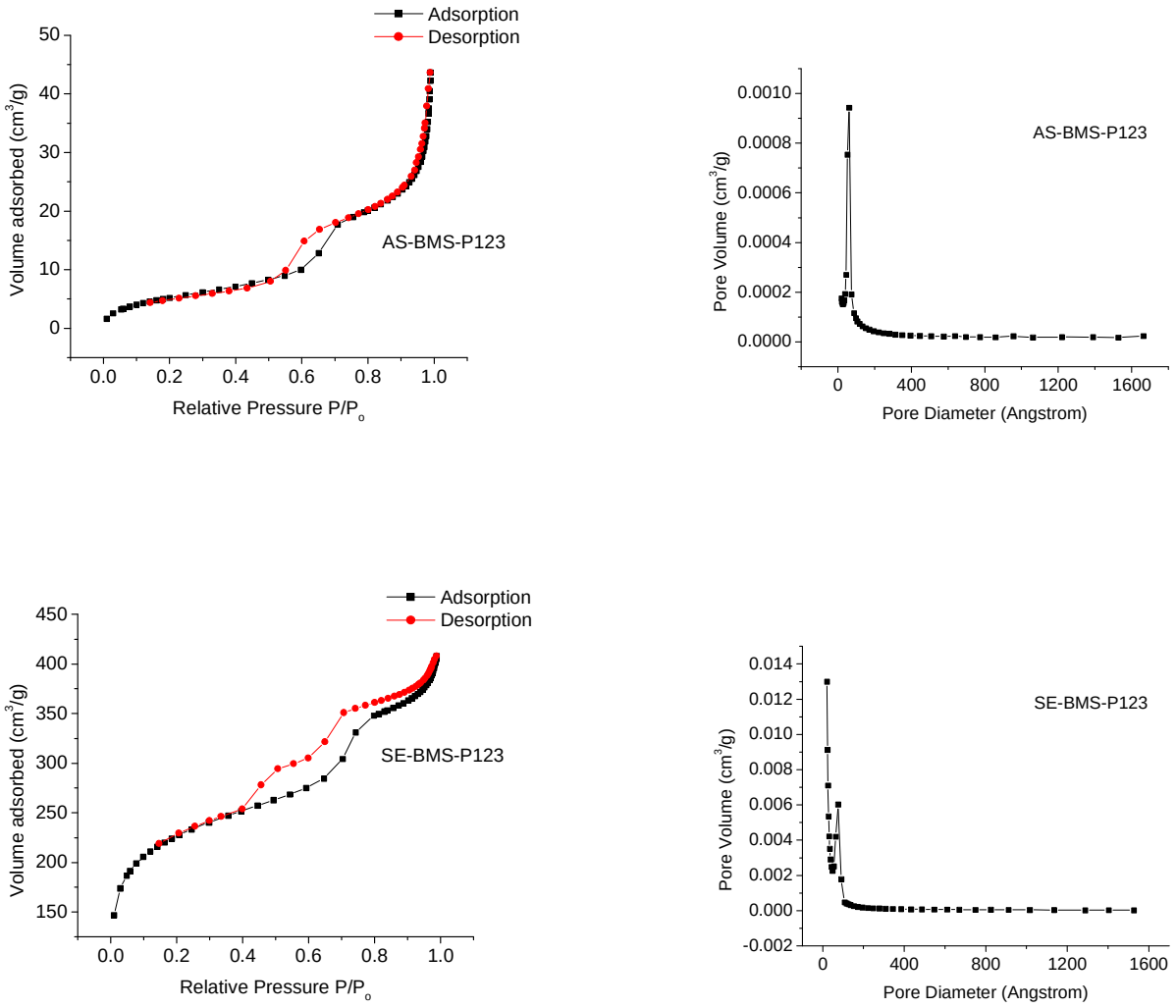

Figure 4.6 Nitrogen adsorption isotherms and the corresponding BJH pore size distributions derived from adsorption and desorption isotherms for a) AS-BMS-P123 and b) SE-BMS-P123 organosilica materials.

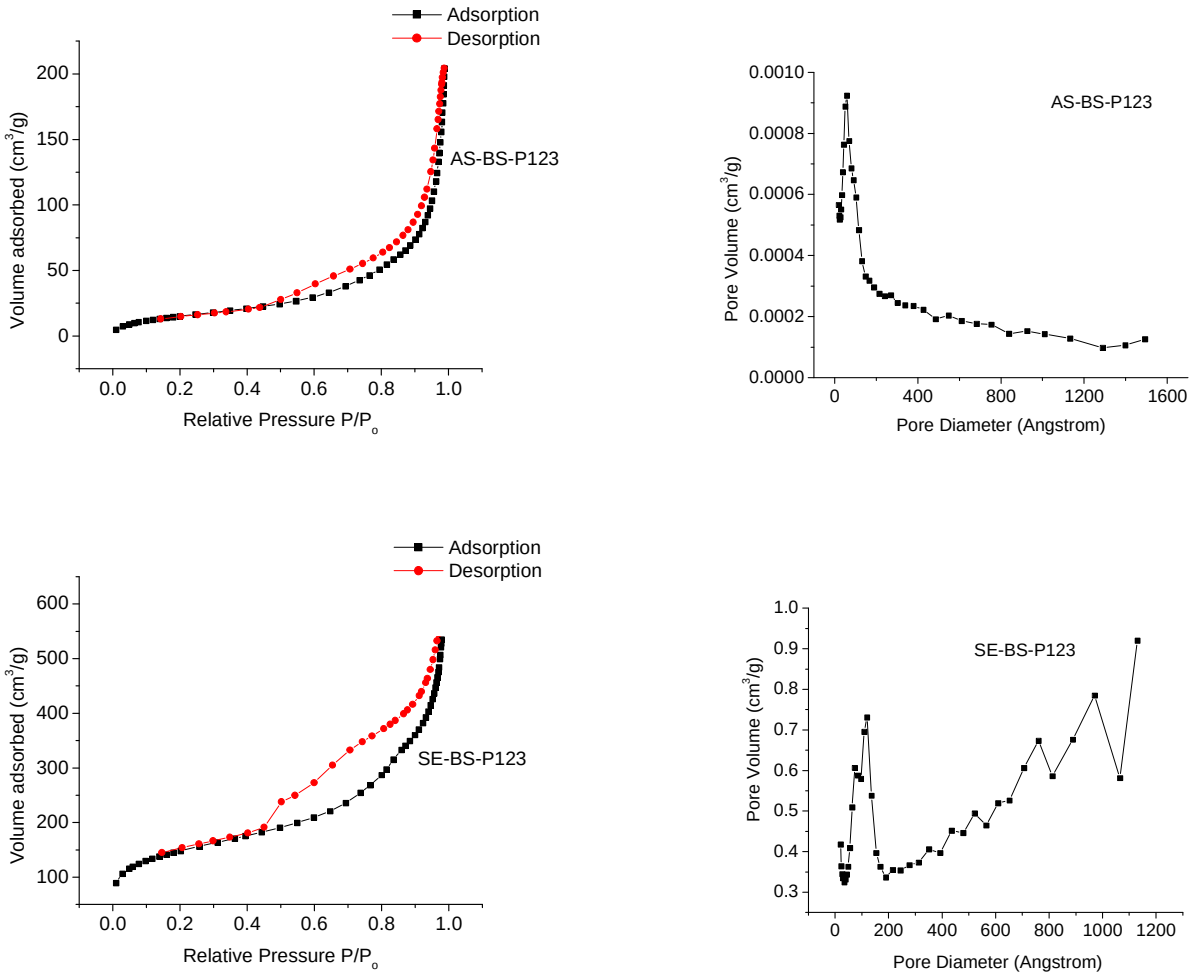

Figure 4.7 Nitrogen adsorption isotherms and the corresponding BJH pore size distributions derived from adsorption and desorption isotherms for a) AS-BS-P123 and b) SE-BS-P123 organosilica materials.

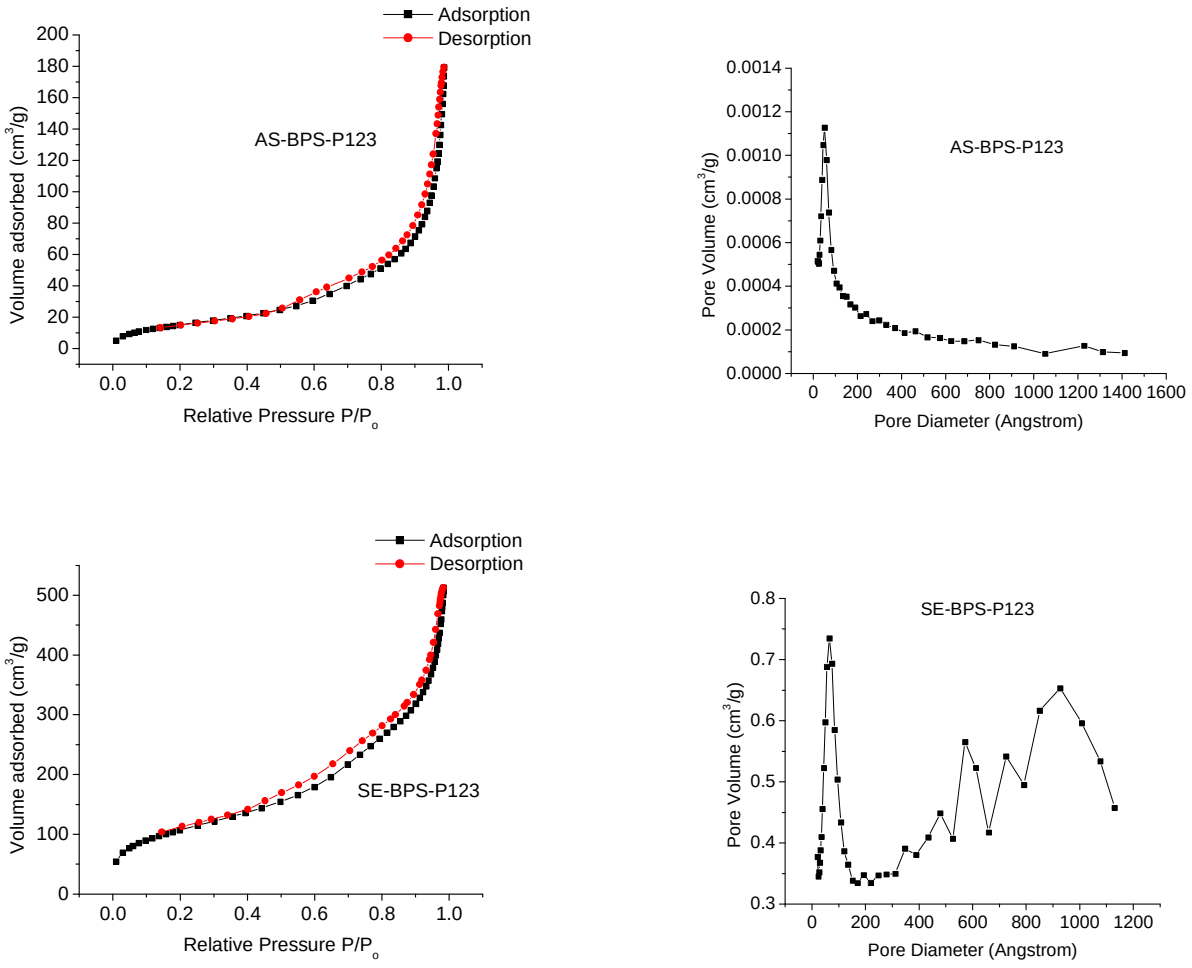

Figure 4.8 Nitrogen adsorption isotherms and the corresponding BJH pore size distributions derived from adsorption and desorption isotherms for a) AS-BPS-P123 and b) SE-BPS-P123 organosilica materials.

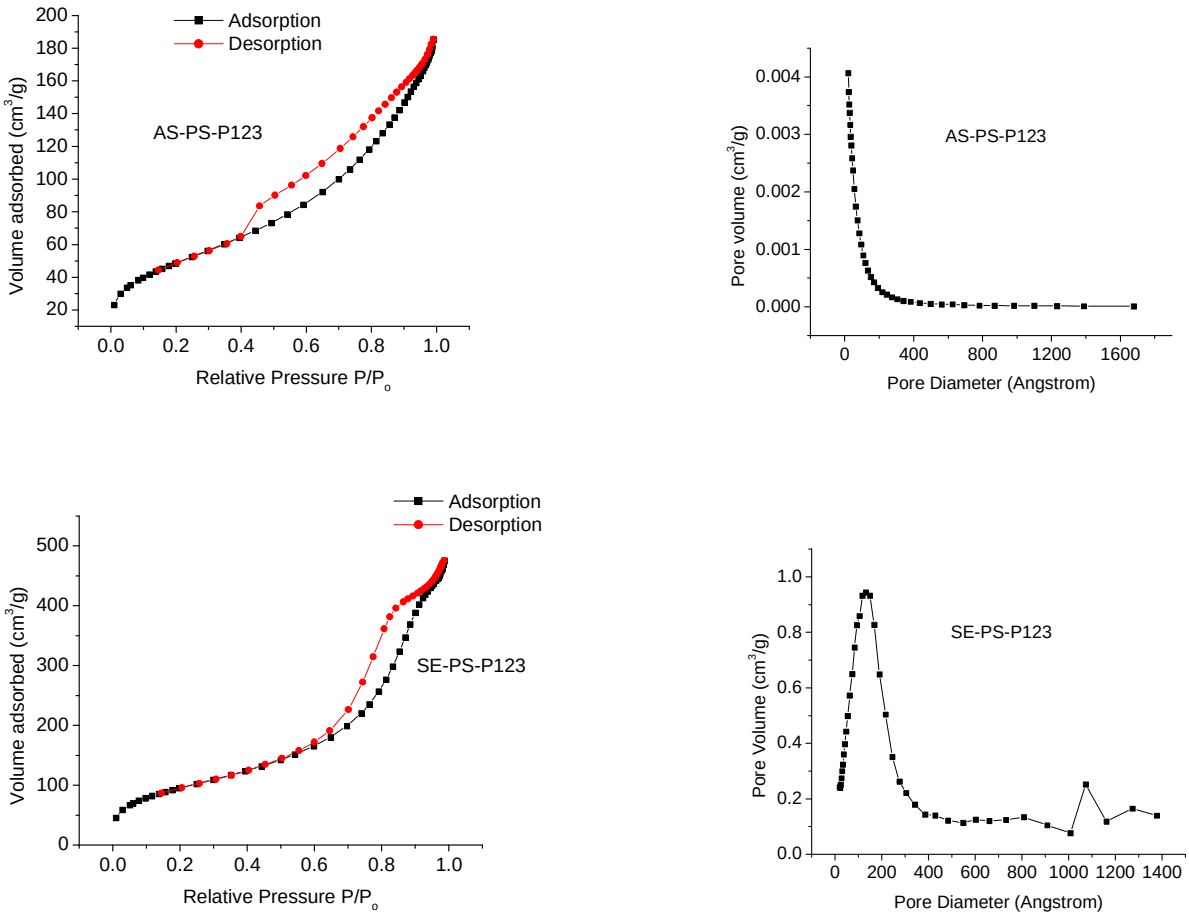

Figure 4.9 Nitrogen adsorption isotherms and the corresponding BJH pore size distributions derived from adsorption and desorption isotherms for a) AS-PS-P123 and b) SE-PS-P123 organosilica materials.

4.1.2 As-synthesized and surfactant extracted periodic mesoporous organosilica materials synthesized using CTAB as structure directing agent.

The methodology for the synthesis of the as-synthesized and surfactant extracted periodic mesoporous organosilica materials made using CTAB as a structure directing agent can be found in section 3.3.2.1 and 3.3.2.2. For sample notations refer to the table of contents.

4.1.2.1 Fourier transform infrared (FTIR) spectroscopy

FTIR spectroscopy was used to detect the presence of organic groups in the as-synthesized and solvent extracted samples synthesized using CTAB as a structure directing agent (Figures 4.10 and 4.11). The as-synthesized and surfactant extracted samples clearly show absorption bands assigned to Si – C stretching vibrations (*) at 786 cm^{-1}. Absorption bands which could be attributed to CTAB (#) at 1096, 1230, 2846 and 2930 cm^{-1} can only be seen in the spectra of all the as-synthesized samples indicating that the surfactant has been removed by solvent extraction. The AS-BMS-CTAB and SE-BMS-CTAB organosilica samples show absorption bands at 1272 and 1412 cm^{-1} which are characteristic of C – H deformations vibrations (^). The AS-BS-CTAB and SE-BS-CTAB organosilica samples show medium absorption bands of C – C stretching vibrations ($) at 1407 and 1499 cm^{-1} and strong absorption bands of C – H stretching (+) at 779 and 804 cm^{-1}. There is an additional weak band at 3025 cm^{-1} also indicating a C – H stretch vibration (+). These bands indicate the presence of aromatic rings in the sample. The AS-PS-CTAB and SE-PS-CTAB samples show an absorption band at 1649 cm^{-1} due to a N – H bend (//).

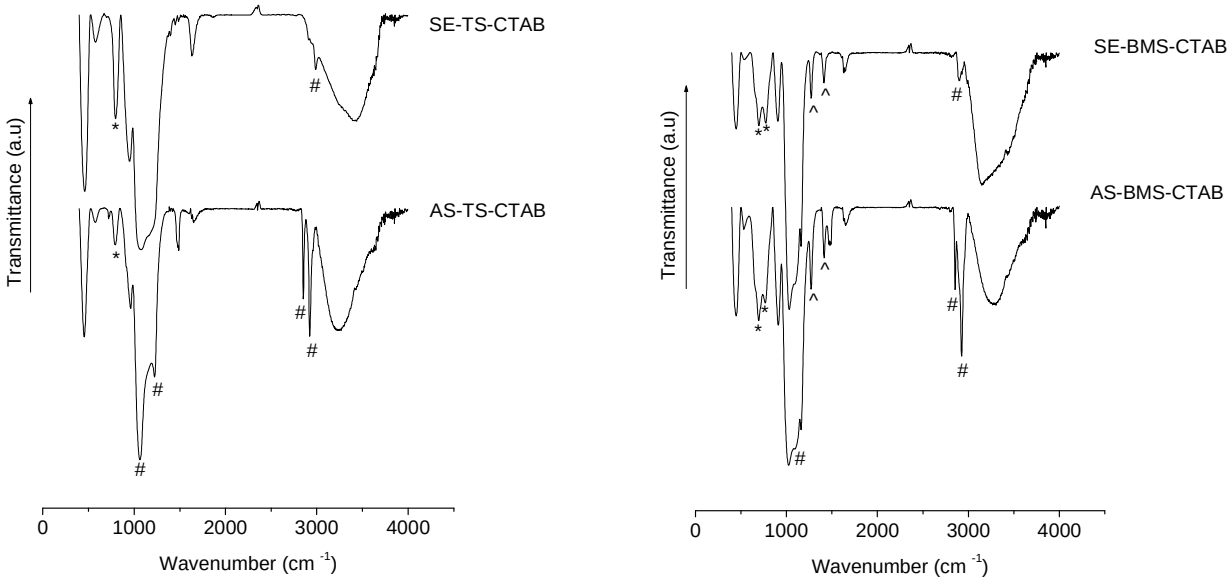

Figure 4.10 FTIR spectra of a) AS-TS-CTAB and SE-TS-CTAB and b) AS-BMS-CTAB and SE-BMS-CTAB mesoporous silica materials. (*) modes assigned to Si – C stretching vibrations, (#) modes assigned to C – H stretching and deformation vibrations of CTAB and (^) modes assigned to C – H deformations vibrations of the framework organic group.

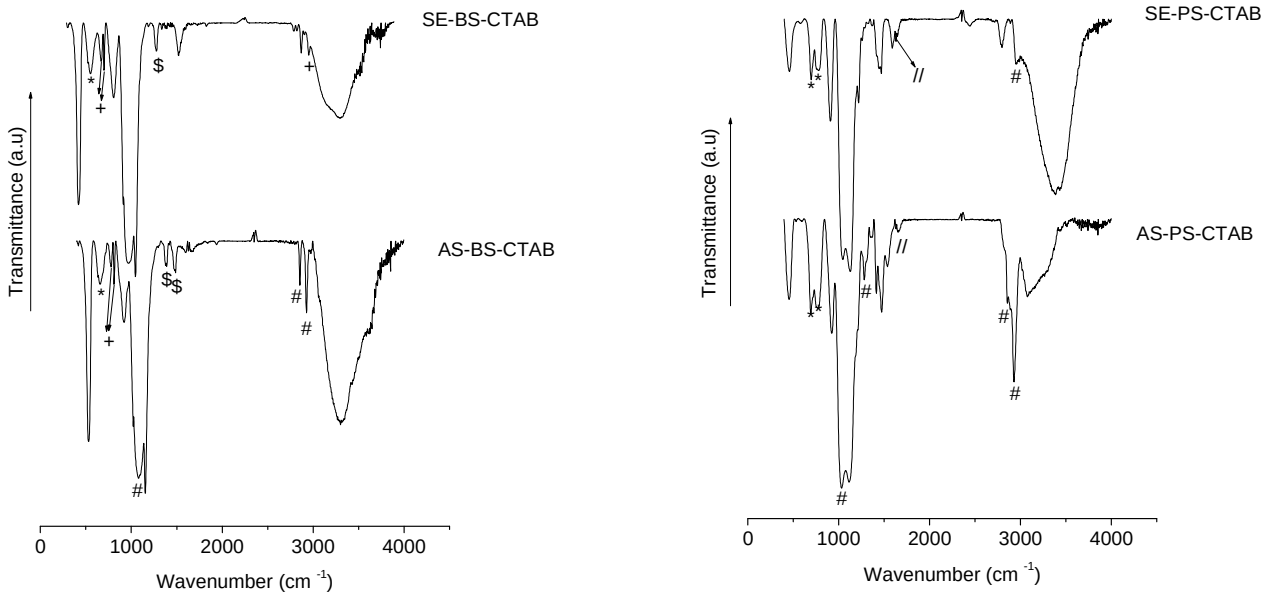

Figure 4.11 FTIR spectra of a) AS-BS-CTAB and SE-BS-CTAB and b) AS-PS-CTAB and SE-PS-CTAB mesoporous silica materials. (*) modes assigned to Si – C stretching vibrations, (#) modes assigned to C – H stretching and deformation vibrations of CTAB, ($) modes assigned to C – C stretching vibrations of the aromatic ring, (+) modes assigned to C – H stretching vibrations of the aromatic ring and (//) modes assigned to N – H bend vibrations.

4.1.2.2 Thermogravimetric analysis

Samples were analysed before and after solvent extraction using thermogravimetric analysis (TGA). Analysis was conducted from room temperature to 1000 ^{o}C at a heating rate of 10 ^{o}C/ minute under a nitrogen atmosphere. The TGA curves of as-synthesized and surfactant extracted samples are shown in Figure 4.12.

AS-TS-CTAB shows a small weight loss in the temperature range of 54-132 ^{o}C of 5 % due to the desorption of water and ethanol molecules. There is a sharp significant weight loss of approximately 33 % in the temperature range 132-292 ^{o}C due to surfactant decomposition. SE-TS-CTAB shows a small weight loss in the temperature range of 67-558 ^{o}C of 8 % due to physisorbed water and ethanol molecules and residual surfactant decomposition.

AS-BS-CTAB shows a sharp weight loss of approximately 50% at 30 ^{o}C which is due to an instrumental error. The thermogravimetric curve for SE-PS-CTAB sample (not shown) was also obtained. It was not shown because it is similar to that of AS-PS-CTAB sample, but however evidence that the surfactant was removed partially in this sample is shown by FTIR spectroscopy and the increase in BET surface area of SE-PS-CTAB sample which shows that some of the surfactant which blocked the pores was removed.

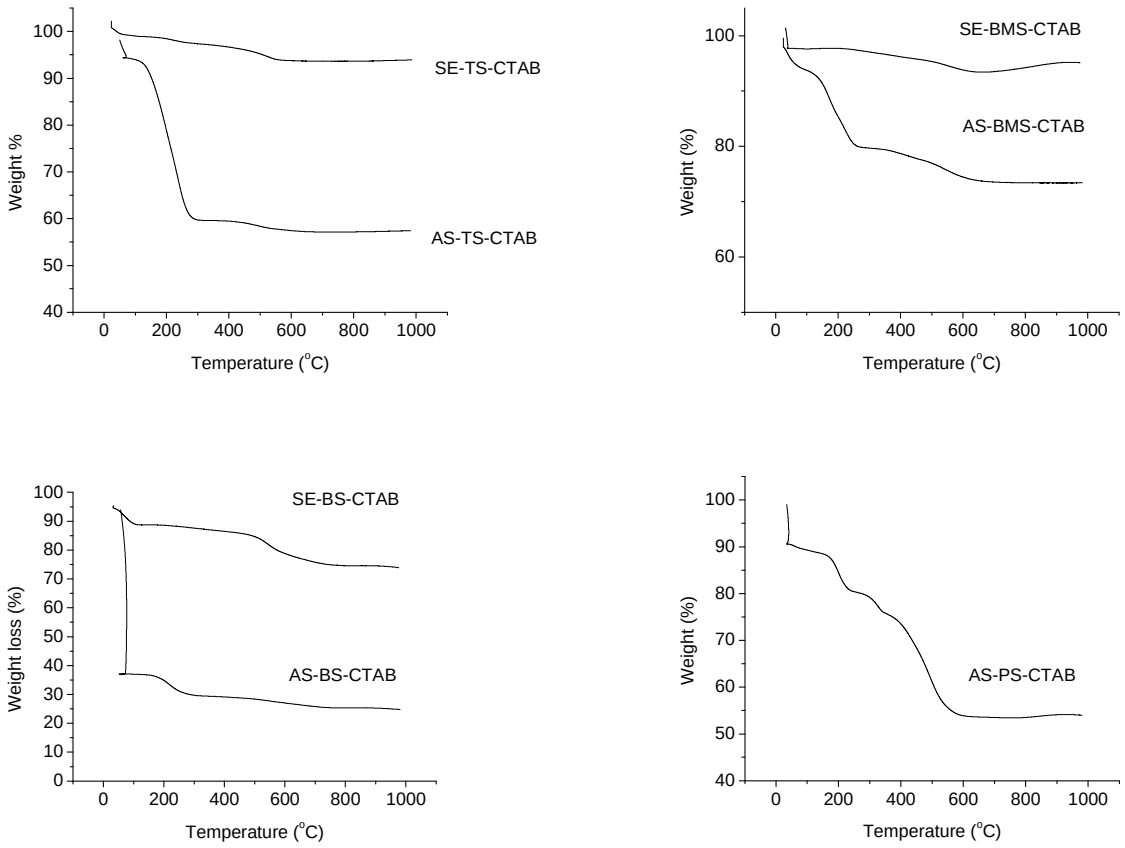

Figure 4.12 TGA curves of a) AS-TS-CTAB and SE-TS-CTAB, b) AS-BMS-CTAB and SE-BMS-CTAB, c) AS-BS-CTAB and SE-BS-CTAB, d) AS-PS-CTAB mesoporous silica materials.

Table 4.3 TGA results of as synthesized and solvent extracted PMOs prepared with CTAB as SDA.

Sample	Temperature range (^{o}C)	% Mass loss	Source of mass loss
AS-TS-CTAB	54 – 132	5	Desorption of water and ethanol molecules
	132 - 292	33	Surfactant decomposition
SE-TS-CTAB	67 – 558	8	Desorption of water and ethanol molecules, residual surfactant decomposition
AS-BMS-CTAB	31 - 127	4	Desorption of water
	127 - 264	13	Surfactant decomposition
	264 – 668	6	Matrix decomposition and water from condensation of internal hydroxyls
SE-BMS-CTAB	52 - 652	9	Decomposition of matrix and residual surfactant
AS-BS-CTAB	168 – 265	6	Surfactant decomposition
	265 – 714	5	Matrix decomposition and water from condensation of internal hydroxyls

Sample	Temperature range (^{o}C)	% Mass loss	Source of mass loss
SE-BS-CTAB	37 – 102	5	Desorption of water and ethanol molecules
	102 – 498	4	Surfactant decomposition
	498 – 750	10	Residual surfactant decomposition and water from condensation of internal hydroxyls.
AS-PS-CTAB	164 – 291	9	Surfactant decomposition
	291 – 571	25	Loss of organic groups of bis(propyl)amine in the framework, loss of water from condensation of internal hydroxyls and matrix decomposition

4.1.2.3 Nitrogen sorption studies

The structural properties (BET surface area, pore volume and average pore diameter) of the as-synthesized and solvent extracted mesoporous materials are shown in Table 4.4. The BJH pore diameters derived from adsorption and desorption isotherms are also listed in Table 4.4. All as-synthesized samples have low surface areas when compared to those of the respective surfactant extracted samples. This is due to the organic groups occupying a significant amount of space in the interior of the pores and hence less area is available for nitrogen sorption. In the surfactant extracted samples the BET surface areas decrease as the chain length of the organic groups increases. SE-TS-CTAB, SE-BMS-CTAB and SE-PS-CTAB have surface areas of 947.4, 901.1 and 331.6 m^2/g respectively. TEOS has no organic groups, BTME has two CH_2 chains and Propylamine has six CH_2 chains attached to a NH_2 group making it very flexible, hence as given the lower BET surface area. However SE-BS-CTAB mesoporous material was an exception, it had the largest BET surface area of 928.6 m^2/g.

The pore volumes increase as the chain length increases from AS-TS-CTAB < AS-BMS-CTAB < AS-BS-CTAB. However an exception is AS-PS-CTAB which has the lowest pore volume. The surfactant extracted samples have larger pore volumes compared to the corresponding as-synthesized materials. AS-TS-CTAB, AS-BMS-CTAB, AS-BS-CTAB and AS-PS-CTAB have total pore volumes of 0.16, 0.18, 0.52 and 0.04 cm^3/g respectively.

Table 4.4 Structural properties of as-synthesized and surfactant extracted PMOs synthesized using CTAB as a structure directing agent.

Sample Name	BET Surface Area (m^2/g)	Total Pore Volume (cm^3/g)	Average Pore Diameter (nm)	BJH Adsorption Pore Diameter (nm)	BJH Desorption Pore Diameter (nm)
AS-TS-CTAB	37.6	0.2	17.1	18.6	19.7
SE-TS-CTAB	947.4	0.9	3.8	3.3	3.3
AS-BMS-CTAB	120.1	0.2	6.0	6.0	5.7
SE-BMS-CTAB	901.1	0.6	2.7	3.5	3.5
AS-PS-CTAB	21.7	0.0	7.3	5.5	5.9
SE-PS-CTAB	331.6	0.2	2.9	3.2	3.2
AS-BS-CTAB	76.3	0.5	27.0	27.8	27.9
SE-BS-CTAB	928.6	1.8	7.8	18.9	18.4

Nitrogen adsorption-desorption isotherms and BJH pore size distribution curves derived from adsorption or desorption isotherms of as-synthesized and surfactant extracted organosilica materials are shown in Figures 4.13 – 4.16. All solvent extracted samples exhibit Type IV isotherms which are characteristic of mesoporous materials, except for SE-BS-CTAB material which exhibits Type I isotherm which is characteristic of materials with cylindrical pores, and have pore sizes in the microporous range [2]. The BJH pore size distribution of SE-BS-CTAB further confirms that the sample contains micropores with maxima of 1.85 nm. The following types of Hysteresis loops were observed: Type H3 for AS-TS-CTAB, AS-BS-CTAB, SE-BS-CTAB and AS-PS-CTAB (aggregates of plate like particles giving rise to slit – shaped pores) and Type H4 for SE-TS-CTAB, AS-BMS-CTAB, SE-BMS-CTAB and SE-PS-CTAB (narrow slit – like pores). AS-TS-CTAB, AS-BS-CTAB and AS-PS-CTAB exhibit Type I isotherms which are characteristic of microporous materials.

The pore size distribution derived from the adsorption isotherms of AS-TS-CTAB, SE-TS-CTAB, SE-PS-CTAB and AS-PS-CTAB show one narrow pore size with maxima at 107.2, 4.9, 2.2 and 2.2 nm respectively. AS-TS-CTAB contains macropores. SE-TS-CTAB, AS-PS-CTAB and SE-PS-CTAB contain mesopores while AS-BS-CTAB contains a mixture of mesopores and micropores. The pore size distribution curve of SE-BMS-CTAB shows one maxima of 3.6 nm, indicating that the sample contains mesopores. The pore size distribution curves for AS-BMS-CTAB also contains mesopores and macropores. The pore size distribution curves for AS-TS-CTAB, AS-BMS-CTAB, AS-BS-CTAB and SE-BS-CTAB mesoporous materials (Figures 4.15a, 4.14a, 4.17a and 4.17b respectively) show maxima for the pore diameters and these do not correlate with those in Table 4.4. This could be due to interparticle absorption in the agglomerates.

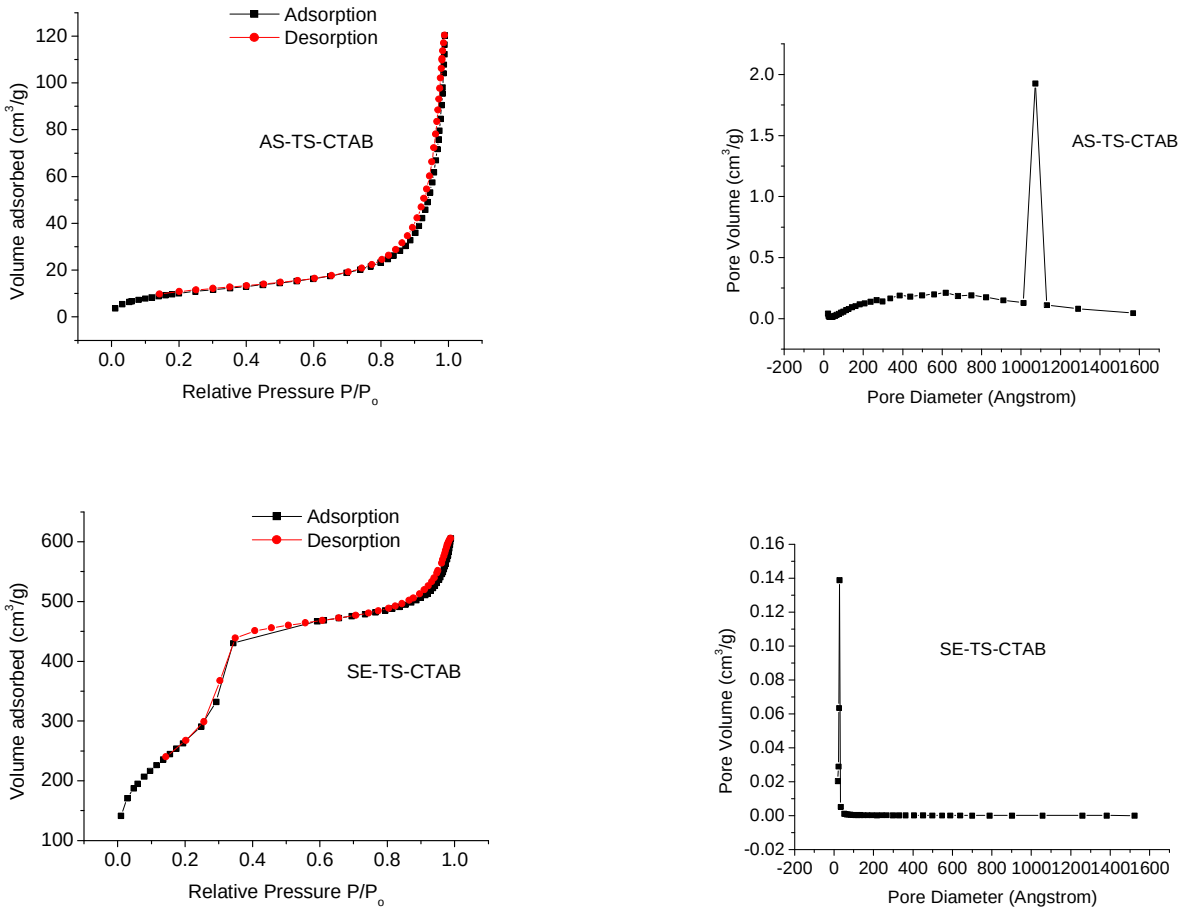

Figure 4.13 Nitrogen adsorption isotherms and the corresponding BJH pore size distributions derived from adsorption and desorption isotherms for a) AS-TS-CTAB and b) SE-TS-CTAB organosilica materials.

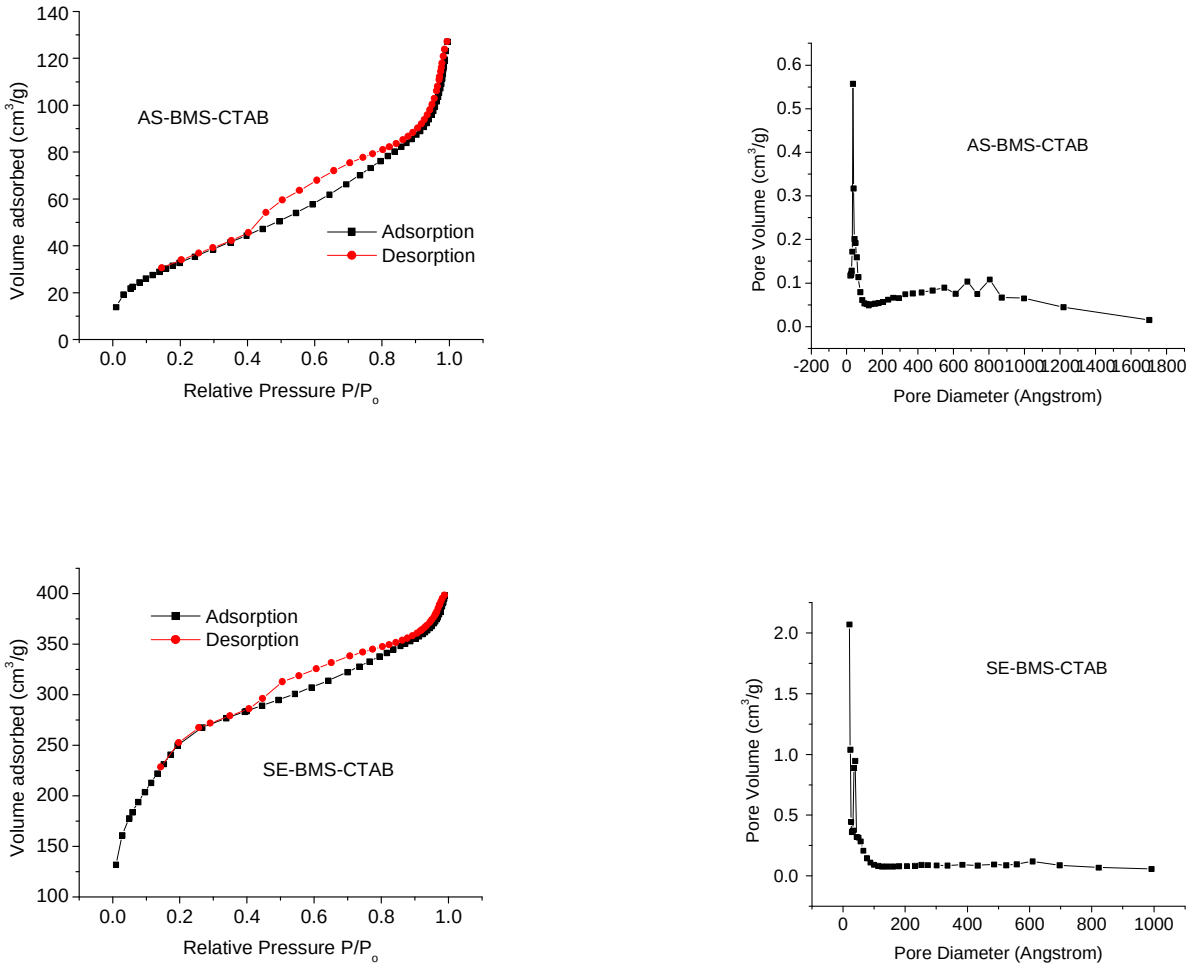

Figure 4.14 Nitrogen adsorption isotherms and the corresponding BJH pore size distributions derived from adsorption and desorption isotherms for a) AS-BMS-CTAB and b) SE-BMS-CTAB organosilica materials.

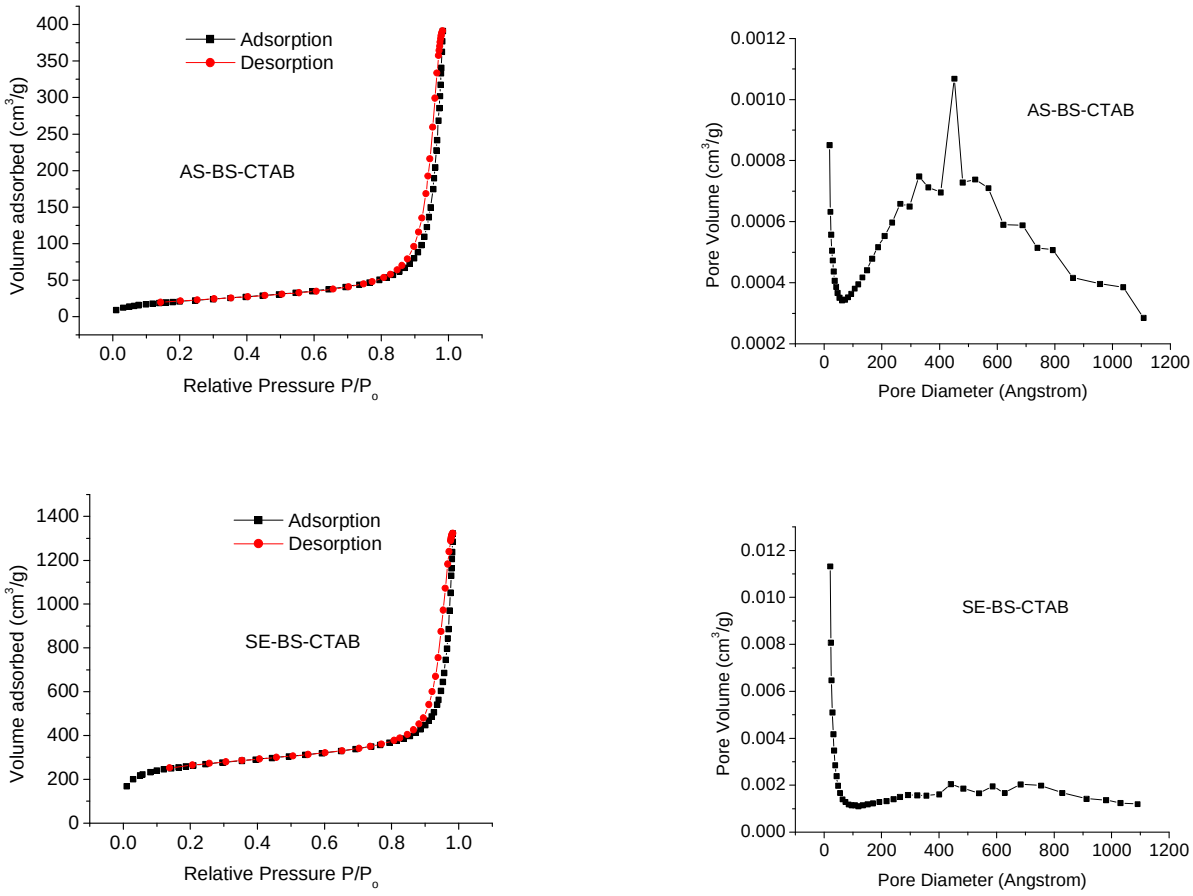

Figure 4.15 Nitrogen adsorption isotherms and the corresponding BJH pore size distributions derived from adsorption and desorption isotherms for a) AS-BS-CTAB and b) SE-BS-CTAB organosilica materials.

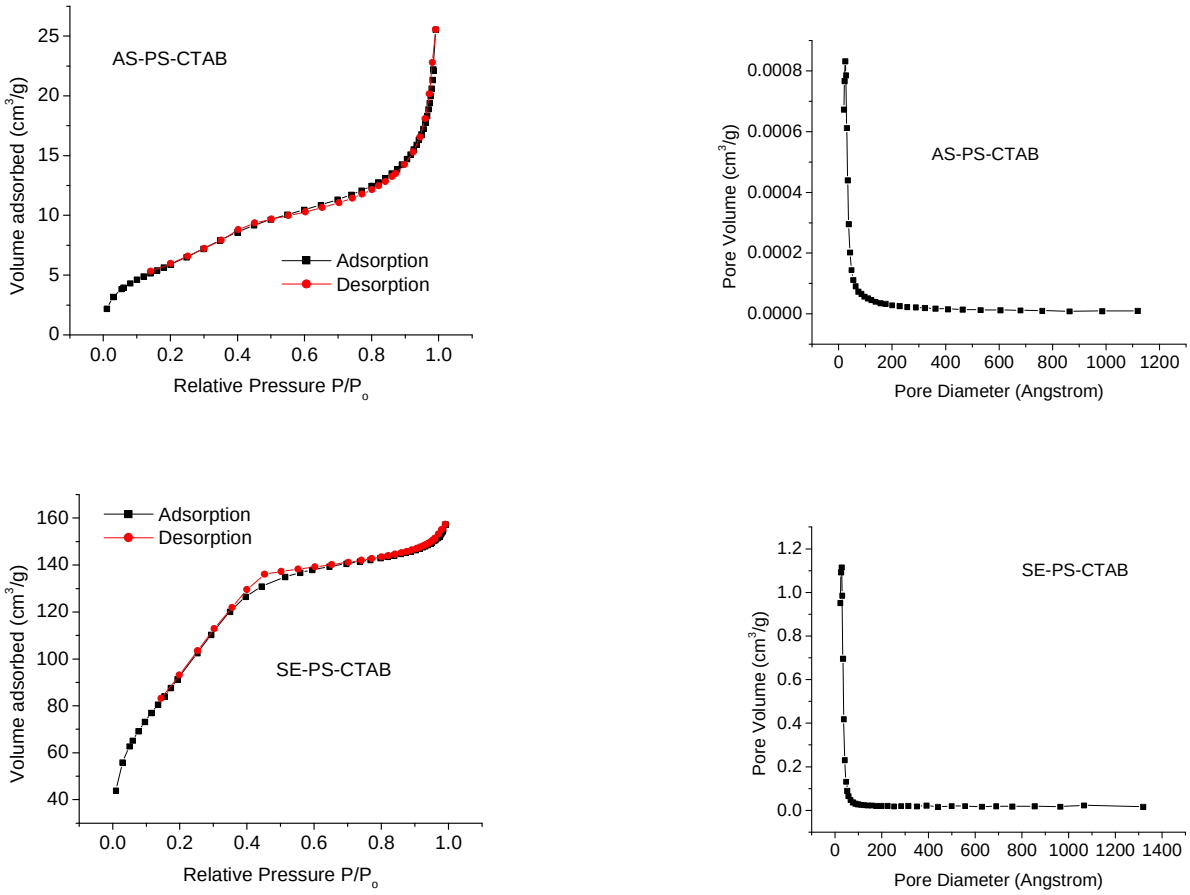

Figure 4.16 Nitrogen adsorption isotherms and the corresponding BJH pore size distributions derived from adsorption and desorption isotherms for a) AS-PS-CTAB and b) SE-PS-CTAB organosilica materials.

4.1.3 Summary of results

FTIR spectroscopy and thermogravimetric analysis confirm the formation of organosilica materials and show that the surfactants Pluronic P123 and CTAB were removed by solvent extraction. The use of the surfactant Pluronic P123 produced periodic mesoporous organosilica materials which had surface areas which followed a systematic trend. It was seen that the size of the organic group had an effect on the surface area obtained on the periodic mesoporous organosilica materials produced. From the results of the surface areas of solvent extracted samples, it was observed that the smaller the chain length of the organosilica precursor, the higher the surface area obtained. It can therefore be concluded that small organic groups (ethane) are more favorable for synthesizing PMOs with high surface areas followed by rigid organic groups (benzene and biphenyl) and lastly flexible organic groups (bis(propyl)amine). The surface areas obtained for SE-TS-P123, SE-BMS-P123 and SE-PS-P123 are 839.4, 802.3 and 344.3 m^2/g respectively. The surface areas of SE-BS-P123 and SE-BPS-P123 were 527.1 and 386.2 m^2/g respectively.

The use of the surfactant CTAB yielded periodic mesoporous organosilica materials which followed a systematic trend, with the exception of SE-BS-CTAB. In the surfactant extracted samples the BET surface areas decrease as the chain length of the organic groups increased. SE-TS-CTAB, SE-BMS-CTAB and SE-PS-CTAB have surface areas of 947.4, 901.1 and 331.6 m^2/g respectively. TEOS has no organic groups, BTME has two CH_2 chains and bis(propyl)amine has six CH_2 chains attached to a NH_2 group making it very flexible hence yielding the lower BET surface area. However SE-BS-CTAB mesoporous material was an exception, it had the largest BET surface area of 928.6 m^2/g. It is evident from BET that the surfactant extracted materials are porous but the structural periodicity must have been confirmed by low angle XRD. Low angle XRD was not done for all the surfactant extracted periodic mesoporous organosilica samples formed due to inadequate resources.

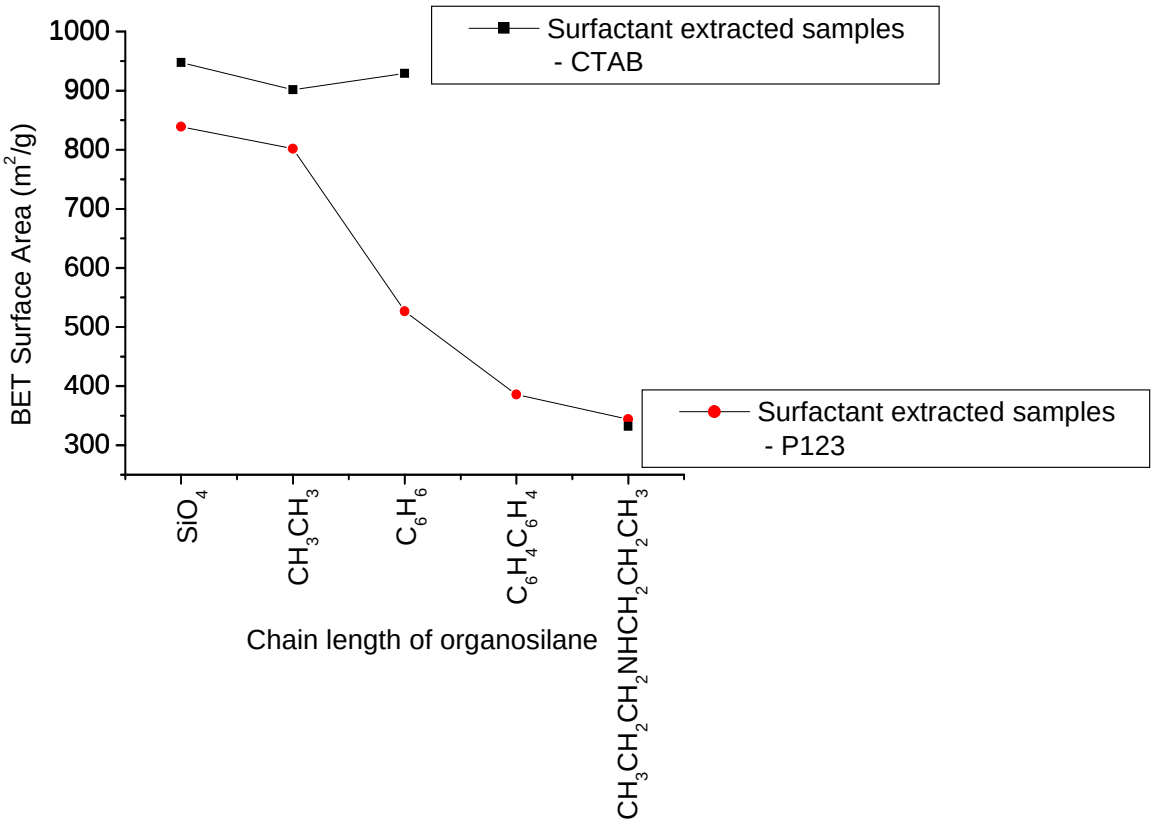

Figure 4.17 Graph showing the correlation between BET surface and the chain length of the organosilane.

From Figure 4.17, it is shown clearly that the surface areas increase as the chain length of the organosilane is decreased for periodic mesoporous organosilanes synthesized using P123 as the structure directing agent. PMOs synthesized using Pluronic P123 as the structure directing agent have lower surface areas than those obtained using CTAB. No PMOs were formed in this study using 4,4-Bis (triethoxysilyl)-1,1 biphenyl as the organosilica precursor and CTAB as the structure directing agent although there was one synthesized in literature. SE-TS-P123 and SE-TS-CTAB had the highest surface areas followed by SE-BMS-P123 and SE-BMS-CTAB. However SE-BS-CTAB had a higher surface area than SE-BMS-CTAB. This was higher than

what was anticipated. It shows that 1,4-Bis (triethoxysilyl) benzene forms PMOs with better structural properties when CTAB as the structure directing agent is used. It can therefore be concluded that CTAB is a better structure directing agent for synthesizing PMOs with better structural properties than CTAB.

4.2 Synthesis of carbon on silica nanocomposite materials

4.2.1 Investigation of the effect of carbonization of different organic – inorganic hybrid materials at a constant temperature.

Three types of as-synthesized mesoporous silica materials were used for this investigation. They each contained different silica sources (TEOS, BTEB and BTMSPA) and were made with the same structure directing agent P123. The as-synthesized samples were sealed under vacuum and carbonized at 1000 ^{o}C for 5 hours. The effect of using the different silica sources was investigated. Refer to section 3.3.3 for methodology and table of contents for notations of symbols.

4.2.1.1 Transmission electron microscopy

Representative TEM images of AS-T-CS 1000 ^{o}C/5 h, AS-B-CS 1000 ^{o}C/5 h and AS-P-CS 1000 ^{o}C/5 h samples are shown in Figures 4.18 – 4.20. TEM images of AS-T-CS 1000 ^{o}C/5 h have confirmed that nearly all of the carbon on silica nanotubes formed are bamboo shaped with no straight carbon nanotubes. The bamboo nanotubes had varying shapes. These were produced in the absence of nitrogen. AS-P-CS 1000 ^{o}C/5 h produced multiwalled carbon on silica nanotubes with very thick internal diameters of between 160 – 170 nm, carbon spheres with average

diameters of 400 nm and amorphous carbon material. AS-P-CS 1000 ^{o}C/5 h surprisingly did not produce bamboo shaped nanostructures even though it contained nitrogen atoms. This might

have been caused by the amount of nitrogen content in the sample being insufficient for the production of the bamboo structure. TEM investigation of AS-B-CS 1000 ^{o}C/5 h samples revealed the presence of carbon on silica nanotubes among the various amorphous carbonaceous materials. The carbon on silica nanotubes obtained for AS-B-CS 1000 ^{o}C/5 h had very thin internal diameters and were long compared to the thick carbon on silica nanotubes obtained for AS-P-CS 1000 ^{o}C/5 h.

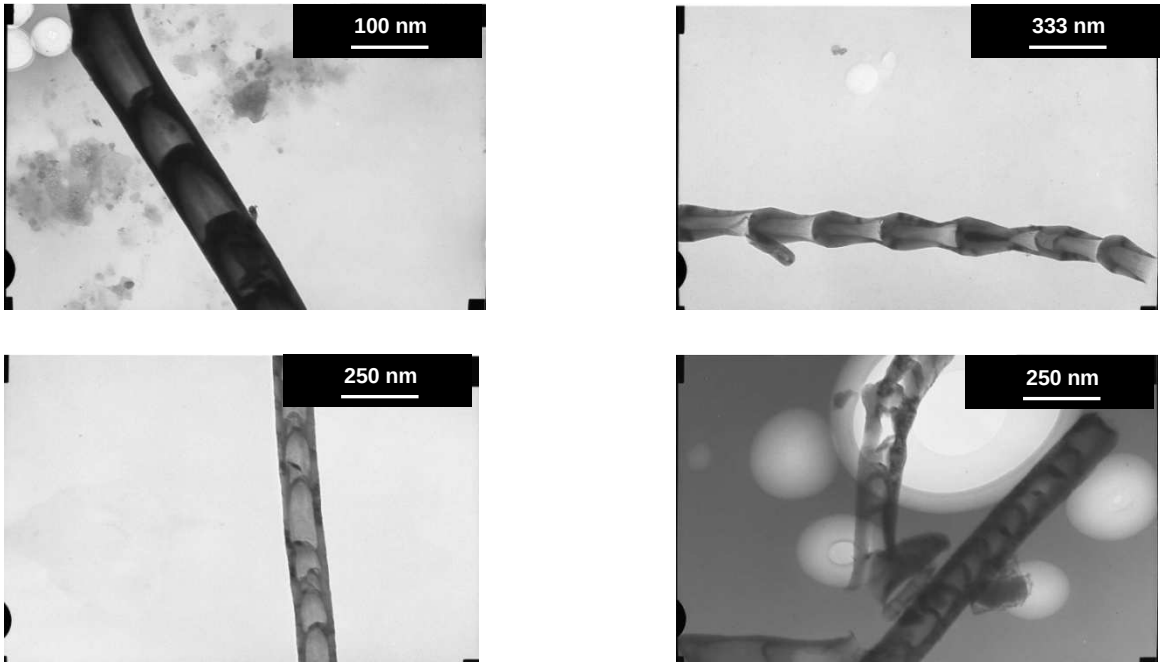

AS-T-CS 1000 ^{o}C/5 h

Figure 4.18 Transmission electron microscopy images of AS-T-CS 1000 ^{o}C/5 h samples.

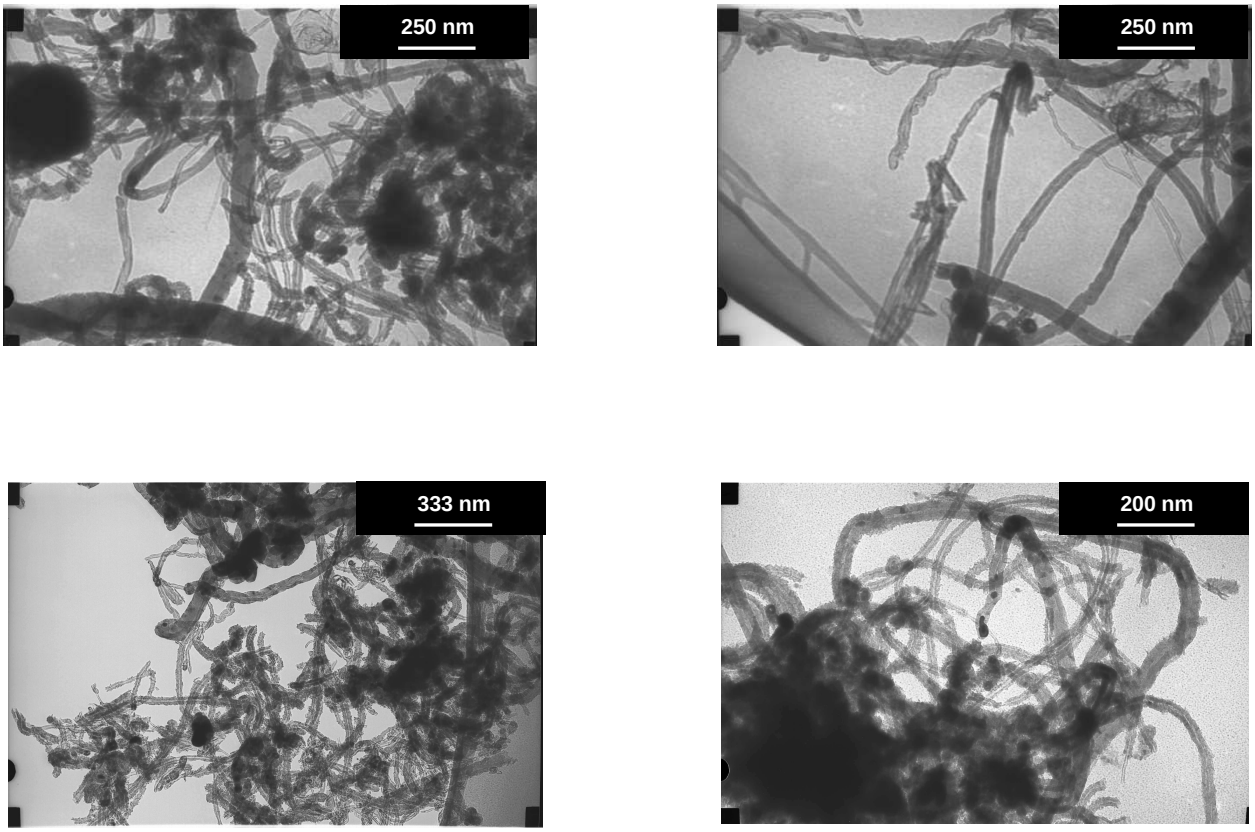

AS-B-CS 1000 ^{o}C/5 h

Figure 4.19 Transmission electron microscopy images of AS-B-CS 1000 ^{o}C/5 h samples.

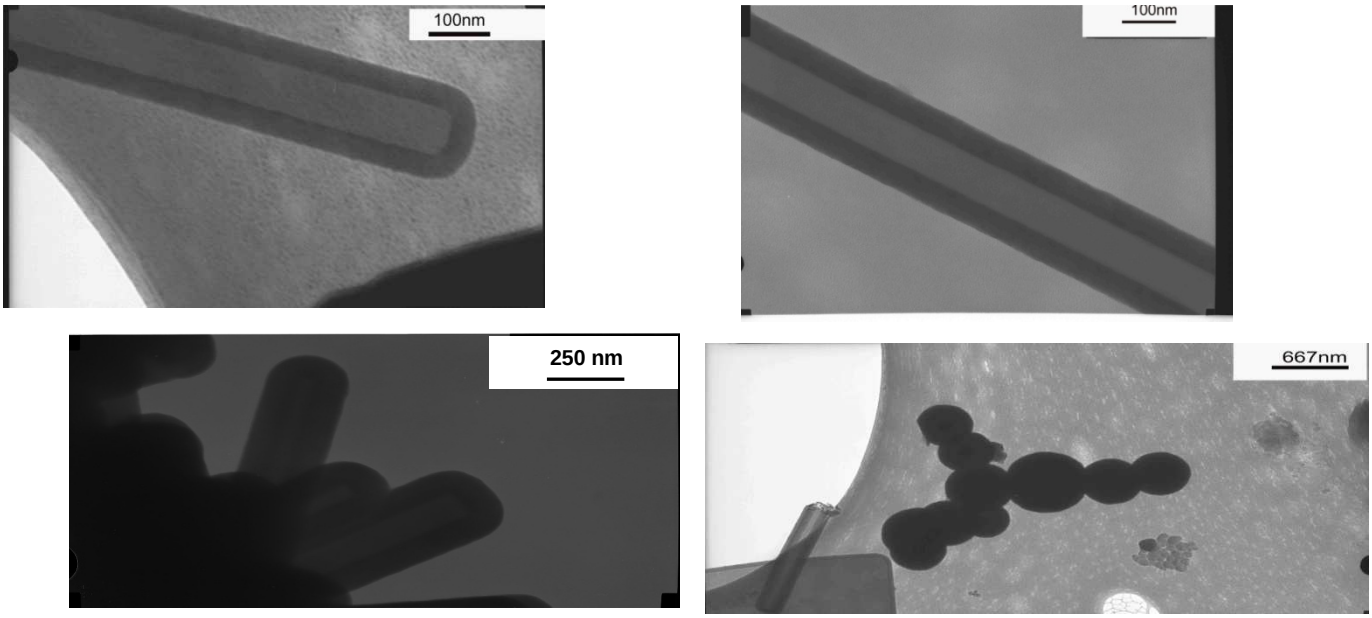

AS-P-CS 1000 ^{o}C/5 h

Figure 4.20 Transmission electron microscopy images of AS-P-CS 1000 ^{o}C/5 h samples.

4.2.1.2 High magnification TEM

High magnification TEM and corresponding EDX Spectra of AS-P-CS 1000 ^{o}C/5 h are shown in Figure 4.21. These were taken to observe the elemental content of the tubes and spheres. The tubes and spheres constitute of mainly carbon, silicon and oxygen, the copper peaks appearing are of the copper grid used to mount the sample. It was observed that if the product was not washed sufficiently with water, large amounts of NaCl were obtained in the product as shown in the EDX spectra in Figure 4.21. The presence of carbon and silica was also confirmed by Raman spectra and TGA analysis done under air atmosphere.

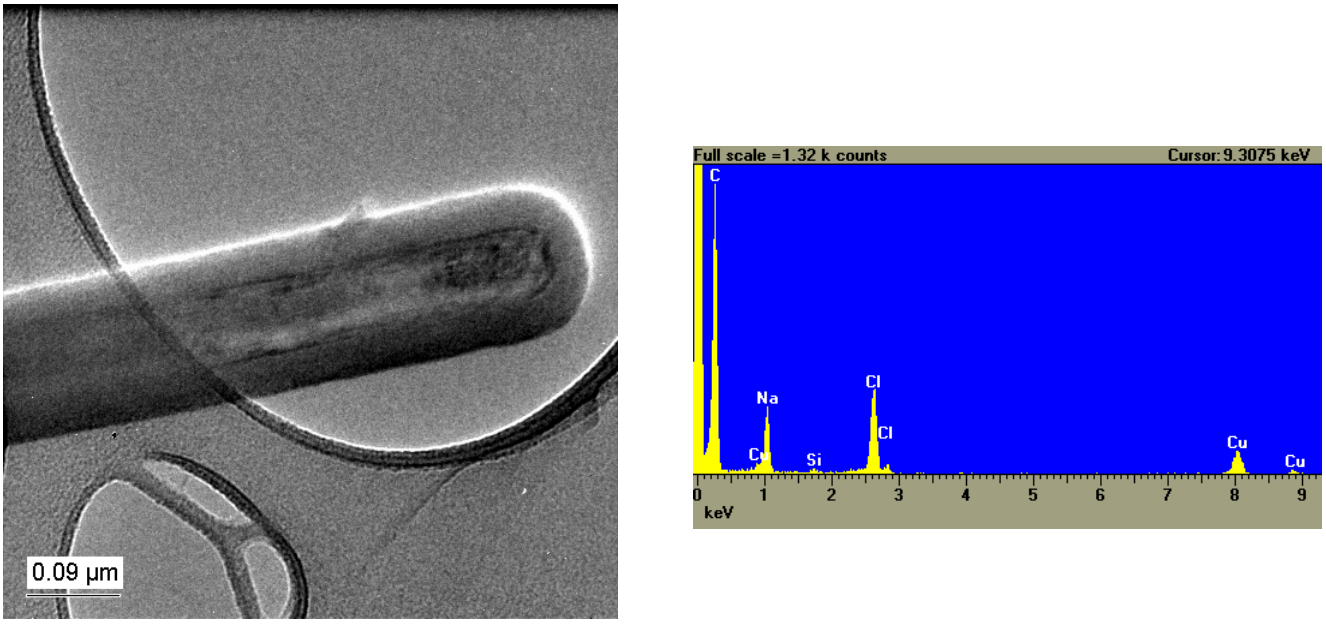

Figure 4.21 High magnification TEM images and corresponding EDX spectra of AS-P-CS 1000 ^{o}C/5 h carbon on silica nanocomposite sample.

4.2.1.3 Raman spectroscopy

Raman spectroscopy was used to elucidate whether the carbon containing products were amorphous or graphitic. The Raman spectra of AS-T-CS 1000 ^{o}C/5 h, AS-B-CS 1000 ^{o}C/5 h and AS-P-CS 1000 ^{o}C/5 h samples are shown in Figure 4.22. The spectrum of all samples had a strong band around 1347 – 1359 cm^{-1} (D-band) which is attributed to the presence of amorphous carbon [3]. Another band was also observed in the samples which varied from 1595 – 1604 cm^{-1} (G-Band) which is related to the symmetric E_{2G} intralayer mode of graphite [3]. However this band was rather broad in all samples, indicating a low degree of graphitization under the applied

synthetic conditions of the samples. The I_D/I_G ratios of AS-T-CS 1000 ^oC/5 h, AS-B-CS 1000 ^oC/5 h and AS-P-CS 1000 ^oC/5 h samples are 0.81, 1.87 and 0.96 (Table 4.5). The disorder of the samples does not follow any systematic trend.

Table 4.5 D- and G-band positions and I_D/I_G ratios of carbon on silica nanocomposites produced by carbonization of different organic-inorganic hybrid materials at constant temperature and time.

Sample Name	D-band position (cm^{-1})	G-band position (cm^{-1})	I_D/I_G Ratio
AS-T-CS 1000 ^oC/5 h	1359	1603	0.81
AS-B-CS 1000 ^oC/5 h	1353	1597	1.87
AS-P-CS 1000 ^oC/5 h	1359	1595	0.96

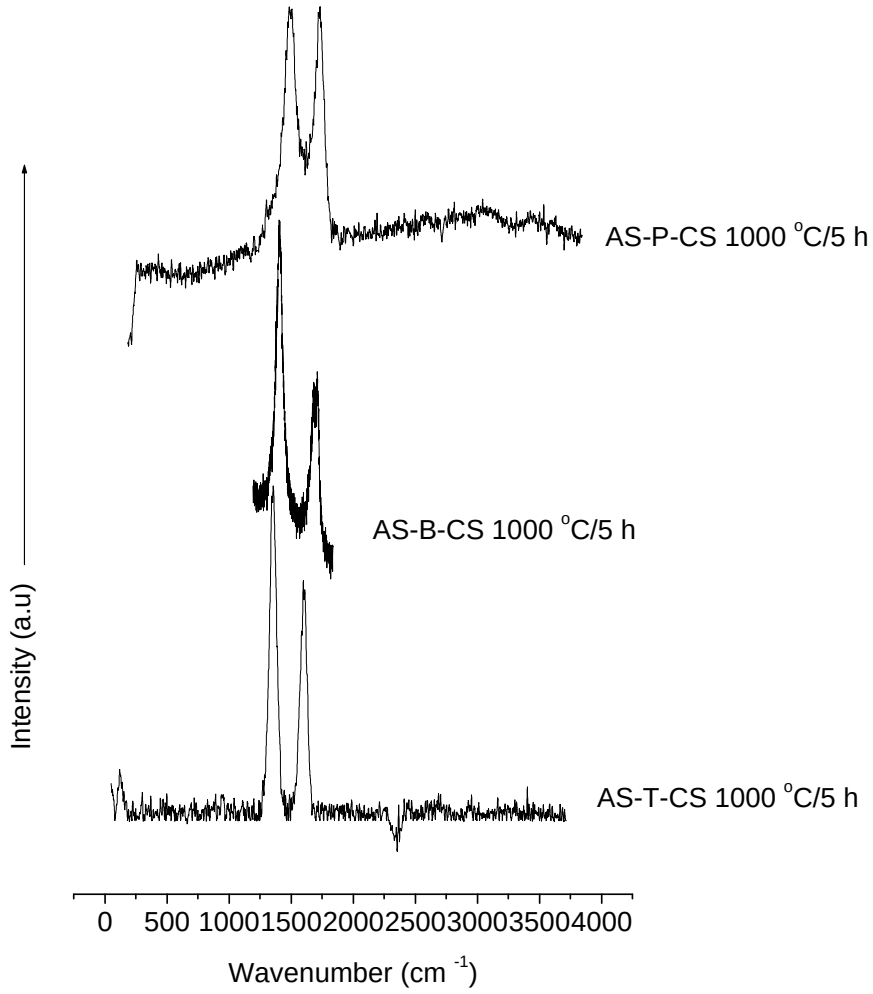

Figure 4.22 Raman spectra of a) AS-T-CS 1000 °C/5 h, b) AS-B-CS 1000 °C/5 h and c) AS-P-CS 1000 °C/5 h samples.

4.2.1.4 Thermogravimetric analysis

Figure 4.23 shows the TGA graphs of AS-T-CS 1000 ^{o}C/5 h, AS-B-CS 1000 ^{o}C/5 h and AS-P-CS 1000 ^{o}C/5 h samples. Analysis was conducted from room temperature to 900 ^{o} C at a heating rate of 10 ^{o}C/min under an air atmosphere. The TGA graph of AS-P-CS 1000 ^{o}C/5 h sample shows a sharp significant weight loss between 416 – 470 ^{o}C of approximately 25% which is due to the oxidation of carbon in oxygen atmosphere. There is another weight loss from 719 – 820 ^{o}C of approximately 9% which might be due to some of the SiO_2 decomposition. The residual SiO_2 content is approximately 63 %. AS-B-CS 1000 ^{o}C/5 h shows a sharp loss from 650 – 776 ^{o}C of approximately 25 % due to the oxidation of carbon in oxygen atmosphere. Residual SiO_2 content in this sample is approximately 75 %. AS-T-CS 1000 ^{o}C/5 h shows a sharp weight loss between 581 and 659 ^{o}C of approximately 13 % due to the oxidation of carbon in oxygen. Residual SiO_2 content is approximately 87 %. The mass losses associated with product decomposition of AS-T-CS 1000 ^{o}C/5 h, AS-B-CS 1000 ^{o}C/5 h and AS-P-CS 1000 ^{o}C/5 h are 581, 650 and 416 ^{o}C respectively. It can be concluded that AS-B-CS 1000 ^{o}C/5 h sample is the most thermally stable, followed by AS-T-CS 1000 ^{o}C/5 h and lastly AS-P-CS 1000 ^{o}C/5 h. Also, the thermal stability of the as-synthesized mesoporous phases is greatly enhanced after they have undergoing the carbonization process.

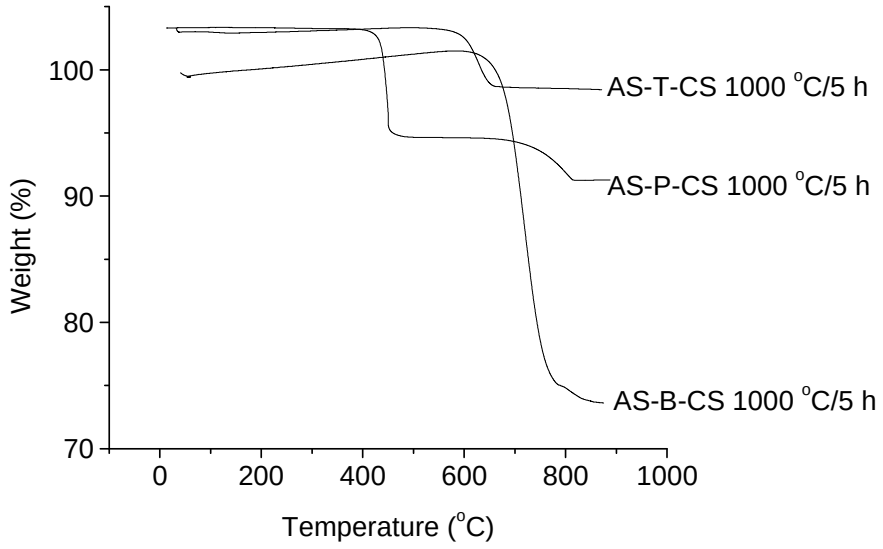

Figure 4.23 TGA curves of a) AS-T-CS 1000 ^{o}C/5 h, b) AS-P-CS 1000 ^{o}C/5 h and c) AS-B-CS 1000 ^{o}C/5 h samples.

4.2.1.5 Summary of results

AS-T-CS 1000 ^{o}C/5 h produced carbon on silica bamboo nanotubes with varying shapes and some amorphous material. The sample is thermally stable up to 581 ^{o}C in an air atmosphere. The presence of silica in the material was confirmed by TGA. AS-P-CS 1000 ^{o}C/5 h produced carbon on silica nanotubes with very thick internal diameters of between 160 – 170 nm, carbon spheres with average diameters of 400 nm and amorphous carbon. The sample is thermally stable up to 416 ^{o}C in an air atmosphere. EDX confirmed the presence of silicon, carbon and oxygen in the various nanostructures obtained for this sample. AS-B-CS 1000 ^{o}C/5 h produced carbon on silica nanotubes with varying small internal diameters and amorphous carbon material. The sample was the most thermally stable of the three materials up to 650 ^{o}C in an air atmosphere. Raman spectroscopy revealed that all samples had a low degree of graphitization and are

therefore amorphous. The I_D/I_G ratios of AS-T-CS 1000 ^oC/5 h, AS-B-CS 1000 ^oC/5 h and AS-P-CS 1000 ^oC/5 h samples are 0.81, 1.87 and 0.96 (Table 4.5). The disorder of the samples does not follow any systematic trend.

4.2.2 Effect of carbonization temperature on properties of AS-B-CS y ^oC/5 h (where y = 700, 800, 900, 1000 or 1100 ^oC) composites.

As-synthesized benzene-bridged silica samples were sealed under vacuum in quartz tubes and the samples were heated at temperatures of 700, 800, 900, 1000 and 1100 ^oC for 5 hours. The effect of varying the carbonization temperature was investigated. The samples were characterized by TEM, TGA, nitrogen physisorption and scanning x-ray photoelectron spectroscopy. Refer to section 3.3.3 for methodology and table of contents for notations of symbols.

4.2.2.1 Transmission electron microscopy

TEM images of as-synthesized benzene organosilica materials pyrolysed at different temperatures under vacuum are shown in Figure 4.24. Table 4.6 summarizes data obtained from TEM micrographs of the products obtained after heating as-synthesized benzene samples at different temperatures.

Table 4.6 Morphologies of carbon on silica nanocomposite materials produced after carbonization of as-synthesized benzene-bridged silica samples at different temperatures.

Sample	Morphology
AS-B-CS 700 ^{o}C/5 h	Amorphous material
AS-B-CS 800 ^{o}C/5 h	Spheres were starting to form but not very distinct and some amorphous material
AS-B-CS 900 ^{o}C/5 h	Very distinct spheres and some amorphous material
AS-B-CS 1000 ^{o}C/5 h	Nanotubes, spheres, beads and some amorphous material
AS-B-CS 1100 ^{o}C/5 h	Spheres and some amorphous material

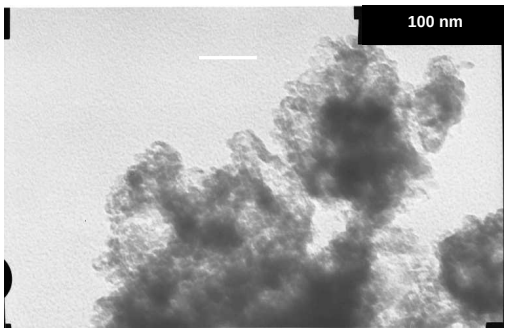

a) AS-B-CS 700 °C/5 h

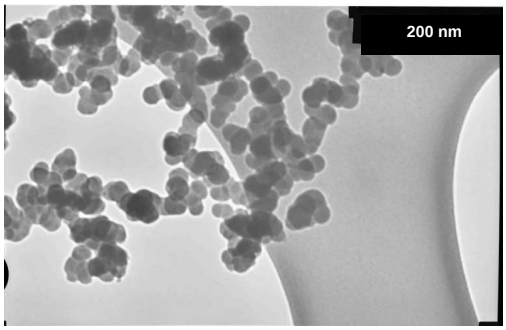

b) AS-B-CS 800 °C/5 h

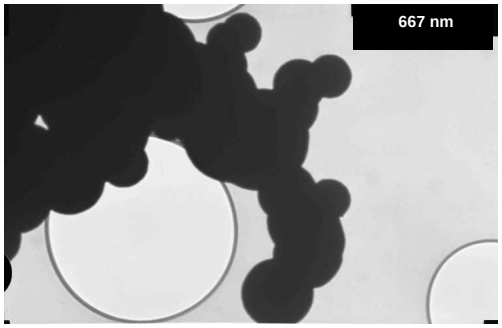

c) AS-B-CS 900 °C/5 h

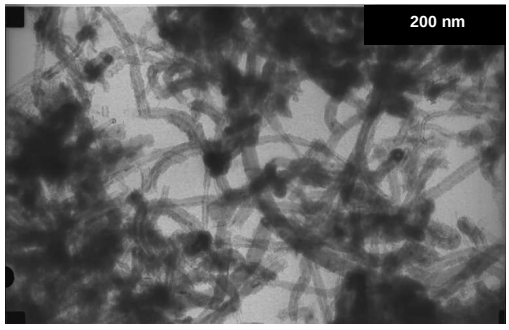

d) AS-B-CS 1000 °C/5 h

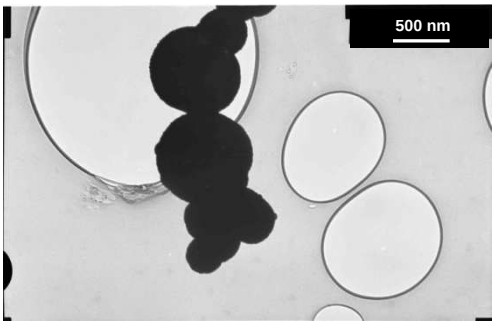

e) AS-B-CS 1100 °C/5 h

Figure 4.24 Representative TEM images of a) AS-B-CS 700 °C/5 h, b) AS-B-CS 800 °C/5 h, c) AS-B-CS 900 °C/5 h, d) AS-B-CS 1000 °C/5 h and e) AS-B-CS 1100 °C/5 h carbon on silica nanocomposite samples.

4.2.2.2 Raman spectroscopy

Raman spectroscopy was used to elucidate whether carbonization of the AS-Benzene organosilica samples at different temperatures would result in amorphous or graphitic carbon containing nanocomposite materials. Raman spectra of AS-B-CS 700 ^{o}C/5 h, AS-B-CS 800 ^{o}C/5 hrs), AS-B-CS 900 ^{o}C/5 h, AS-B-CS 1000 ^{o}C/5 h and AS-B-CS 1100 ^{o}C/5 h are shown in Figure 4.25. The spectra of all samples had strong bands around 1347 – 1359 cm^{-1} (D-band) which are attributed to the presence of amorphous carbon [3]. Another band was also observed in the samples which varied from 1595 – 1604 cm^{-1} (G-Band) which is related to the symmetric E_{2G} intralayer mode of graphite [3]. This band was rather broad in all samples, indicating a low degree of graphitization under the applied synthetic conditions used to make the samples. Generally, the D-band to G-band ratio is used to evaluate the defects in carbon materials. The I_D/I_G ratios (Table 4.7) suggest that, as the carbonization temperature increased, the degree of disorder also increased. Indeed, the products of AS-BS-P123 samples produced with carbonization temperatures of 700, 800, 900 and 1000 ^{o}C gave rise to I_D/I_G ratios of 0.81, 1.07, 1.32 and 1.53 respectively. There was however a decrease in the I_D/I_G ratio of AS-B-CS 1100 ^{o}C/5 h sample of 1.33 and this could be due to a change in the morphology of the structures.

Table 4.7 D- and G-band positions and I_D/I_G ratios of AS-BS-P123 samples heated at different temperatures.

Sample Name	D-band Position (cm^{-1})	G-Band Position (cm^{-1})	I_D/I_G Ratio
AS-B-CS 700 ^oC/5 h	1328	1597	0.81
AS-B-CS 800 ^oC/5 h	1336	1597	1.07
AS-B-CS 900 ^oC/5 h	1343	1603	1.32
AS-B-CS 1000 ^oC/5 h	1350	1597	1.53
AS-B-CS 1100 ^oC/5 h	1350	1589	1.33

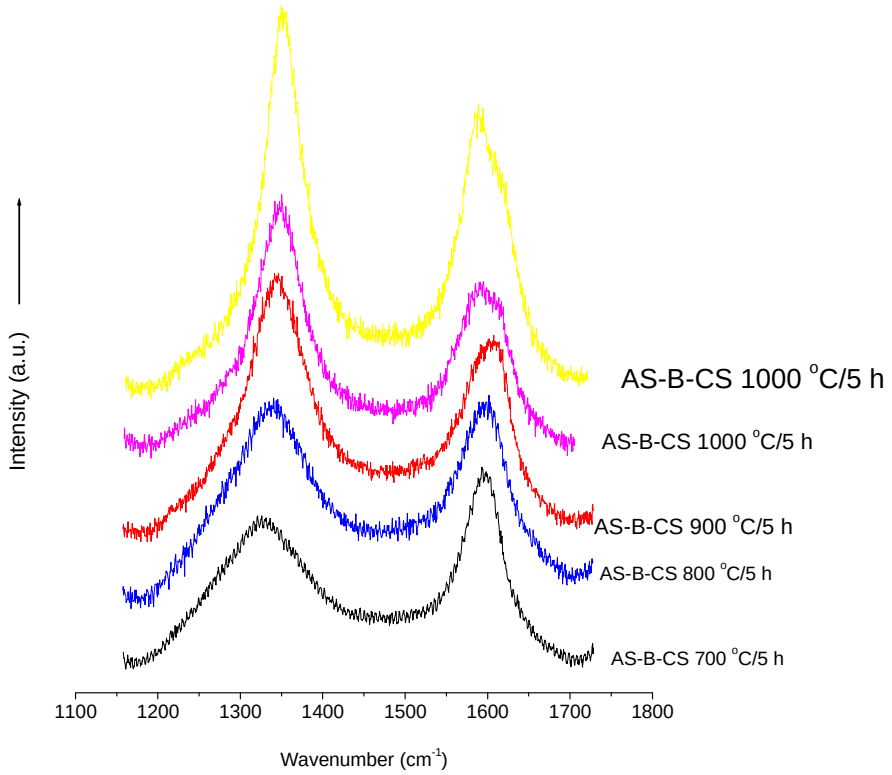

Figure 4.25 Raman spectra of a) AS-B-CS 700 ^{o}C/5 h, b) AS-B-CS 800 ^{o}C/5 h, c) AS-B-CS 900 ^{o}C/5 h, d) AS-B-CS 1000 ^{o}C/5 h and e) AS- B-CS 1100 ^{o}C/5 h carbon on silica nanocomposites samples.

4.2.2.3 Thermogravimetric analysis

Thermogravimetric weight changes were recorded in air to evaluate the thermal stability of the carbon on silica nanocomposite materials produced after heating AS-BS-P123 at different temperatures under vacuum for 5 hours (Figure 4.26). The temperature at which the major loss changes occurred of the carbon on silica nanocomposites produced increased as the carbonization temperature increased from 700 ^{o}C to 1000 ^{o}C. At 1100 ^{o}C carbonization temperature, the temperature at which the major loss changes occurred decreased. The AS-B-CS

700 ^{o}C/5 h, AS-B-CS 800 ^{o}C/5 h, AS-B-CS 900 ^{o}C/5 h, AS-B-CS 1000 ^{o}C/5 h and AS- B-CS 1100 ^{o}C/5 h show major weight loss changes at 635, 716, 768, 776 and 612 ^{o}C respectively in an air atmosphere. Significant weight losses corresponding to the oxidation of the carbon occurred between 480 – 780 ^{o}C for the carbon on silica nanocomposite samples. The carbon contents for AS-B-CS 700 ^{o}C/5 h, AS-B-CS 800 ^{o}C/5 h, AS-B-CS 900 ^{o}C/5 h, AS-B-CS 1000 ^{o}C/5 h and AS- B-CS 1100 ^{o}C/5 h are 17.5, 14.87, 15.4, 17.7 and 17.8 % respectively. The carbon content of AS-B-CS 1000 ^{o}C /5 h is lower than that of composites reported by Lu and co-workers [4], who using BTEB as an organosilica precursor observed a 36.5% weight carbon content. Lu and co-workers synthesized their mesoporous carbon silica composite by carbonizing the benzene/silica/surfactant hybrid powder in a nitrogen atmosphere using the CVD method at 900 ^{o}C for 4 hours. Residual SiO_2 was the remaining component in all materials after oxidation of carbon and it ranged between 73 and 79 %. Derivative plots (Figure 4.27) clearly show that as carbonization temperature increases, peak minima shift to higher decomposition temperatures, indicating higher thermal stability of the composites.

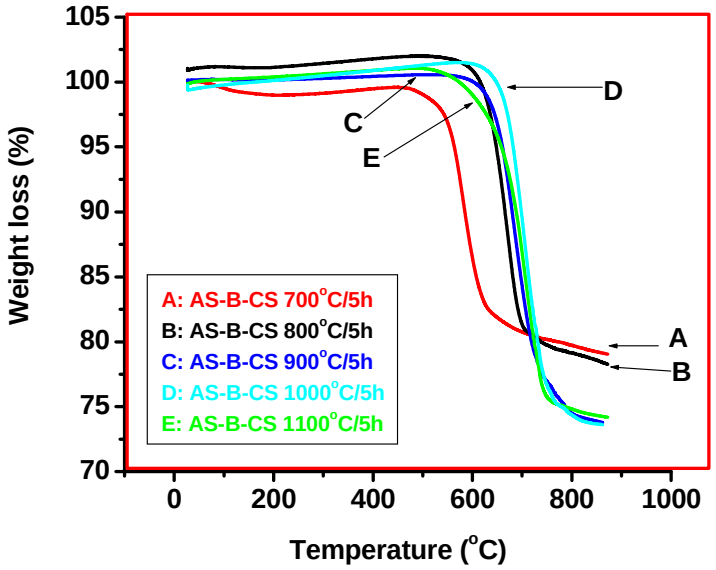

Figure 4.26 TGA curves of a) AS-B-CS 700 ^{o}C/5 h, b) AS-B-CS 800 ^{o}C/5 h, c) AS-B-CS 900 ^{o}C/5 h, d) AS-B-CS 1000 ^{o}C/5 h and e) AS-B-CS 1100 ^{o}C/5 h carbon on silica nanocomposites samples.

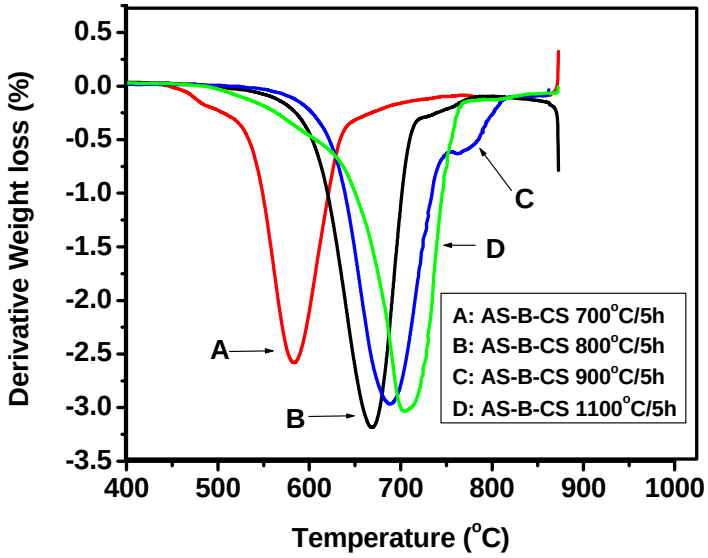

Figure 4.27 Derivative TGA curves of a) AS-B-CS 700 °C/5 h, b) AS-B-CS 800 °C/5 h, c) AS-B-CS 900 °C/5 h and d) AS-B-CS 1100 °C/5 h carbon on silica nanocomposite samples.

4.2.2.4 Nitrogen sorption studies

The textural properties of the carbon on silica nanocomposites produced after heating mesoporous phenyl-bridged organosilica/surfactant mesophases at different temperatures are summarised in Table 4.8. The low surface areas and pore volumes are perhaps due to pore blockage as described below. A possible explanation for the apparent lack of mesoporosity for all samples is that the carbonization efficiency is so high at temperatures from 700 to 1100 °C that rapid formation of carbon deposit blocks some of the mesopores. The formation of carbon on silica nanocomposites relies on the decomposition (burn off) of the surfactant molecules (to generate pore channels) and the conversion of the benzene organic groups to carbon generating a silica/carbon framework. At these high pyrolysis temperatures (700, 800, 900, 1000 and 1100

^{o}C) the carbonization may convert the surfactant molecules directly to carbon which blocks the pores rather than being burnt off.

Table 4.8 Textural properties of carbon on silica nanocomposites produced using as-synthesized benzene-bridged organosilica materials heated at different carbonization temperatures.

Sample Name	BET Surface Area (m^2/g)	Total Pore Volume (cm^3/g)	Average Pore Diameter (nm)	BJH Adsorption Pore Diameter (nm)	BJH Desorption Pore Diameter (nm)
AS-B-CS 700 ^oC/5 h	5.2	0.0	25.8	69.9	68.2
AS-B-CS 800 ^oC/5 h	17.3	0.1	28.9	41.0	19.0
AS-B-CS 900 ^oC/5h	41.2	0.2	17.6	17.1	14.4
AS-B-CS 1000 ^oC/5h	7.8	0.0	22.1	23.4	20.0
AS-B-CS 1100 ^oC/5h	29.9	0.1	19.2	17.9	13.0

4.2.2.5 Scanning X-ray photoelectron spectroscopy

XPS was used to discern the chemical state of the produced carbon on the silica nanostructures. AS-B-CS 1000 ^{o}C/5 h was analysed using XPS. XPS results confirmed the presence of carbon, oxygen and silicon in atomic concentrations (%) 35.9, 51 and 13.1% respectively.

4.2.2.6 Summary of results

AS-BS-P123 samples heated at different carbonization temperatures produced different carbon on silica nanostructures which included spheres and nanotubes. Amorphous material (approximately 60%) was also produced. The presence of silicon and carbon in the carbon on silica nanocomposites produced was further confirmed by the use of XPS (AS-B-CS 1000 ^{o}C/5 h sample). Raman data showed that as the carbonization temperature is increased, the degree of disorder of the materials also increased. The temperature at which major loss changes occurred due to the oxidation of carbon increased as the carbonization temperature increased up to 1000 ^{o}C. Low surface areas and pore volumes were obtained for all mesoporous phenyl-bridged organosilica/surfactant mesophases heated at different temperatures. This may be due to the high carbonization efficiency at temperatures from 700 ^{o}C to 1100 ^{o}C that there is rapid formation of carbon deposits which blocks some of the mesopores. Also at these high pyrolysis temperatures, the carbonization may be so fast that the surfactant molecules are directly converted to carbon which blocks the pores rather than being burnt off.

4.2.3 The effect of variation of carbonization time on the morphology of carbon on silica nanocomposites formed from AS-PS-P123 organosilica materials

The effect of variation of carbonization time was investigated. AS-PS-P123 mesoporous silica samples were sealed under vacuum and heated to 1000 ^{o}C at different carbonization times of 30 minutes, 1 hour and 5 hours in a muffle furnace. The effect of carbonization time on the resulting carbon on silica nanocomposites produced was investigated. Refer to section 3.3.3 for methodology and table of contents for notations of symbols.

4.2.3.1 Transmission electron microscopy

Serp *et al* [5] classified structures produced by carbon according to their size into fullerenes C_n, carbon onions (2 – 20 nm, with closed graphite layer) [6], carbon spheres (50 nm to 1 µm) [7,8] and carbon beads (above 1 µm) [9]. TEM images and the corresponding diameter distribution graphs of AS-P-CS 1000 ^{o}C/0.5 h, AS-P-CS 1000 ^{o}C/1 h and AS-P-CS 1000 ^{o}C/5 h are shown in Figures 4.30 – 4.32.

AS-P-CS 1000 ^{o}C/0.5 h mesoporous silica samples produced carbon on silica beads. The size distribution of the particles was determined by TEM examination of 76 particles. The diameters of the carbon beads ranged from 0.8 to 3.2 µm and the diameters of most carbon beads were from 1.8 – 2.0 and 1.2 – 1.4 µm. (see from Figure 4.28). The TEM images indicate the carbon beads appear to be of perfect spheres.

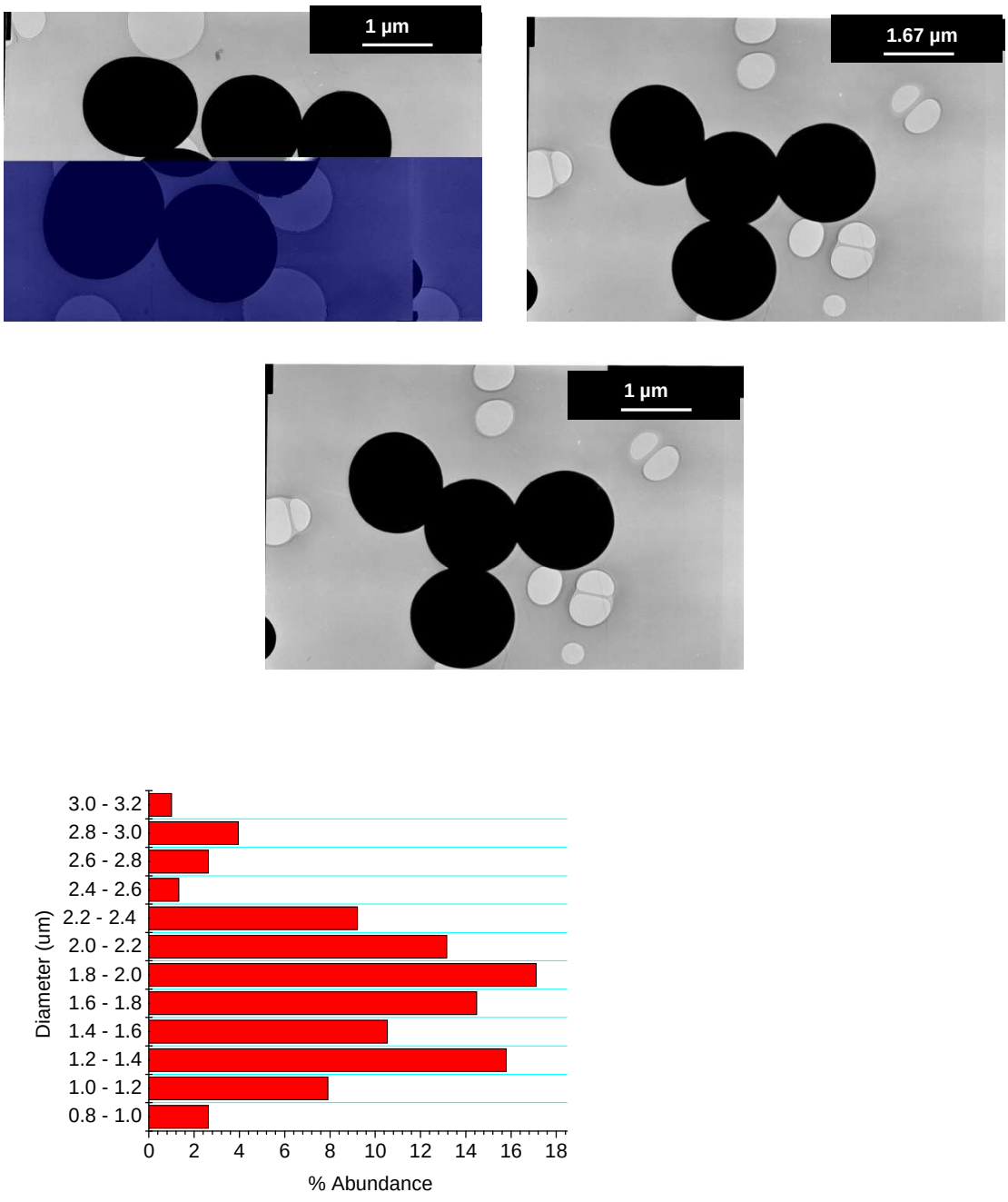

Figure 4.28 TEM images of AS-P-CS 1000 ^{o}C/0.5 h and the corresponding diameter distribution graph of carbon on silica beads.

The size distribution of the particles of AS-P-CS 1000 ^{o}C/1 h was determined by TEM examination of 96 particles. The diameters of the carbon beads ranged from 1.2 to 4.6 µm and the diameters of most carbon beads were from 1.8 – 2.4 µm. (see from Figure 4.29). Only carbon on silica beads and amorphous material were observed.

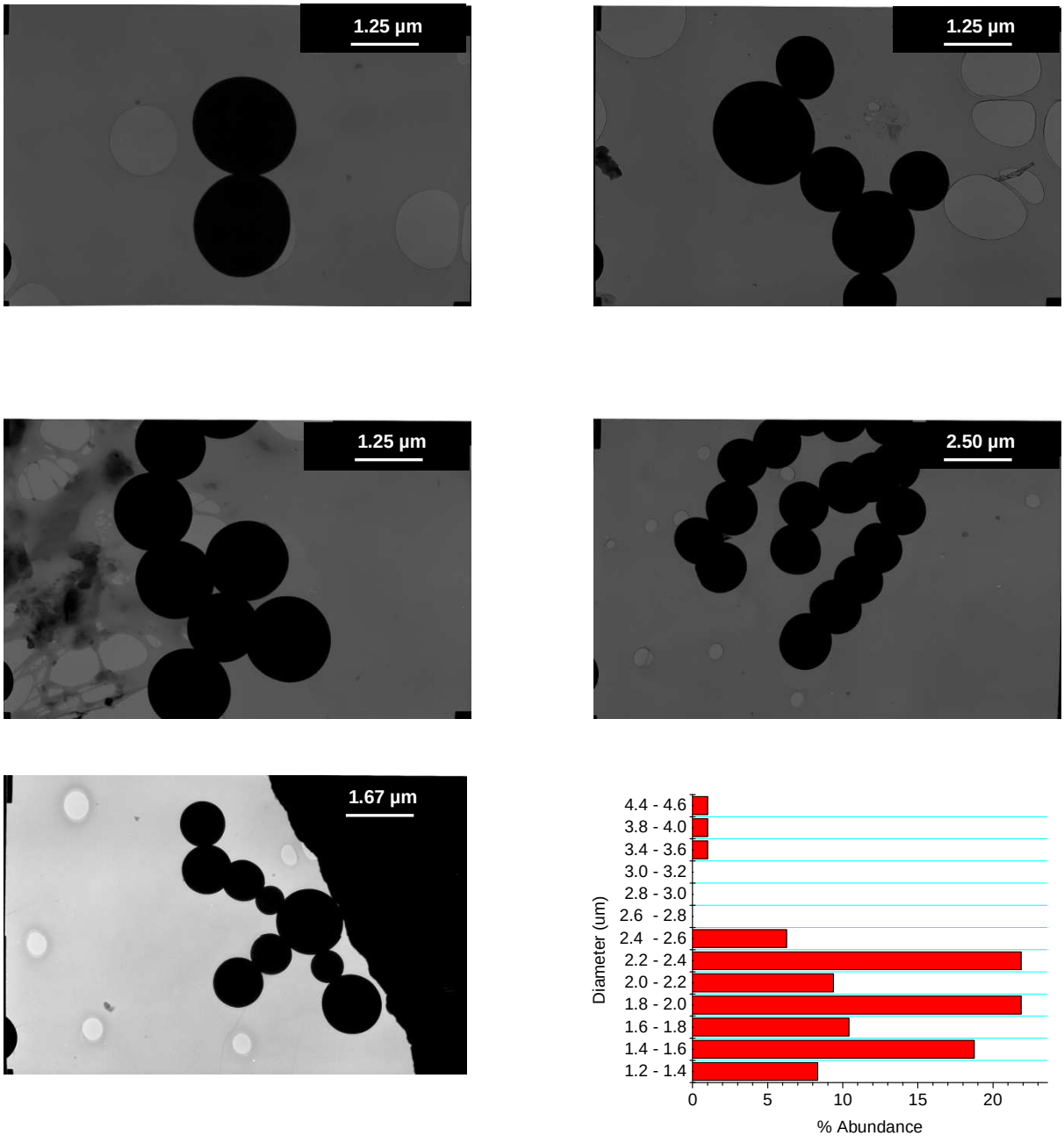

Figure 4.29 TEM images of AS-P-CS 1000 ^{o}C/1 h and the corresponding diameter distribution graph of carbon on silica beads.

AS-P-CS 1000 ^{o}C/5 h samples showed different morphologies of carbon on silica nanotubes, spheres, beads and amorphous carbon material in some areas (Figure 4.30). The diameters of the carbon nanotubes ranged from 225 – 275 nm, the outer wall diameters vary between 75 – 100 nm, the middle wall thickness varies from 25 – 113 nm. The size distribution of the sphere and bead particles was not obtained because their yield was very low (approximately 5 %).

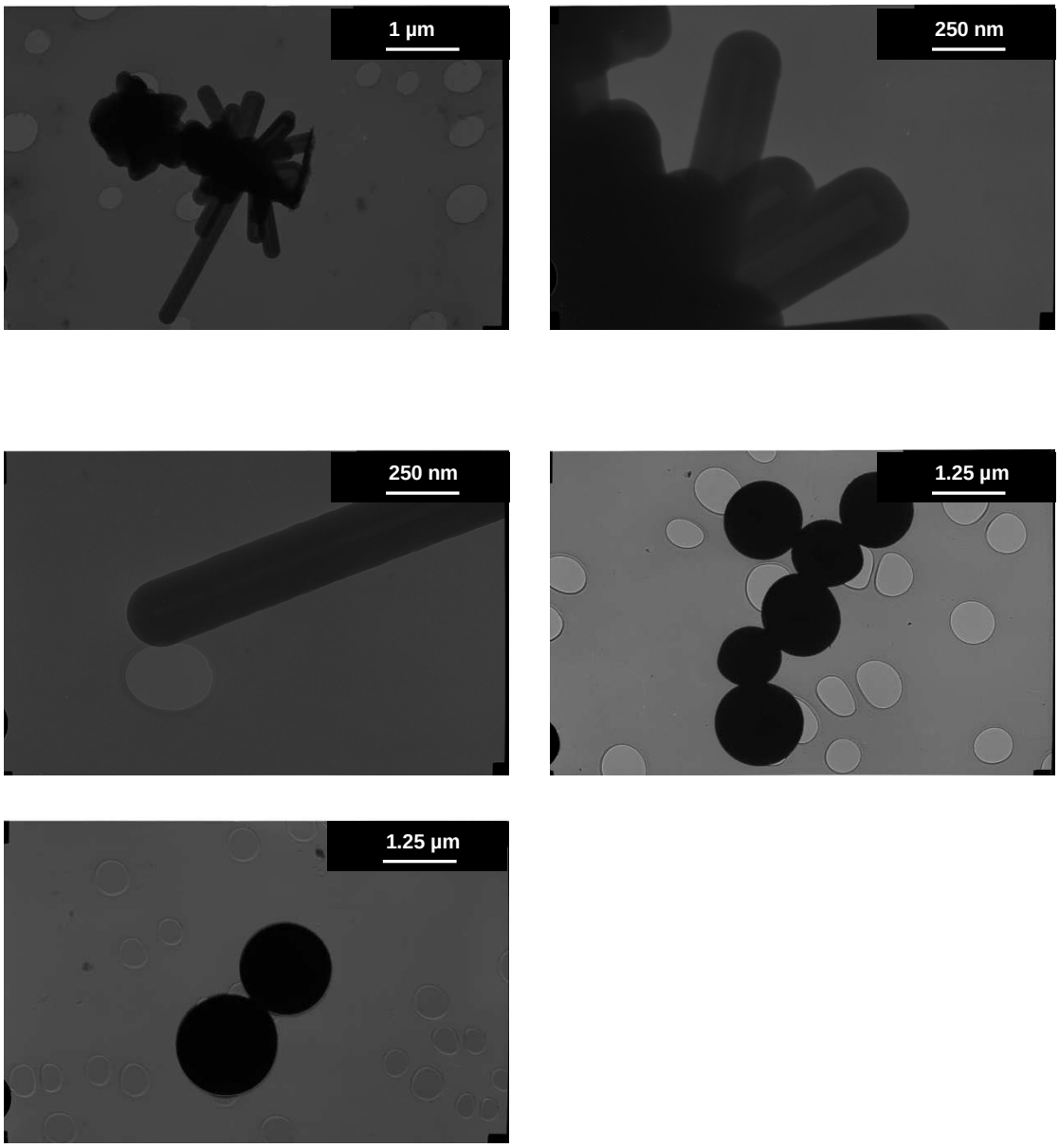

Figure 4.30 TEM images of AS-P-CS 1000 ^{o}C/5 h samples.

4.2.3.2 Thermogravimetric analysis

The thermal stability of AS-P-CS 1000 ^{o}C/5 h, AS-P-CS 1000 ^{o}C/1 h and AS-P-CS 1000 ^{o}C/0.5 h carbon on silica nanocomposite samples was investigated by TGA (Figure 4.31). The temperature at which major loss changes occurred (due to oxidation of carbon) of the carbon on silica nanocomposites produced increased as the carbonization time was increasing from 0.5 hours to 5 hours. The major loss changes of AS-P-CS 1000 ^{o}C/5 h, AS-P-CS 1000 ^{o}C/1 h and AS-P-CS 1000 ^{o}C/0.5 h occurred at 557, 561 and 572 ^{o}C respectively in an air atmosphere.

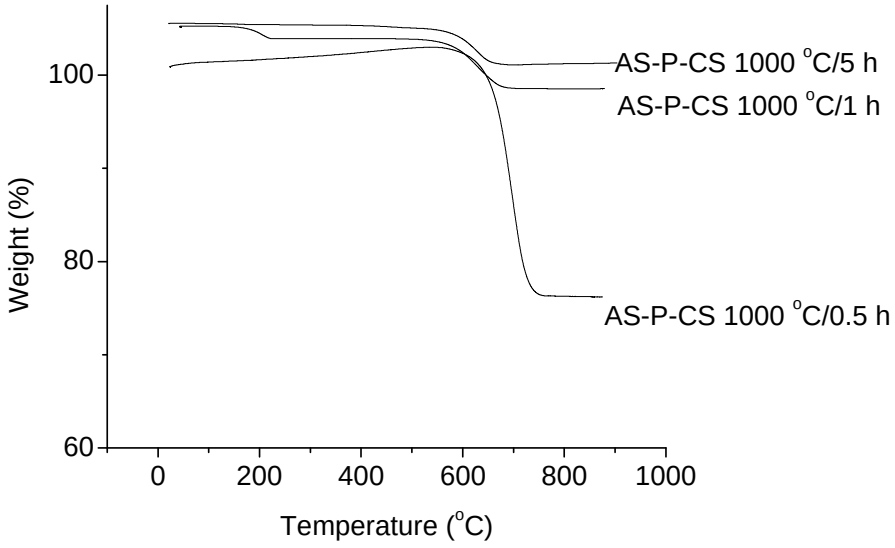

Figure 4.31 TGA curves of a) AS-P-CS 1000 ^{o}C/5 h, b) AS-P-CS 1000 ^{o}C/1 h and c) AS-P-CS 1000 ^{o}C/0.5 h carbon on silica nanocomposites samples.

4.2.3.3 Raman spectroscopy

Raman spectroscopy was used to ascertain whether the variation of carbonization time had any effect on the quality of the carbon on silica nanostructures produced. Figure 4.32 shows the Raman spectra of the AS-P-CS 1000 ^{o}C/5 h, AS-P-CS 1000 ^{o}C/1 h and AS-P-CS 1000 ^{o}C/0.5 h carbon on silica nanocomposite samples. Two significant peaks lying at about 1355 and 1600 cm^{-1} correspond to the D-band and G-band respectively. The D-band is explained by defects, dislocations and lattice distortions in the carbon containing structures. The G-band is attributed to the ordered graphite structure [10]. In the AS-P-CS 1000 ^{o}C/0.5 h carbon on silica sample there is a peak at around 3000 cm^{-1} which is an overtone. The I_D/I_G ratios of AS-P-CS 1000 ^{o}C/5 h, AS-P-CS 1000 ^{o}C/1 h and AS-P-CS 1000 ^{o}C/0.5 h are 0.96, 0.82 and 0.65 respectively (Table 4.9). From the table it can be seen that as the carbonization time is increased, the degree of disorder of the carbon on silica nanostructures increases.

Table 4.9 D- and G-band positions and I_D/I_G ratios of carbon on silica nanocomposites produced by the carbonization of AS-PS-P123 samples at different times.

Sample Name	D-band Position (cm^{-1})	G-Band Position (cm^{-1})	I_D/I_G Ratio
AS-P-CS 1000 ^{o}C/5 h	1357	1596	0.96
AS-P-CS 1000 ^{o}C/1 h	1359	1600	0.82
AS-P-CS 1000 ^{o}C/0.5 h	1359	1595	0.65

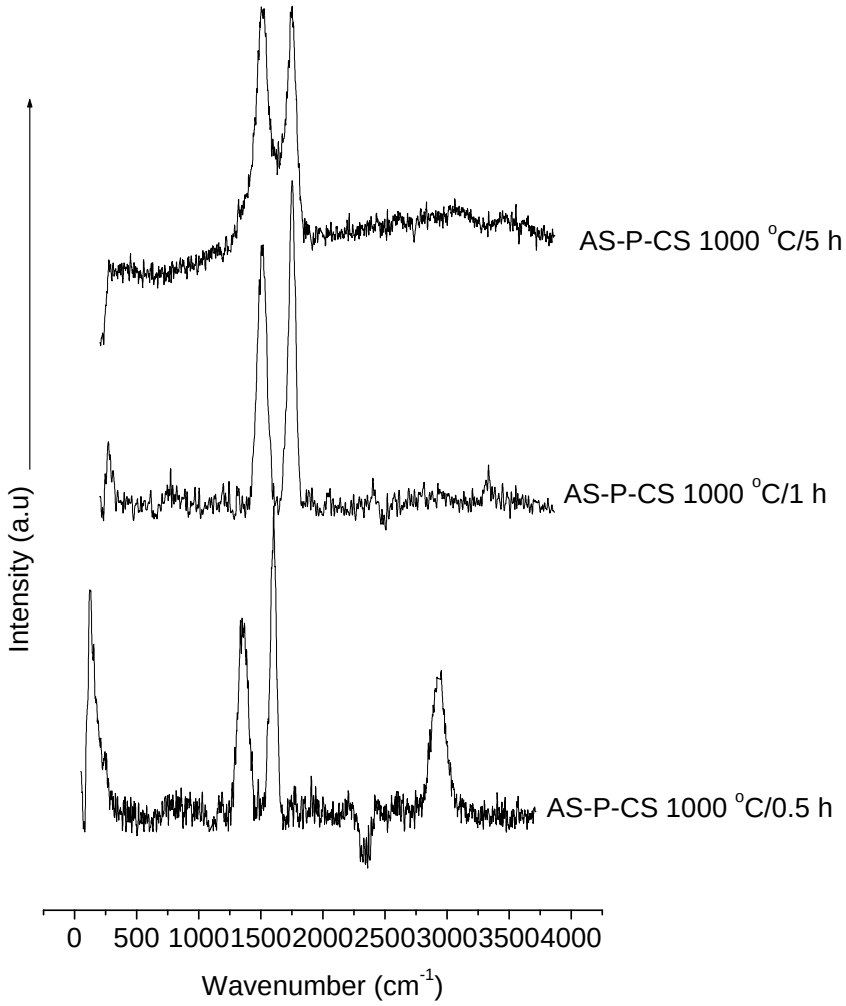

Figure 4.32 Raman spectra of a) AS-P-CS 1000 °C/5 h, b) AS-P-CS 1000 °C/1 h and c) AS-P-CS 1000 °C/0.5 h carbon on silica nanocomposite samples.

4.2.3.4 Summary of the results

Table 4.10 shows the summary of TEM results obtained of AS-P-CS 1000 ^{o}C/*x* h (where *x* = 0.5, 1 and 5 hrs) carbon on silica nanocomposite samples. From the TEM results it can be seen that longer pyrolysis times yields various shaped carbon on silica nanocomposites and shorter pyrolysis times yields only amorphous material and beads. AS-P-CS 1000 ^{o}C/5 h produced carbon on silica nanocomposites of nanotubes, spheres, beads and amorphous material. Both AS-P-CS 1000 ^{o}C/1 h and AS-P-CS 1000 ^{o}C/0.5 h carbon on silica nanocomposites produced amorphous material and beads. Most carbon on silica beads of AS-P-CS 1000 ^{o}C/1 h and AS-P-CS 1000 ^{o}C/0.5 h had sizes which ranged from 1.8 – 2.4 and 1.2 – 2.0 µm respectively. Shorter pyrolysis times of 0.5 h produced carbon on silica beads with smaller diameters which ranged from 1.2 – 2.0 µm and pyrolysis times of 1 h produced carbon on silica beads with larger diameters of 1.8 – 2.4 µm. The Raman data showed that as the carbonization time is increased, the degree of disorder in the carbon on silica nanocomposites also increases. This result is in agreement with Katok *et al* [11] who saw that longer pyrolysis times (more than 1 hour) yielded more of amorphous material. The thermal stability of the carbon on silica nanocomposite samples decreased as the carbonization time was increased.

Table 4.10 Summary of TEM results obtained of AS-P-CS 1000 ^{o}C/*x* h (where *x* = 5, 1 and 0.5 hrs) carbon on silica nanocomposite samples.

Sample	Morphology of product	Diameter distribution (μm)	Peak range (μm)
AS-P-CS 1000 ^{o}C/5 h	Amorphous material, nanotubes, spheres and beads		0.2 – 0.3 (nanotubes)
AS-P-CS 1000 ^{o}C/1 h	Amorphous material and beads	1.2 – 4.6	1.8 – 2.4
AS-P-CS 1000 ^{o}C/0.5 h	Amorphous material and beads	0.8 – 3.2	1.2 – 2.0

4.3 References

[1] R. Mokaya, Z. Yang, Y. Xia, *Journal of Materials Chemistry*, **16**, 3417 (2006).

[2] S.J. Grey, K.S. W. Sing, *Adsorption, Surface Area and Porosity*, Academic Press, London, (1982).

[3] Y. Zhang, G. Hu, D. O`Hare, Y. Sun, *Carbon*, **44**, 1969 (2006).

[4] J. Pang, V.T. John, D. A. Loy, Z. Yang, Y. Lu, *Advanced Materials*, **17**, 704 (2005)

[5] P. Serp, R. Feurer, P. Kalck, Y. Kihn, J. L. Faria, J. L. Figueiredo, *Carbon*, **39**, 621 (2001).

[6] D. Ugarte, *Nature*, **359**, 707 (1992).

[7] Q. Wang, F. Y. Cao, Q. W. Chen, C. Chen, *Materials Letters*, **59**, 3738 (2005).

[8] Y. Z. Piao, K. J. An, J. Y. Kim, T. Y. Yu, T. W. Hyeon, *Journal of Materials Chemistry*, **16**, 2984 (2006).

[9] V. G. Pol, M. Motiei, A. Gedanken, J. Calderon-Moreno, M. Yoshimura, *Carbon*, **42**, 111 (2004).

[10] F. Tuinstra, J. L. Koenig, *The Journal of Chemical Physics*, **53**, 1126 (1970).

[11] K. V. Katok, V. A. Tertykh, S. Ya. Brichka, G. P. Prikhod'ko, *Journal of Thermal Analysis and Calorimetry*, **86**, 109 (2006).

CHAPTER FIVE

CONCLUSION

The surfactant-templated sol-gel method was used to synthesize as-synthesized and surfactant extracted periodic mesoporous organosilica materials. Five different silica sources were used: tetraethylorthosilicate (TEOS), 1,2-bis(trimethoxysilyl)ethane (BTME), 1,4-bis(triethoxysilyl)benzene (BTEB), 4,4-bis (triethoxysilyl)-1,1 biphenyl (BTEBP) and bis[(3-trimethoxysilyl)propyl]-amine (BTMSPA). Two structure directing agents were used, triblock copolymer (Pluronic P123) and cetyltrimethylammonium bromide (CTAB). The chain length of the organic moiety and the nature of the structure directing agents were varied in order to study their effect on the morphology, thermal stability and on the surface properties (namely surface area, pore volume, pore size and pore size distribution) of the materials synthesized.

Carbon on silica nanocomposites were synthesized by directly carbonizing the organosilica/surfactant phases at different temperatures under an inert atmosphere produced by first sealing the mesoporous silica materials in quartz tubes under vacuum. This resulted in carbon on silica nanocomposites with various nanostructures (e.g. nanotubes, spheres, beads, etc). The effect of carbonization time, carbonization temperature, and the nature of the silica/organosilica precursor on the morphology, graphitic/amorphous nature, thermal stability, and textural properties of carbon on silica nanocomposites produced was investigated.

FTIR spectroscopy and thermogravimetric analysis confirm the formation of organosilica materials and show that the surfactants Pluronic P123 and CTAB were removed by solvent extraction. Solvent extraction yielded materials with high surface areas, high pore volumes and pore sizes in the mesopores region. The pore sizes for solvent extracted samples synthesized using Pluronic P123 and CTAB as SDAs were in ranges of 3.1 – 8.3 nm and 2.7 – 7.8 nm respectively. All surfactant extracted samples synthesized using Pluronic P123 as a SDA exhibit

Type IV isotherms which is typical of mesoporous materials. All surfactant extracted samples synthesized using CTAB as a SDA exhibit Type IV isotherms except for SE-BS-CTAB material which exhibits Type I isotherm which is characteristic of materials with cylindrical pores.

The use of the surfactant Pluronic P123 produced periodic mesoporous organosilica materials which had surface areas which followed a systematic trend. It was seen that the size of the organic group had an effect on the surface area obtained on the periodic mesoporous organosilica materials produced. From the results of the surface areas of solvent extracted samples, it was observed that the smaller the chain length of the organosilica precursor, the higher the surface area obtained. It can therefore be concluded that small organic groups (ethane) are more favorable for synthesizing PMOs with high surface areas followed by rigid organic groups (benzene and biphenyl) and lastly flexible organic groups (bis(propyl)amine). The surface areas obtained for SE-TS-P123, SE-BMS-P123 and SE-PS-P123 are 839.4, 802.3 and 344.3 m^2/g respectively. The surface areas of SE-BS-P123 and SE-BPS-P123 were 527.1 and 386.2 m^2/g respectively.

The use of the surfactant CTAB yielded periodic mesoporous organosilica materials which followed a systematic trend, with the exception of SE-BS-CTAB. In the surfactant extracted samples the BET surface areas decrease as the chain length of the organic groups increased. SE-TS-CTAB, SE-BMS-CTAB and SE-PS-CTAB have surface areas of 947.4, 901.1 and 331.6 m^2/g respectively. TEOS has no organic groups, BTME has two CH_2 chains and bis(propyl)amine has six CH_2 chains attached to a NH_2 group making it very flexible hence yielding the lower BET surface area. However SE-BS-CTAB mesoporous material was an exception, it had the largest BET surface area of 928.6 m^2/g. It is evident from BET that the materials are porous but the structural periodicity must have been confirmed by low angle XRD. Low angle XRD was not done for all the surfactant extracted periodic mesoporous organosilica samples formed due to inadequate resources.

the surface areas increase as the chain length of the organosilane is decreased for periodic mesoporous organosilanes synthesized using P123 as the structure directing agent (Figure 4.19). PMOs synthesized using Pluronic P123 as the structure directing agent have lower surface areas than those obtained using CTAB. No PMOs were formed in this study using 4,4-Bis (triethoxysilyl)-1,1 biphenyl as the organosilica precursor and CTAB as the structure directing agent although there was one synthesized in literature. SE-TS-P123 and SE-TS-CTAB had the highest surface areas followed by SE-BMS-P123 and SE-BMS-CTAB. However SE-BS-CTAB had a higher surface area than SE-BMS-CTAB. This was higher than what was anticipated. It shows that 1,4-Bis (triethoxysilyl) benzene forms PMOs with better structural properties when CTAB as the structure directing agent is used. It can therefore be concluded that CTAB is a better structure directing agent for synthesizing PMOs with better structural properties than CTAB.

The carbonization of as-synthesized and surfactant extracted mesoporous materials in quartz tubes under an inert atmosphere using resulted in a diverse range of carbon on silica nanostructures. AS-T-CS 1000 ^{o}C/5 h produced carbon on silica bamboo nanotubes with varying shapes and some amorphous material. The sample is thermally stable up to 581 ^{o}C in an air atmosphere. The presence of silica in the material was confirmed by TGA. AS-P-CS 1000 ^{o}C/5 h produced carbon on silica nanotubes with very thick internal diameters of between 160 – 170 nm, carbon spheres with average diameters of 400 nm and amorphous carbon. The sample is thermally stable up to 416 ^{o}C in an air atmosphere. EDX confirmed the presence of silica, carbon and oxygen in the various nanostructures obtained for this sample. AS-B-CS 1000 ^{o}C/5 h produced carbon on silica nanotubes with varying small internal diameters and amorphous carbon material. The sample was the most thermally stable of the three materials up to 650 ^{o}C in an air atmosphere. Raman spectroscopy revealed that all samples had a low degree of graphitization and are therefore amorphous. The I_D/I_G ratios of AS-T-CS 1000 ^{o}C/5 h, AS-B-CS 1000 ^{o}C/5 h and AS-P-CS 1000 ^{o}C/5 h samples are 0.81, 1.87 and 0.96 (Table 4.5). The disorder of the samples does not follow any systematic trend.

AS-BS-P123 samples heated at different carbonization temperatures produced different carbon on silica nanostructures which included spheres and nanotubes. Amorphous material (approximately 60%) was also produced. The presence of silicon and carbon in the carbon on silica nanocomposites produced was further confirmed by the use of XPS (AS-B-CS 1000 ^{o}C/5 h sample). Raman data showed that as the carbonization temperature is increased, the degree of disorder of the materials also increased. The temperature at which major loss changes occurred due to the oxidation of carbon increased as the carbonization temperature increased up to 1000°C. Low surface areas and pore volumes were obtained for all mesoporous phenyl-bridgedorganosilica/surfactant mesophases heated at different temperatures. This may be due to the high carbonization efficiency at temperatures from 700 ^{o}C to 1100 ^{o}C that there is rapid formation of carbon deposits which blocks some of the mesopores. Also at these high pyrolysis temperatures, the carbonization may be so fast that the surfactant molecules are directly converted to carbon which blocks the pores rather than being burnt off.

AS-PS-P123 materials were heated to 1000 ^{o}C but the pyrolysis times were varied. From the TEM results it was seen that longer pyrolysis times yields various shaped carbon on silica nanocomposites and shorter pyrolysis times yields only amorphous material and beads. AS-P-CS 1000 ^{o}C/5 h produced carbon on silica nanocomposites of nanotubes, spheres, beads and amorphous material. Both AS-P-CS 1000 ^{o}C/1 h and AS-P-CS 1000 ^{o}C/0.5 h silica on carbon nanocomposites produced amorphous material and beads. Most carbon on silica beads of AS-P-CS 1000 ^{o}C/1 h and AS-P-CS 1000 ^{o}C/0.5 h had sizes which ranged from 1.8 – 2.4 and 1.2 – 2.0 µm respectively. Shorter pyrolysis times of 0.5 h produced carbon on silica beads with smaller diameters which ranged from 1.2 – 2.0 µm and pyrolysis times of 1 h produced carbon on silica beads with larger diameters of 1.8 – 2.4 µm. The Raman data showed that as the carbonization time is increased, the degree of disorder in the carbon on silica nanocomposites also increases. The thermal stability of the carbon on silica nanocomposite samples decreased as the carbonization time was increased. The aims and objectives of this study were achieved.